creative commons
COMMONS DEED

저작자표시-비영리-변경금지 2.0 대한민국

이용자는 아래의 조건을 따르는 경우에 한하여 자유롭게

- 이 저작물을 복제, 배포, 전송, 전시, 공연 및 방송할 수 있습니다.

다음과 같은 조건을 따라야 합니다:

저작자표시. 귀하는 원저작자를 표시하여야 합니다.

비영리. 귀하는 이 저작물을 영리 목적으로 이용할 수 없습니다.

변경금지. 귀하는 이 저작물을 개작, 변형 또는 가공할 수 없습니다.

- 귀하는, 이 저작물의 재이용이나 배포의 경우, 이 저작물에 적용된 이용허락조건을 명확하게 나타내어야 합니다.
- 저작권자로부터 별도의 허가를 받으면 이러한 조건들은 적용되지 않습니다.

저작권법에 따른 이용자의 권리는 위의 내용에 의하여 영향을 받지 않습니다.

이것은 이용허락규약(Legal Code)을 이해하기 쉽게 요약한 것입니다.

Disclaimer

dCollection

Ph.D. Dissertation of Engineering

Assessment of urban ecosystem structure and connectivity using multi-scale LiDAR datasets

다중 규모 LiDAR 데이터를 활용한 도시생태계 구조 및 연결성 평가

August 2021

Graduate School of Seoul National University
Interdisciplinary Program in
Landscape Architecture

Heejoon Choi

Assessment of urban ecosystem structure and connectivity using multi-scale LiDAR datasets

Advisor: Youngkeun Song

A dissertation submitted in partial fulfillment of the requirements for the Degree of Doctor of Philosophy in Interdisciplinary Program in Landscape Architecture in Seoul National University

August 2021

Heejoon Choi

Approved by Thesis Committee

Chair	Dong Kun Lee
Vice Chair	Young ruel Ryu
Examiner	Wanmo Kang
Examiner	Junsuk Kang
Examiner	Younkeun Song

Publications

Please note that Chapters 2–4 of this dissertation proposal were written as standalone papers (see below). Chapters 3 and 4 were published in 2019 and 2021, respectively, and Chapter 2 has been under minor revision.

CHAPTER 2

Choi, H., & Song, Y. (2021). Comparing tree structures derived among airborne, terrestrial and mobile LiDAR systems in urban parks. *GIScience & Remote Sensing.* (Minor Revision)

CHAPTER 4

Choi, H., Song, Y., & Jang, Y. (2019). Urban Forest Growth and Gap Dynamics Detected by Yearly Repeated Airborne Light Detection and Ranging (LiDAR): A Case Study of Cheonan, South Korea. *Remote Sensing*, 11(13). doi:10.3390/rs11131551

CHAPTER 5

Choi, H., Song, Y., Kang, W., Thorne, J. H., Song, W., & Lee, D. K. (2021). LiDAR-derived three-dimensional ecological connectivity mapping for urban bird species. *Landscape Ecology*. doi:10.1007/s10980-020-01165-8

Abstract

Assessment of urban ecosystem structure and connectivity using multi-scale LiDAR datasets

Heejoon Choi
Interdisciplinary Program in Landscape Architecture
Graduate School, Seoul National University
Supervised by Professor Youngkeun Song

Integrated multiscale light detection and ranging (LiDAR) datasets are required for managing urban ecosystems because 1) LiDAR datasets can represent various spatial structures across the urban landscape and 2) the multitemporal LiDAR approach can derive the changes of urban landscape structures. This dissertation aimed to find the various spatiotemporal availabilities (i.e., from the tree-level spatial scale to the city-level regional scale with the multitemporal approach) of LiDAR or laser scanning (LS) datasets for monitoring urban ecosystems in the following three chapters.

Chapter 2: Collecting tree inventory data in urban areas is important for managing green areas. Surveying using airborne laser scanning (ALS) is effective for collecting urban tree structures but less efficient regarding the economic costs and its operation. Terrestrial laser scanning (TLS), and mobile laser scanning (MLS) datasets could have the potential in complementing those of ALS in the respect to efficiency. However, to the best of my knowledge, there were limited studies for seeking the similarities and variations among the canopy metrics derived from various LiDAR platforms. In Chapter 2, I compared structural canopy metrics among ALS, TLS, and MLS datasets in the urban parks. The purpose of Chapter 2 was to test whether the estimates of tree metrics differed depending on single or clustered trees and to test whether the errors in LiDAR-derived metrics were related to the tree structures. Small, urban parks were selected for surveying trees using the three LiDAR platforms. The ALS datasets were acquired on 14 May, 2017. The TLS and MLS datasets were acquired from 10–11 May, 2017, and 21–25 April, 2020, respectively. The tree point clouds were classified into single and clustered trees. The structural metrics were compared in each pair (i.e., ALS and TLS, ALS and MLS, and TLS and MLS pairs). The heights related metrics (e.g., percentile heights and the distribution of the heights values), the complexity metric (e.g., the Rumple index) and area were calculated for comparisons. The root mean square error (RMSE), bias, and the Pearson's correlation coefficient (r) were calculated to evaluate the difference in each metric among the LiDAR platforms. The results showed that

ZMAX, max and mean CHM, and area showed good consistencies (RMSE% < 15 %, Bias% < 15 %, and r > 0.900). Especially, the biases of CHM-derived metrics did not present significant differences ($p > 0.05$) regardless of single or clustered trees. Moreover, the biases from the comparisons in each pair showed linear relations with the tree heights and vertical canopy complexity (i.e., Pearson's correlation coefficient showed significant; $r > |0.29|$, $p < 0.05$). My results could be references when combining multiple LiDAR systems to estimate the canopy structures of urban park areas.

Chapter 3: Understanding forest dynamics is important for assessing the health of urban forests, which experience various disturbances, both natural (e.g., treefall events) and artificial (e.g., making space for agricultural fields). Therefore, quantifying three-dimensional (3D) changes in canopies is a helpful way to manage and understand urban forests better. Multitemporal ALS datasets enable me to quantify the vertical and lateral growth of trees across a landscape scale. The goal of Chapter 3 is to assess the annual changes in the 3-D structures of canopies and forest gaps in an urban forest using annual airborne LiDAR datasets for 2012–2015. The canopies were classified as high canopies and low canopies by a 5 m height threshold. Then, I generated pixel- and plot-level canopy height models and conducted change detection annually. The vertical growth rates and leaf area index showed consistent values year by year in both canopies, while the spatial distributions of the canopy and leaf area profile (e.g., leaf area density) showed inconsistent changes each year in both canopies. In total, high canopies expanded their foliage from 12 m height, while forest gap edge canopies (including low canopies) expanded their canopies from 5 m height. Annual change detection with LiDAR datasets might inform about both steady growth rates and different characteristics in the changes of vertical canopy structures for both high and low canopies in urban forests.

Chapter 4: Although many studies have considered urban structure when investigating urban ecological networks, few have considered the 3D structure of buildings as well as urban green spaces. In Chapter 4, I examined an urban ecological network using the 3D structure of both green spaces and buildings. Using breeding-season bird species observations and ALS data collected, I assessed the influence of 3D structural variables on species diversity. I used correlation analyses to determine if vertical distribution, volume, area, and height of both buildings and vegetation were related to bird species diversity. Then I conducted circuit theory-based current flow betweenness centrality (CFBC) analysis using the LiDAR-derived structural variables. I found that the volumes of buildings and 8–10 m vegetation heights were both highly correlated with species richness per unit area. There were significant differences between 2D and 3D connectivity analysis using LiDAR-derived variables among urban forest patches, boulevards, and apartment complexes. Within

urban forest patches and parks, 3D CFBC represented canopy structural characteristics well, by showing high variance in spatial distributions. The 3D CFBC results indicated that adjacent high-rise buildings, dense apartment complexes, and densely urbanized areas were isolated, as characterized by low centrality values, but that vegetation planted in open spaces between buildings could improve connectivity by linking isolated areas to core areas. My research highlights the importance of considering 3D structure in planning and managing urban ecological connectivity.

In this dissertation, the availability of integrated multiscale LiDAR datasets was found via three standalone studies. It was revealed that 3D information could enhance the quality of urban landscape monitoring and ecological connectivity analysis by elaborately explaining spatial structures. However, the spatiotemporal scales of each standalone study were limited to the city scale and to five years. The recently launched Global Ecosystem Dynamics Investigation (GEDI) would help to solve these limitations. Furthermore, the GEDI dataset could help researchers understand the relationship between ecosystem structures and their functions.

Keyword: LiDAR, Airborne laser scanner, Terrestrial laser scanner, Mobile laser scanner, 3D point cloud, Vegetation structure, Urban landscape structure, Urban ecosystem
Student Number: 2018-35951

Table of Contents

List of Figures

List of Tables

Chapter 1. Introduction

1. Background

1.1. Urbanization and the importance of urban green spaces

Globally, 55% of the world's population lived in urban areas in 2018. By 2050, 68% of the world's population is projected to become urbanized (United Nations 2019), which would cause the rapid development of urban and suburban areas. Accelerated urbanization is considered one of the greatest threats to biodiversity and environments (Zhou et al. 2011). To sustain healthy environments in urban areas, appropriate vegetation plans and management should be considered because these activities reduce the ecological trade-offs that result from urban development (Plummer et al. 2020). Suitable vegetation plans and management can especially introduce diverse species and improve local biodiversity while providing various ecosystem services (Sandström et al. 2006; Savard et al. 2000); (Fontana et al. 2011; Plummer et al. 2020; Sahraoui et al. 2021). To conduct appropriate planning to manage urban ecosystems, it is critical to quantify urban ecosystem structures to be objectively informed of their status.

1.2. Urban landscape and Light detection and ranging application

In urban scales, managing urban ecosystems requires all spatial information across the urban landscape, including high resolution of horizontal and vertical datasets since urban landscape consists of various spatial structures. Furthermore, measuring vertical information which is essential for understanding biodiversity function of green spaces providing various habitat (i.e., ecological niches) (Rutten et al. 2015). However, it is challenging to quantify spatial information of urban ecosystems only with two-dimensional (2D) imageries or several spectral bands (Casalegno et al. 2017). Using advanced techniques such as operating high-resolution light detection and ranging (LiDAR) and data processing can represent diverse structures of urban ecosystems. Recently, therefore, these advanced technologies (i.e., geospatial technologies and ecological informatics) are being applied to solve the ecological and environmental problems and related questions (D'Urban Jackson et al. 2020; Lepczyk et al. 2021).

Green space surveys are conducted in many countries via onsite sampling of plots that are considered representative of the whole study site. In addition, airborne photogrammetry and satellite imagery are applied to measure the diameter at breast height, stand height, basal area, and species composition using terrestrial field sampling data. However, these traditional methods have certain limitations related to the subjective interpretation of measurement results, low measurement accuracy,

and lack of information about vertical canopy structures because of their complex structure (Latifi et al. 2016; Sasaki et al. 2013; Whitehurst et al. 2013). For overcoming the limitations of existing research methods, there is a need for techniques that can support the assessment of forest structures and biodiversity, such as LiDAR remote sensing (Coops et al. 2016).

Many studies have used LiDAR sensors to assess horizontal and vertical tree structures (Song et al. 2016; White et al. 2016; Zhao et al. 2018). LiDAR is one of the most accurate active remote sensing tools. A laser scanner collects object imagery in a three-dimensional (3D) perspective (i.e., a point cloud dataset) by calculating the time intervals between emitting laser pulses and receiving their reflections from target objects. There are three LiDAR platforms or systems, depending on where the sensors are loaded or which systems are used; airborne laser scanning (ALS), terrestrial laser scanning (TLS), and mobile laser scanning (MLS or handheld laser scanning) (Hyyppä et al. 2020). Although ALS can cover large areas (local to region levels), there are concerns that they collect sparse sub-canopy data for forests due to the specifications of the LiDAR sensors, such as the laser footprint, pulse repetition rate, and flight altitude; The footprint of the laser is not small enough to penetrate the gaps in tree canopies or the laser is blocked by the high canopies (Bater et al. 2011; Goodwin et al. 2006; Wang et al. 2019; White et al. 2016). TLS can generate a highly dense point cloud, but tree heights may be underestimated because of the occlusion effects of the lower canopy (Hilker et al. 2012; Krooks et al. 2014; Wang et al. 2019), whereas ALS estimates of tree heights < 10 m show good agreement regardless of stand complexity (Wang et al. 2019; Wu et al. 2020). Although TLS can collect accurate data from tree structures, it has disadvantages in collecting top-canopy data and in surveying regional areas with limited access. Recently, the use of MLS in canopy studies has increased. MLS has been developed in the field of robotics and has adopted simultaneous localizing and mapping (SLAM) robotics systems. MLS is more convenient than TLS for collecting 3D datasets of extensive areas (Heo et al. 2019; Hyyppä et al. 2020; Liang et al. 2016a; Schneider et al. 2019).

1.2.1. Combination with airborne LiDAR and terrestrial LiDAR data for surveying structures of urban green spaces

ALS datasets may be useful for administrators to plan and manage their urban areas; however, the economic cost of ALS makes it difficult to collect consistent multi-temporal ALS datasets that correspond to urban land-use changes (White et al. 2016). TLS and MLS may solve the acquisition problems for these temporal data (Bauwens et al. 2016; Bienert et al. 2018). However, there are few studies of which LiDAR-derived structural variables of green areas can be used in common among the different LiDAR systems. Most studies have been conducted using single LiDAR

systems with field surveys for validation. Hilker et al. (2012) concluded that tree-level (i.e., collecting individual tree data) measurements were more accurate using TLS than using ALS, whereas height estimation was more accurate using ALS. Pyörälä et al. (2019) and LaRue et al. (2020) compared ALS-derived canopy metrics with TLS-derived wood properties and found that several wood properties were predictable from the ALS datasets. Ojoatre et al. (2019) and Bazezew et al. (2018) estimated forest biomass by integrating ALS and TLS datasets.

Although a few studies have integrated the different LiDAR systems (Hilker et al. 2012; LaRue et al. 2020; Pyörälä et al. 2019), more relevant studies are needed to manage the green spaces in urban areas. Moreover, more in-depth understanding is required as to which tree-structure variables derived from ALS, TLS, and MLS can substitute for and complement each other.

1.2.2. Multi-temporal urban forest gap monitoring

Quantifying forest gaps is essential for monitoring the stability of the forest structure because these disturbances can change the light environment and drive forest dynamics (Asner et al. 2013; Fisher et al. 2008; Kane et al. 2011; Whitmore 1989). Physical disturbances in forest canopies usually result from deforestation (e.g., making space for agricultural fields) and tree-fall events (Asner et al. 2013). Forest gaps could be characterized by their size distribution. The areas of forest gaps in natural forests follow the power-law distribution with the frequencies. Usually, small openings (formed by wind damaged or tree mortality) in natural forests dominate areas in the size distribution and show larger scaling exponents, while frequent large openings show smaller scaling exponents. Therefore, by comparing the scaling exponents with other forests, it is possible to compare the degrees of disturbances (Kane et al. 2011; Whitmore 1989).

Urban forests are usually fragile to disturbances because the dense human population leads to severe conditions that can damage the forest directly (e.g., land-cover changes from forested to urbanized areas) (Steenberg et al. 2016). Forest damage such as deforestation and landcover changes could result in relatively larger openings than small openings in forests and the human activities in there may hinder the forest equilibrium or change the forest ecosystems (Vepakomma et al. 2018). Particularly in South Korea, small and large mountainous urban forests are very common as they remain green areas after development and many people use them for leisure activities, agriculture, and private graveyards that are accompanied with canopy openings (Kim et al. 2013). Although many policies try to conserve these urban forests in South Korea, land use in urban forests is complexed and can easily undergo harsh disturbances (Ryu et al. 2017). Therefore, it is important to monitor forest gaps in urban forests where various natural or anthropogenic disturbances can

occur.

For applications of multi-temporal ALS in urban forests, a few studies about the forest dynamics (e.g., forest growth and forest gap dynamics) in an urban forest have been conducted. Ossola and Hopton (2018b) measured urban tree loss dynamics in cities' residential landscapes using bi-temporal (five-year period) LiDAR datasets. They particularly noted the changes in urban trees over time caused by human management and urban tree removal for hazard prevention or artistic preference. Since the urban forests are characteristically vulnerable to various and frequent disturbances, particularly in terms of physical damage (Liu et al. 2015; McWilliam et al. 2010; Ossola and Hopton 2018b), canopy loss occurs frequently that could finally result in artificial canopy openings. However, to the best of my knowledge, most studies with airborne LiDAR datasets have focused on the forest gaps which are usually treefall gaps in the natural forests (Vepakomma et al. 2018; Vepakomma et al. 2008) and few studies are related to artificial canopy openings in cities. In the same manner of the effect on the surrounding environment of forest gaps, artificial openings could affect the adjacent environment (Dalagnol et al. 2019) and may also affect the changes in surrounding canopy structures. Therefore, it is important to monitor urban forests continuously (Cumming et al. 2008) including both forest gaps and their artificial canopy openings.

1.2.3. Ecological connectivity analysis using LiDAR

Urban ecological networks provide solutions-based tools to decision-makers regarding urban conservation challenges (Choe and Thorne 2019; Lepczyk et al. 2017; Nor et al. 2017; Sandstrom et al. 2006). Well-managed ecological networks resulting from the use of these tools could improve biodiversity and sustainability in cities by providing ecosystem services such as hydrological regulation, air purification, and positive effects on human health (Barton and Pretty 2010; Steenberg et al. 2016).

Ecological networks can be quantified by connectivity indices, which provide a measure of how landscape patterns affect ecological processes. Centrality metrics are a form of connectivity indices (Carroll et al. 2012). Centrality values vary among landscape patches and generally imply at least some connectivity within landscapes, at least functionally, even when patches are not physically connected in space (Kindlmann and Burel 2008). Thus, urban ecological connectivity assessments can be effectively used to evaluate landscape function within cities (Casalegno et al. 2017; Cook 2002; Dickson et al. 2019; Grafius et al. 2017; Tian et al. 2017; Urban and Keitt 2001; Zeller et al. 2012).

Networks in urban ecosystems reflect heterogeneous landscape patterns with characteristics such as variation in vegetation patches and both vegetation and

anthropogenic structure (e.g., buildings) (Farinha-Marques et al. 2017; Lepczyk et al. 2017). Including vegetation measures as well as measures of building structures (e.g., height and volume) in assessments of urban ecological networks is essential, particularly when considering urban bird species, as these structures represent habitat structure and composition for such species (Xie et al. 2016). Urban ecology studies have often focused on avian species because the extent of ecological connectivity in a given area is related to bird species diversity (Evans et al. 2009b; Goddard et al. 2010; Kang et al. 2015). Avian species typically use green spaces as both corridors and habitat by selecting and moving within vegetation in both vertical and horizontal directions (e.g., by using the top or middle of canopies, and tree interior or edges) (Casalegno et al. 2017; Conole and Kirkpatrick 2011). Therefore, considering the horizontal and vertical distributions of green spaces is essential to understanding between-patch connectivity for birds (Casalegno et al. 2017). In addition, because buildings in urban ecosystems often segregate urban green patches and act as barriers against the urban bird species (Hale et al. 2012), the configuration of structures including building volume, distribution, and height should be considered when designing urban green space connectivity. However, most urban network studies have treated structures only in 2-dimensions and used vertical information such as tree heights or structures by categorizing values (Grafius et al. 2017; Matsuba et al. 2016).

There are great opportunities for applying 3D datasets to the field of ecology and environment. A 3D dataset could help elucidate the relationship between urban morphologies and urban heat environment. Tian et al. (2019) identified the relationship between air temperature and 3D landscape indices such as building to vegetation volume ratio. Zhang et al. (2019) used the 3D index (e.g., sky fraction) derived from the Google street map to estimate land surface temperatures. Moreover, using a 3D dataset could enhance the understanding of bird species movements. For example, Liu et al. (2020b) and Tattoni and Ciolli (2019) emphasized the importance of 3D data for the bird corridors. Liu et al. (2020b) used digital elevation models (DEMs) and building heights for understanding the impacts of urban vertical expansion on the birds' migratory patterns, and Tattoni and Ciolli (2019) also applied a DEM for finding potential stopover sites in the birds' migratory routes.

Many studies have demonstrated that including vegetation structure is critical to assessing ecological connectivity (Casalegno et al. 2017; Chen et al. 2014; Coops et al. 2016; Dalponte et al. 2019; Guo et al. 2018; Melin et al. 2018; Plowright et al. 2017; Shao et al. 2019). For example, Coops et al. (2016) found that airborne LiDAR-derived indices such as the standard deviation of canopy height, green cover ratio, and canopy height diversity were related to bird species diversity; these metrics were successfully used, along with other environmental variables, to estimate bird

species diversity across broad areas. Casalegno et al. (2017) characterized urban habitat structure using LiDAR data from local to landscape scales and were among the first to assess connectivity among green space patches in urban areas using LiDAR data. LiDAR-derived structural variables have enormous potential for assessing connectivity across spatial scales and thus informing biodiversity conservation and monitoring strategies. Finally, Kedron et al. (2019) developed 3D urban landscape indices using a LiDAR dataset.

Although ecological and connectivity networks include both anthropogenic and vegetation structure, existing research has not typically employed 3D analyses to estimate all structural variables. Two-dimensional variables would have limitations in representing these diverse structures of urban ecosystems.

2. Purpose

In this dissertation, I aimed to find various spatiotemporal (i.e., from the tree-level spatial scale to city-level regional scale with a multi-temporal approach) availabilities using LiDAR to monitor urban ecosystems. I focused on finding the relationship between urban vegetation/building structures and urban biotic environments through three standalone studies. First, I quantified urban vegetation and building structures as metrics. Then, I compared the vegetation metrics among ALS, TLS, and MLS systems to find their consistencies. Second, I addressed the structural metrics to engage in the temporal monitoring of annual changes in an urban forest and found the differences in changes according to whether there were forest gaps or not. Third, I conducted a study to find the relationship between urban vegetation/building structures and urban-living bird species and applied the derived biodiversity-related metrics to analyze ecological connectivity in an urban area.

In Chapter 2, I compared structural tree variables among ALS, TLS, and MLS datasets and sought alternative structural variables that could be applied when an ALS dataset was not available. I aimed to test whether the estimates of tree metrics differed depending on whether the trees were single or clustered and whether the errors in LiDAR-derived metrics were related to tree structure.

In Chapter 3, I assessed the annual changes in the 3D structures of canopies and forest gaps in an urban forest using annual airborne LiDAR datasets. To determine how much urban forest structures have changed, I estimated 1) the distribution of the growth area and damaged areas (e.g., vertical and later growth and damaged areas), 2) changes in vertical leaf area density profile, and 3) the dynamics of opening and closing forest canopies during 2012–2015.

In Chapter 4, I examined an urban ecological network using the 3D structure of both green spaces and buildings. My specific objectives of Chapter 4 are to define which LiDAR-derived urban bird species diversity variables to use in creating a

connectivity surface (landscape resistance and landscape permeability) and then test a modeled urban ecological network created using them. Related research questions are: 1) What are the contributions of the urban green spaces to the 3D connectivity with regard to land-use types; and 2) What are the characteristics of 3D-based connectivity results compared to 2D-based connectivity results?

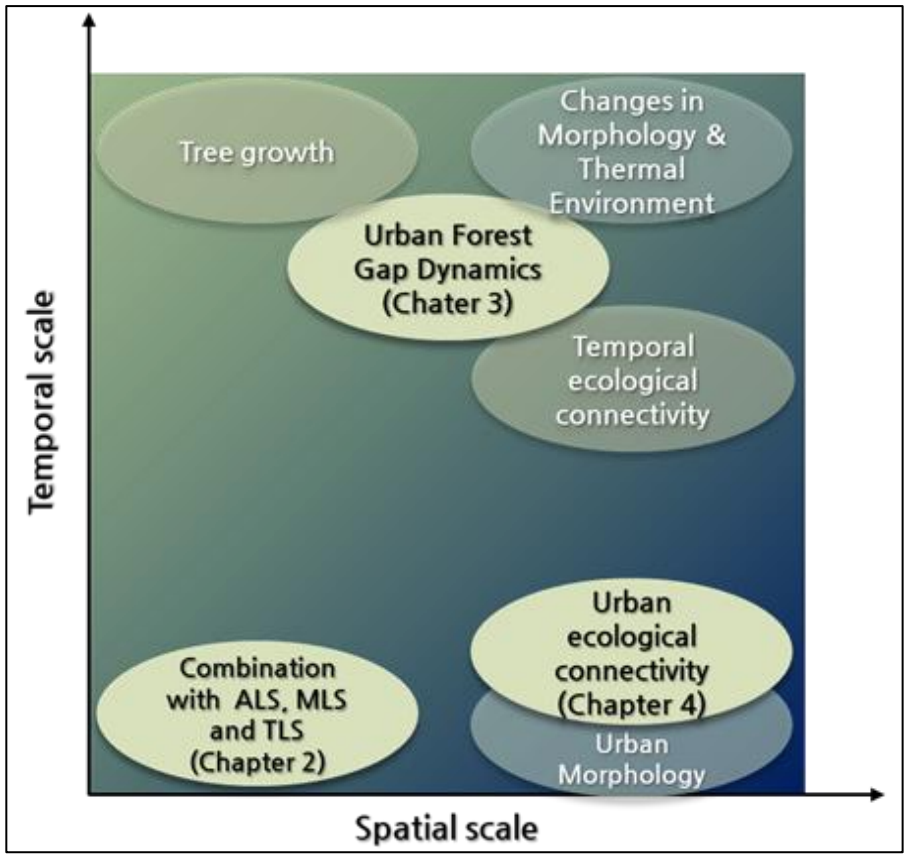

Figure 1.1 Urban ecosystem monitoring using light detection and ranging remote sensing and its related studies by the spatial and temporal scales dealt with in this dissertation

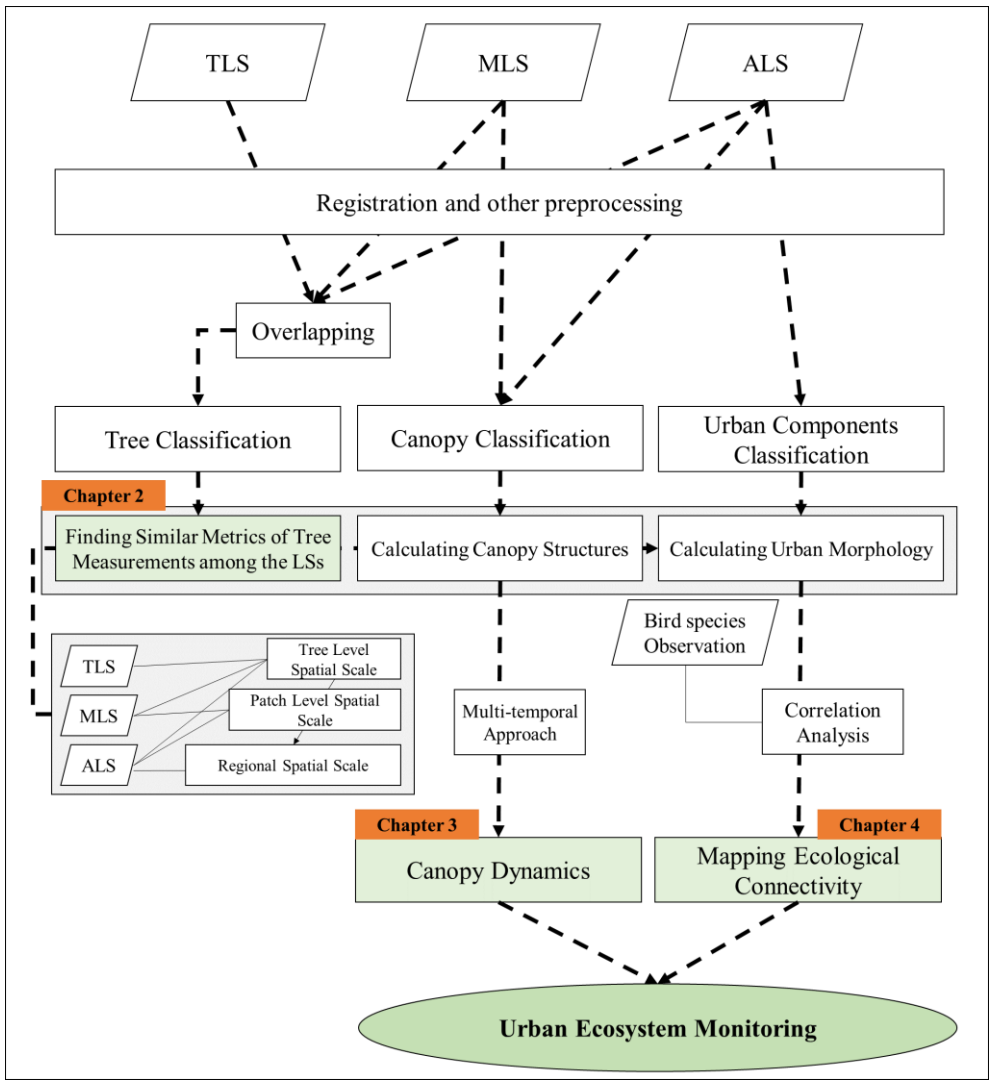

Figure 1.2 Study flow of this dissertation

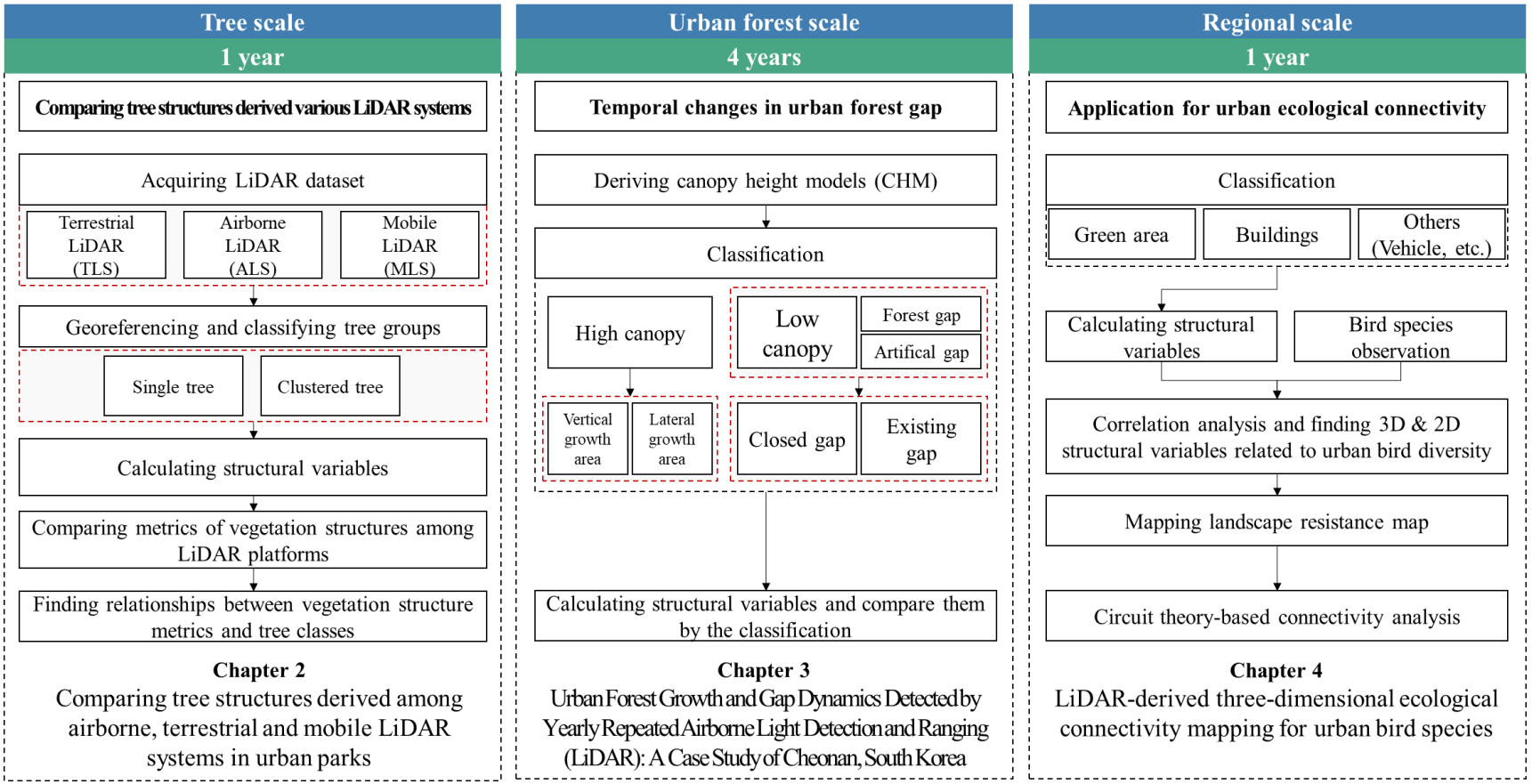

Figure 1.3 Study flow of each chapter

Chapter 2. Comparing tree structures derived among multiple LiDAR systems in urban parks

1. Introduction

A detailed dataset of cityscape tree structures is needed to provide well-managed and designed green spaces. Estimates of both horizontal (i.e., canopy cover) and vertical (i.e., vertical canopy distribution) tree structures are essential to manage and monitor green areas because these parameters identify tree vigor and relate to ecosystem functions and urban biodiversity (Nadrowski et al. 2010; Omasa et al. 2006; Smith et al. 2019; Song et al. 2016). Owing to the importance of estimating tree structures and the limitations imposed by using two-dimensional spatial datasets (e.g., airborne imagery and satellite imagery) to describe the vertical information of tree structures, there is an urgent need for more elaborate spatial datasets created using high resolution remote sensing systems and data processing such as light detection and ranging (LiDAR) remote sensing (Eitel et al. 2016; Lefsky et al. 2002; Lepczyk et al. 2021).

Many studies have used LiDAR sensors to assess horizontal and vertical tree structures (Choi et al. 2019; Song et al. 2016). LiDAR is one of the most accurate active remote sensing tools. A laser scanner collects object imagery in a three-dimensional (3D) perspective (i.e., a point cloud dataset) by calculating the time intervals between emitting laser pulses and receiving their reflections from target objects. There are three LiDAR platforms or systems, depending on where the sensors are loaded or which systems are used; airborne laser scanning (ALS), terrestrial laser scanning (TLS), and mobile laser scanning (MLS or handheld laser scanning) (Hyyppä et al. 2020). Although ALS can cover large areas (local to region levels), there are concerns that ALS collect sparse sub-canopy data for forests due to the specifications of the LiDAR sensors, such as the laser footprint, pulse repetition rate, and flight altitude; The footprint of a laser is not small enough to penetrate the gaps in tree canopies or is blocked by high canopies (Bater et al. 2011; Goodwin et al. 2006; Wang et al. 2019; White et al. 2016). TLS can generate a highly dense point cloud, but tree heights may be underestimated because of the occlusion effects of the lower canopy (Hilker et al. 2012; Krooks et al. 2014; Wang et al. 2019), whereas ALS estimates of tree heights < 10 m show good agreement regardless of stand complexity (Wang et al. 2019; Wu et al. 2020). Although TLS can collect accurate data from tree structures, it has disadvantages in collecting top-canopy data and in surveying regional areas with limited access. Recently, the use of MLS in canopy studies has increased. MLS has been developed in the field of robotics and has adopted simultaneous localizing and mapping (SLAM) robotics systems. MLS is more convenient than TLS for collecting 3D datasets of extensive areas (Heo et al.

2019; Hyyppä et al. 2020; Liang et al. 2016b; Schneider et al. 2019). Moreover, forest inventory results using MLS have shown good agreement compared to TLS-derived results (Su et al. 2020; Wang and Fang 2020).

ALS datasets may be useful for city planners to plan and manage their urban areas; however, the economic cost of ALS makes it difficult to collect consistent multi-temporal ALS datasets that correspond to urban land-use changes (White et al. 2016). TLS and MLS may solve the acquisition problems for these temporal data (Bauwens et al. 2016; Bienert et al. 2018). However, to the best of my knowledge, there are few studies of which LiDAR-derived structural variables of green areas can be used in common among the different LiDAR systems. Most studies have been conducted using single LiDAR systems with field surveys for validation. Hilker et al. (2012) concluded that tree-level (i.e., collecting individual tree data) measurements are more accurate using TLS than using ALS, whereas height estimation is more accurate using ALS. Pyörälä et al. (2019) and LaRue et al. (2020) compared ALS-derived canopy metrics with TLS-derived wood properties and found that several wood properties are predictable using the ALS datasets. Ojoatre et al. (2019) and Bazezew et al. (2018) estimated forest biomass by integrating ALS and TLS datasets.

Each LiDAR system has its pros and cons in terms of its purpose of use. Stand-alone LiDAR systems can successfully estimate tree structures (Heo et al. 2019; Su et al. 2020; Wu et al. 2020). However, the estimated tree structure measurements could be different depending on which LiDAR system is used. This may lead to confusion and reduce confidence when evaluating tree structures and their derived products, such as the plant area index (PAI), biomass, and carbon stocks. A standalone LiDAR system does not capture entire spaces both vertically and horizontally; ALS is weak at sensing understory canopy structures, and TLS and MLS are unfavorable in sensing top canopies and covering broad areas. Therefore, assessing consistencies among the different LiDAR systems should be conducted in advance. Although a few studies have integrated different LiDAR systems (Hilker et al. 2012; LaRue et al. 2020; Pyörälä et al. 2019), a greater depth of understanding regarding the similarities, variations, or consistencies among measurements resulting from LiDAR metrics is required. By comparing canopy metrics indifferent LiDAR systems, it would be possible to determine a methodology for combining metrics to substitute for and complement each other.

Therefore, this study compares tree structure variables among ALS, TLS, and MLS datasets and seeks alternative structural variables that could be applied when an ALS dataset is not available. Specifically, this work aims to determine whether the estimates of different metrics differ depending on whether trees are standalone or clustered and whether the errors in LiDAR-derived metrics are related to tree

structures.

2. Methods and materials

2.1. Study site and tree classification

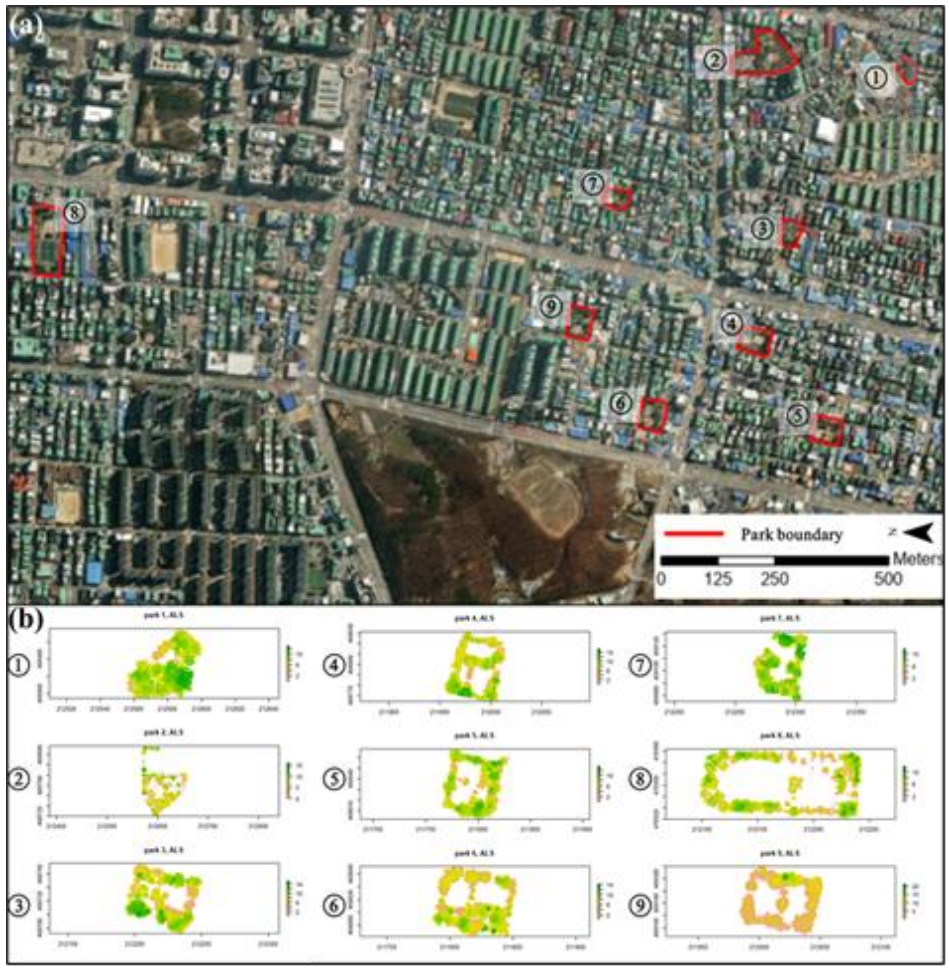

Figure 2.1 Study site (a, red boundary: parks surveyed using ALS, TLS, and MLS) and vegetation height information on numbered parks in this study (b)

I selected small, isolated, urban parks, categorized as children's parks, in Cheonan City, South Korea. I surveyed nine small parks using TLS and MLS to acquire the LiDAR data (Figure 2.1). These small, isolated, urban parks typically consisted of trees lower than 22 m in height, a playground facility, and pergolas. I considered that the vegetation structures consisted of types of single and clustered trees typical of parks in South Korea.

The surveyed vegetation in the parks consisted of general tree species found commonly in South Korea. Generally, sub-canopies (e.g., *Acer palmatum* and *Chaenomeles sinensis*), and high canopies (e.g., *Zelkova serrata*, *Sophora japonica*,

and *Ulmus davidiana* var. *japonica*) form the canopy structures in the parks. The surveyed trees and their shapes were shown in Figure 2.2.

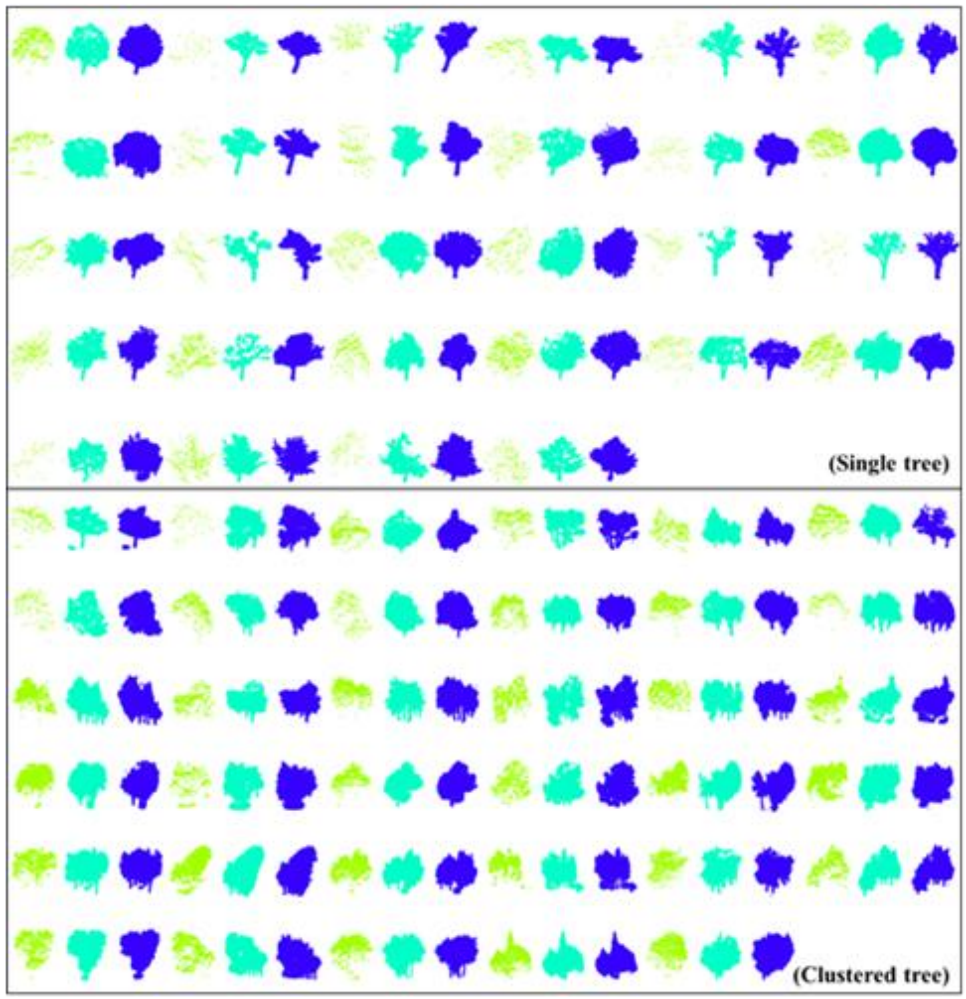

Figure 2.2 Sampled single trees (top) and clustered trees (down) (yellow green: airborne laser scanning; cyan: terrestrial laser scanning; blue: mobile laser scanning)

2.2. LiDAR survey and processing

Table 2.1 Configuration of the LiDAR sensors used in this study

Specification	ALS	TLS	MLS
Equipment	IGI LiteMapper 6800	FARO Focus 350 laser scanner	Kaarta Stencil (Velodyne16 sensor)
System	Mounted on an aircraft	Mounted on a tripod	Mounted on a hand-held computer (SLAM system, 1. 5 m height above ground level)
Range	38,000 m (width: 1,155 m)	0.6 m to 350 m	1 m to 30 m
Accuracy	<±10 cm	<±0.5 cm	<±3 cm
Point density	2-8 point/㎡	> 1,000 point/㎡	> 1,000 point/㎡
Field of view	60°	Verticality: 0~300° Horizontality: 0~360°	Verticality: 30~330° Horizontality: 0~360°
Sensing method and locations	ALS system, flying at an altitude of 1000 m	Positioned several locations at a height of 1.5 m above ground level	SLAM system. Moving while sensing and following loop trajectories
Projection	WGS 1984 52N	Local (Georeferenced by ALS)	Local (Georeferenced by ALS)
Data acquisition	14 MAY 2017	10–11 MAY 2017	21 APR–01 MAY 2020

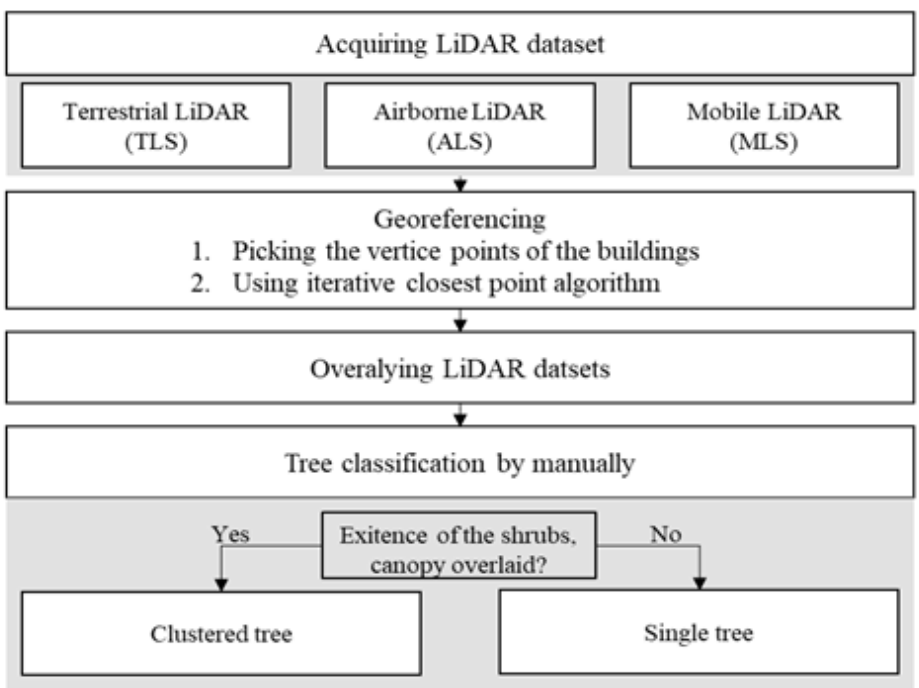

Figure 2.3 LiDAR data processing and tree classification

Table 2.1 lists the sensor specifications. The TLS dataset was acquired from May 10–11, 2017 during a foliated season. The TLS instrument was placed at several positions in each park to reduce the occlusion effects of trunks, twigs, branches, or other objects. Furthermore, I located the sphere-shaped targets for the registration process; the sphere-shaped targets were used as the control points in each collected scene. After scanning the parks, I merged the separate scenes from each position into one complete scene using FARO SCENE software (FARO, Lake Mary, FL, US). The TLS dataset was georeferenced to the ALS dataset by manually picking more than 30 points of the building vertices in both the ALS and TLS datasets and using the iterative closest point (ICP) algorithm in the CloudCompare program (https://www.danielgm.net/cc/) (Figure 2.3). The positional errors (i.e., the root-mean-square error [RMSE]) between the terrestrial-based LiDAR systems (i.e., TLS and MLS) and ALS were between 0.15–0.5 m (Figure 2.4).

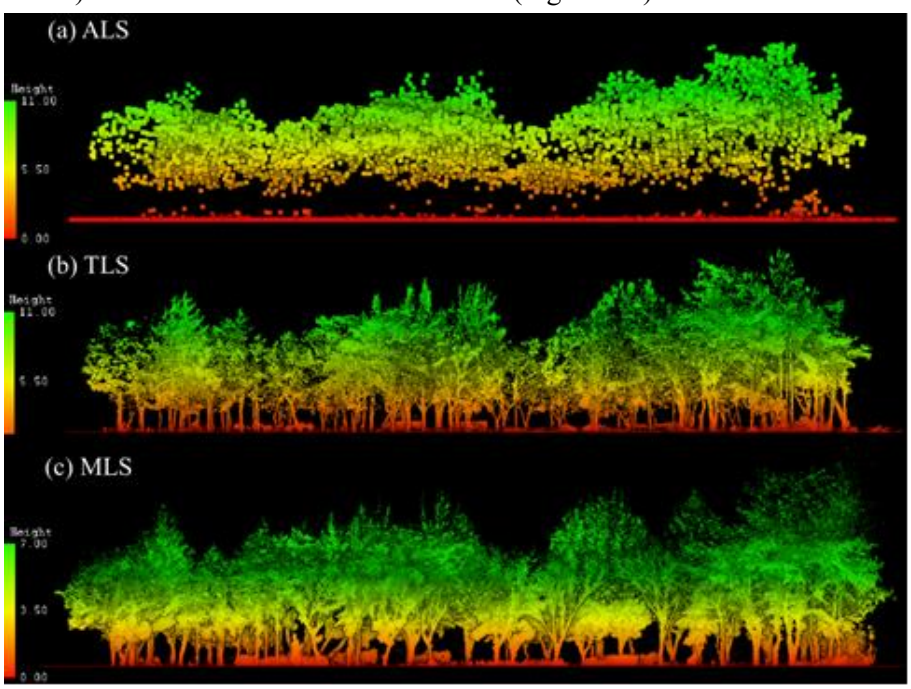

Figure 2.4 Examples of registered and normalized point clouds (a, b, and c are a park point cloud from the airborne laser scanning, terrestrial laser scanning, and mobile laser scanning, respectively)

The MLS dataset was acquired from April 21–25, 2020 mostly during the same season as when the TLS dataset was acquired. Because the MLS was acquired three years after the ALS and TLS acquisition, coexisting trees in between years were selected for comparisons. Since the MLS system incorporated simultaneous localizing and mapping (SLAM) (Maddern et al. 2017; Pandey et al. 2011; Zhang et al. 2016), I was able to avoid occlusion effects and obtain almost complete 3D scenes of the parks by walking inside and outside the parks. Moreover, I made a closed loop

route for the sensing trajectories to improve the quality of the MLS dataset (Zhang et al. 2016).

The ALS datasets were acquired on 14 May 2017 using an IGI LiteMapper 6800 sensor (Samah Aerial Survey Co.). The study sites were surveyed following eight flight lines at an altitude of 1,000 m with a 50% width overlap of the scanned areas. The beam divergence was 0.3 mrad, and the field of view was 60°. The point density was > 5 points/m^2. The dataset was preprocessed and classified using algorithms built into TerraScan software (Terrasolid, Helsinki, Finland) on a MicroStation (Bentley Systems, PA, USA) platform. Non-tree objects were manually deleted, including benches, fences, playground facilities, and building structures.

Following registration or georeferencing using the LiDAR systems (i.e., two pairs: ALS-TLS and TLS-MLS), the point clouds were classified into ground and non-ground points using CloudCompare software (https://www.danielgm.net/cc/). Next, the point clouds were normalized by subtracting the height of the ground from the non-ground points to calculate the absolute height (z, m) values.

Table 2.2 shows the classification of the trees. The vegetation was manually classified into single trees and clustered trees (where canopies combined, Figure 2.5) to test for errors in the LiDAR-derived metrics based on the vegetation type. All classifications were conducted manually, and I excluded the point cloud of any vegetation that had an irregular shape due to occlusion effects.

Table 2.2 Tree classification

Classification	**NO.**	**Average of canopy area (m^2)**	**Maximum canopy area (m^2)**	**Minimum canopy area (m^2)**	**Average of canopy height (m)**	**Maximum canopy height (m)**
Clustered trees	35	214.63	762.07	16.94	7.29	21.26
Single tree	28	44.29	142.97	5.74	6.55	14.69

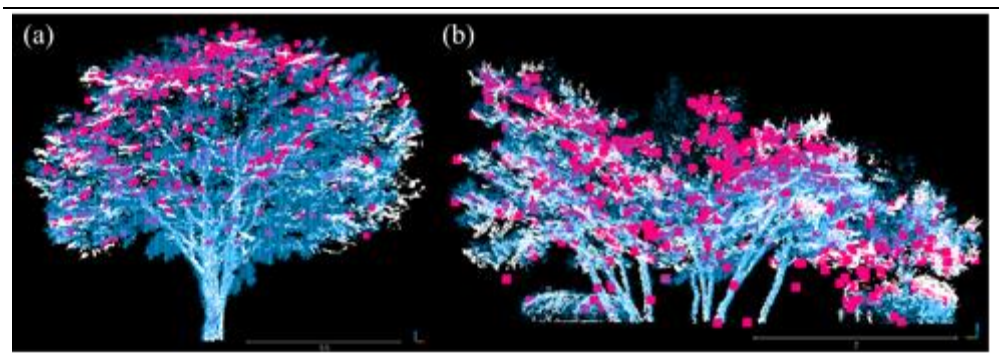

Figure 2.5 Examples of single trees (a) and clustered trees (b) (purple: airborne laser scanning; white: terrestrial laser scanning; sky blue: mobile laser scanning); Classification was conducted manually using CloudCompare software after overlaying the georeferenced airborne laser scanning, terrestrial laser scanning, and mobile laser scanning datasets.

2.3. Deriving the structural variables of the parks

The structural variables, as shown in Table 2.3, were calculated using the lidR (Roussel et al. 2020) and TreeLS (Conto 2020) packages of R software (R Core Team 2021). Height-related metrics, such as the maximum value of height (ZMAX), mean value of height (ZMEAN), 95th percentile height (Zq95), and standard deviation of height (ZSD), are generally used to estimate tree biomass (Goodwin et al. 2006; Hilker et al. 2010; LaRue et al. 2020). Moreover, these metrics describe the vegetation structures; ZMAX is the highest point in the trees and ZMEAN is the average value of the heights of the points (z). Zq95 is the 95th percentile heights of the point clouds. Canopy height model (CHM)-related metrics, such as maxCHM, meanCHM, and Std. of CHM are associated with the forest biomass. These CHM-related metrics were used to describe the canopy surfaces, because ALS was able to detect the canopy surfaces, which were then described by the CHM. The CHMs were calculated by subtracting the digital surface model (DSM) from the digital elevation model (DEM) using CloudCompare and ArcGIS pro softwares (ESRI, Redlands, CA, USA) to describe the absolute heights of the canopies at the study sites. The resolution of the CHM was 0.5 m. I also calculated the CHM-derived metrics from the LiDAR sensors and ascertained whether the TLS and MLS values were similar to those of ALS.

The Rumple Index is calculated by dividing the 3D surface area by the 2D surface area, which generally represents the complexity of the canopy (Parker et al. 2004). A high Rumple Index value implies a highly complex canopy structure (Kane et al. 2010; Parker et al. 2004).

Finally, PAI was derived from the voxelized point clouds. PAI is defined as the one-sided area of vegetation, including both woody and leaf parts, per unit ground area (Hosoi and Omasa 2009; Zhu et al. 2020). The classified point clouds were voxelized as 1 m^3 (1 m × 1 m × 1 m) units to alleviate the effects of differences in the point density of each LiDAR system (Table 2.1). The PAI was calculated by summing up the plant area density (m^2/m^3) of the classified point clouds.

Table 2.3 Summary of the variables derived from airborne, terrestrial and mobile LiDAR scans

Variable	Description	Unit	Reference
ZMAX	Maximum value of z (height, m) of a point cloud	m	Roussel et al. 2020
ZMEAN	Mean value of z (height, m) of a point	m	
Zq95	95th percentile heights of a point cloud above	m	
ZSD	Standard deviation of a point cloud above	m	
maxCHM	Maximum canopy height derived from the canopy height model (CHM) (1-m resolution)	m	Calculated in CloudCompare
meanCHM	Mean height derived from the CHM (1-m resolution)	m	software(https://www.da

Variable	Description	Unit	Reference
Std. of CHM	Standard deviation of the CHM (1-m resolution)	m	nielgm.net/cc/) and ArcGIS pro (ESRI, Redlands, CA, USA)
Rumple index	Canopy complexity calculated by dividing the 3D surface area by the 2D surface area (CHM/ortho area) of the parks	m^2/m^2	Roussel et al. 2020 Parker et al. 2004
Area	Green area based on the point cloud	m^2	Roussel et al. 2020
Plant area index	One-sided area of vegetation, including both woody and leaf parts, per unit ground area. The voxel size was set as 1 m × 1 m × 1 m, vertical distance, dz, was set to 2.5 m, and the constant k was set as 0.5	m^2/m^2	Roussel et al. 2020 Hosoi and Omasa 2009

2.4. Assessing the accuracy of the LiDAR-derived indices

Comparisons were conducted in pairs. The Pearson's correlation coefficient (r), root mean square error (RMSE), relative RMSE (%), bias and relative bias (%) were calculated in three pairs (Wang et al. 2019) for the tree-structure metrics. Comparisons were made between ALS-based vs TLS-based metrics, ALS-based vs MLS-based metrics, and TLS-based vs MLS-based metrics.

The RMSE was derived from the linear regression from each pair (i.e., ALS-TLS, ALS-MLS, and TLS-MLS). The ALS dataset metrics were considered to be a reference because I assumed that TLS and MLS underestimated canopy height (Hilker et al. 2012). The TLS data served as the reference values for the TLS-MLS metrics pair. The relative RMSE (%) was calculated by dividing the mean values of the reference data from the RMSE. Bias was calculated by subtracting the mean values of the reference data from the mean of the compared values, and relative bias (%) was derived after dividing the mean values of the reference data from the bias.

Furthermore, I conducted a t-test to determine whether the calculated tree measurements showed significant differences depending on whether they were derived from single or clustered trees. Pearson's correlation test was conducted to determine whether the calculated measurements have a linear relationship with the canopy structures. The Pearson's correlation coefficient (r) has a value between -1 to 1. If the r value is close to 1, then it indicates that the two compared datasets show a strongly positive linear relationship and vice versa. All calculations were conducted using R software (R Core Team, 2021).

3. Results

3.1. Comparing height metrics among the three LiDAR systems

Table 2.4 Assessment and comparison of the indices of tree structures determined using the LiDAR systems

Metrics	ZMAX					ZMEAN				
Evaluation	RMSE (m)	RMSE (%)	Bias (m)	Bias (%)	r	RMSE (m)	RMSE (%)	Bias (m)	Bias (%)	r
ALS VS. TLS*	0.43	4.45	-0.27	-2.81	0.990	0.86	13.70	1.84	29.11	0.815
ALS VS. MLS*	0.44	4.52	-0.78	-8.11	0.989	1.34	21.16	2.52	39.97	0.447
TLS VS. MLS**	0.52	5.27	-0.51	-5.16	0.984	0.74	16.53	0.69	15.31	0.406
Metrics	**Zq95**					**ZSD**				
Evaluation	**RMSE (m)**	**RMSE (%)**	**Bias (m)**	**Bias (%)**	**r**	**RMSE (m)**	**RMSE (%)**	**Bias (m)**	**Bias (%)**	**r**
ALS VS. TLS*	1.10	12.66	1.07	12.34	0.882	0.44	26.67	-0.24	-14.34	0.762
ALS VS. MLS*	1.31	15.16	1.69	19.48	0.826	0.41	24.68	-0.14	-8.65	0.801
TLS VS. MLS**	1.09	14.41	0.62	8.15	0.764	0.34	17.86	0.09	4.98	0.762

*Biases were calculated by subtracting the TLS and MLS values from the ALS values.
**Biases were calculated by subtracting the MLS values from the TLS values

Table 2.4 and Figure 2.6 show comparisons of the height-related metrics among the three datasets. ZMAX was the most consistent variable among the three LiDAR systems, although evaluation of ZMAX indicated that ZMAX was sometimes underestimated by ALS, considering the biases (Table 2.4). The ALS dataset had a low-density point cloud (5 points/m^2 to 8 points/ m^2), meaning that points representing tree apices could be missing (Zhao et al. 2018). On the other hand, MLS ZMAX values were higher than those derived from TLS and ALS. Since the MLS dataset was acquired 3 years after the ALS and TLS datasets, I assumed that canopy growth had occurred, and this was shown by the higher positive biases compared to ALS and TLS. Figure 6a demonstrates the higher ZMAX values of MLS. In the scatter plots of the MLS pairs, the dots and linear regression graphs are generally located below the 1:1 line, indicating higher ZMAX values than for the other two LiDAR platforms (Figure 2.6a). Since ZMEAN and Zq95 values can easily be affected by the location of the LiDAR, resulting in discrepancies in the point cloud density, differences were more considerable than in ZMAX. A comparison of ZMEAN and Zq95 showed that the dots in the ZMEAN plots were more scattered than those in the Zq95 plots (Figure 2.6b and Figure 2.6c), indicating that Zq95 was more stable and provided an alternative LiDAR metric to that of ZMEAN. A comparison of ZMEAN and Zq95 values revealed that ALS values were higher than those derived by the other two LiDAR systems. Notably, in the case of ZMEAN and Zq95, there were closer linear relationships for the ALS-TLS pairs than for the ALS-MLS and TLS-MLS pairs.

Since ZMEAN and Zq95 values can easily be affected by the location of the LiDAR, resulting in discrepancies in the point cloud density, differences were more considerable than in ZMAX. A comparison of ZMEAN and Zq95 showed that the dots in the ZMEAN plots were more scattered than those in the Zq95 plots (Figure 6b and Figure 6c), indicating that Zq95 was more stable and provided an alternative LiDAR metric to that of ZMEAN. A comparison of ZMEAN and Zq95 values revealed that ALS values were higher than those derived by the other two LiDAR systems. Notably, in the case of ZMEAN and Zq95, there were closer linear relationships for the ALS-TLS pairs than for the ALS-MLS and TLS-MLS pairs (Table 2.4 and Figure 2.6b and Figure 2.6c).

ZSD values revealed a linear relationships among the LiDAR systems (the Pearson's coefficient r values were higher than 0.7), but the values were not very precise (RMSE (%) was almost 20% and with low biases). In particular, ZSD derived from TLS showed relatively low consistencies with the ZSD from ALS and MLS (Pearson's r for ALS-TLS and TLS-MLS were lower than the TLS-MLS pair).

By comparing single and clustered trees, the coefficients of determination (R^2 values) of the height-related metrics of clustered trees, except for ZMAX, were lower than those derived for single trees (see R^2 in Figure 2.6).

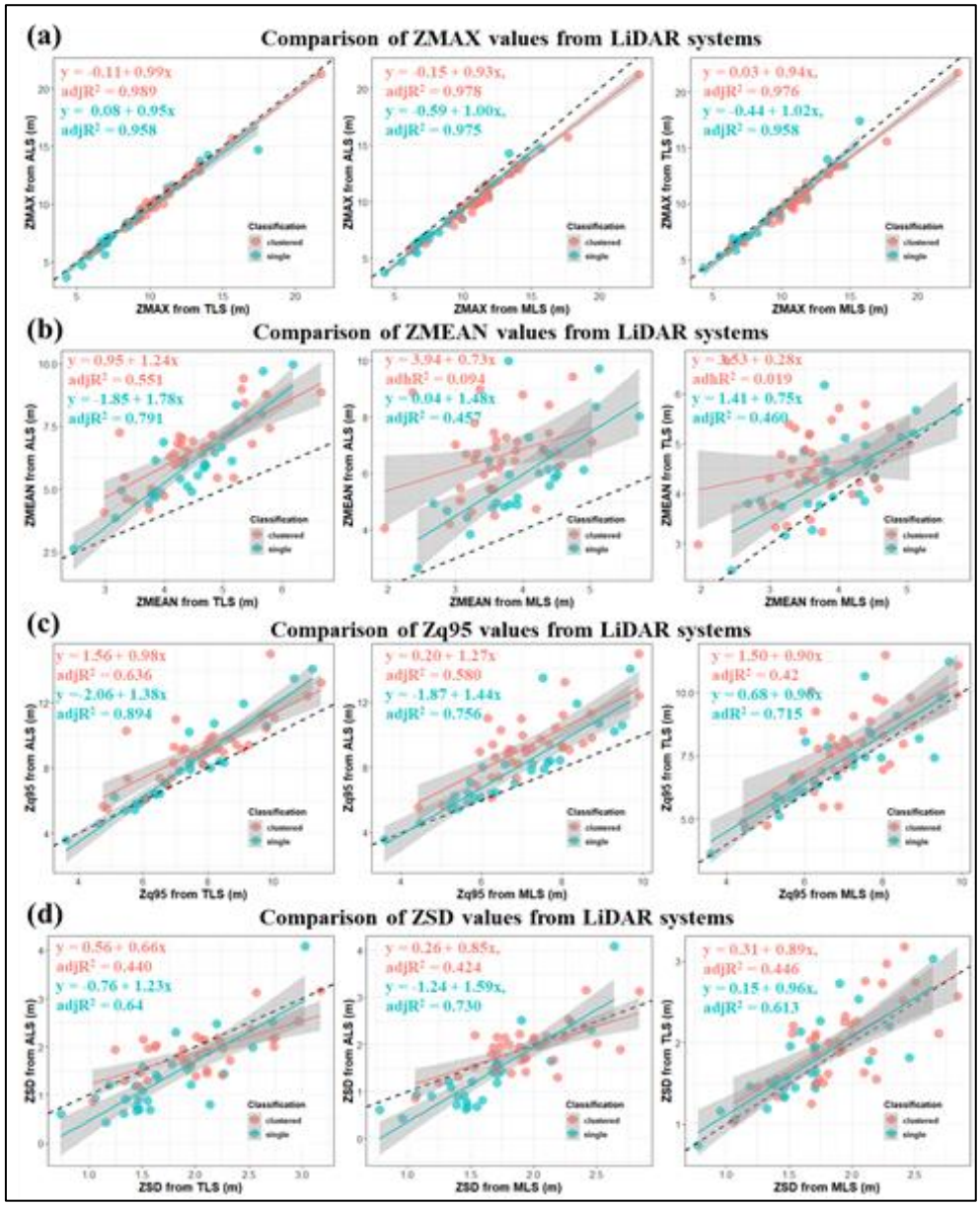

Figure 2.6 Comparison of height related metrics among the LiDAR systems (dashed line is the 1:1 line; grey band is the 95 % confidence interval)

3.2. Comparing CHM-derived canopy height metrics from each LiDAR systems

Table 2.5 Assessment and comparison of the tree-structure indices determined using the LiDAR systems

Metrics	Max CHM					Mean CHM					Std. of CHM				
Evaluation	RMSE (m)	RMSE (%)	Bias (m)	Bias (%)	r	RMSE (m)	RMSE (%)	Bias (m)	Bias (%)	r	RMSE (m)	RMSE (%)	Bias (m)	Bias (%)	r
ALS VS. TLS*	0.43	4.45	-0.27	-2.81	0.990	0.27	3.87	-0.14	-2.11	0.986	0.20	13.21	-0.01	-0.48	0.953
ALS VS. MLS*	0.44	4.52	-0.78	-8.11	0.989	0.36	5.19	-0.65	-9.45	0.975	0.25	16.67	-0.02	-1.21	0.923
TLS VS. MLS**	0.52	5.27	-0.51	-5.16	0.985	0.39	5.54	-0.51	-7.19	0.967	0.20	13.38	-0.01	-0.73	0.945

*Biases were calculated by subtracting the TLS and MLS values from the ALS values.
**Biases were calculated by subtracting the MLS values from the TLS values.

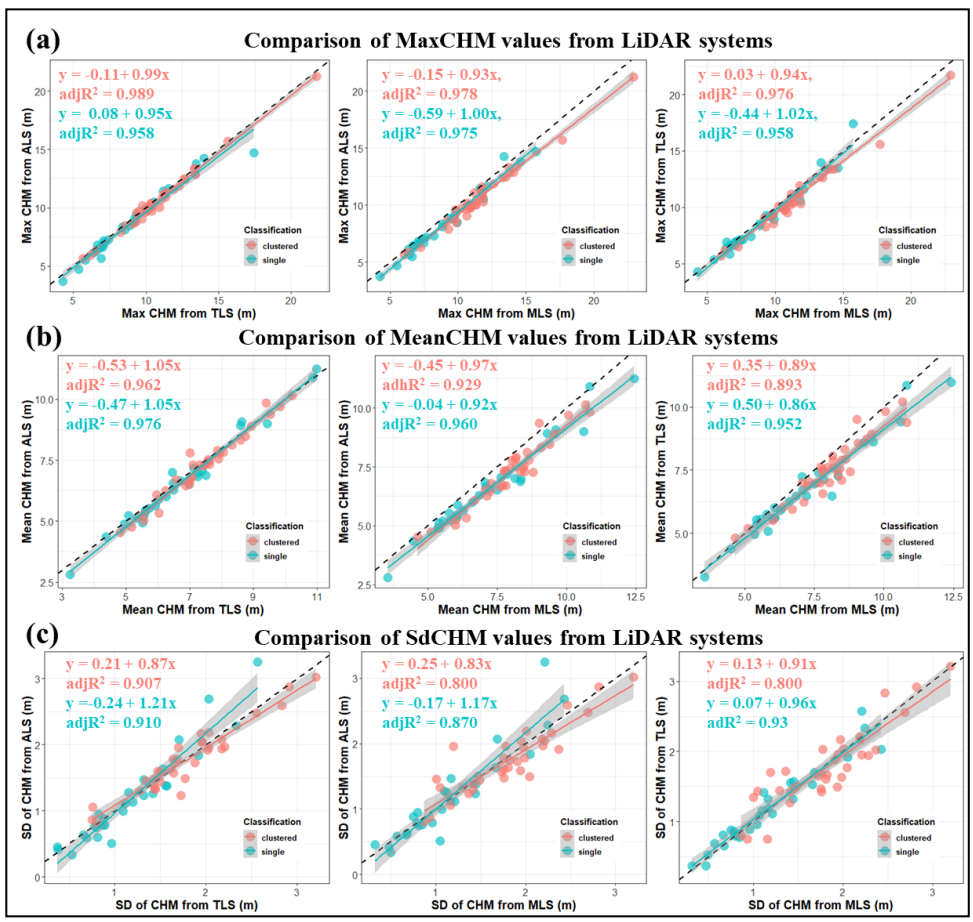

Figure 2.7 Comparison of the CHM-derived heights metrics among the LiDAR systems (dashed line is the 1:1 line; grey band is the 95 % confidence interval)

Table 2.5 and Figure 2.7 show comparisons of CHM-derived height metrics among

the LiDAR platforms. The maxCHM describes the same results as the ZMAX in the evaluations and the scatter plots. A comparison of the meanCHM results showed low RMSEs and biases (≤ 0.39 m and ≤ 0.65 m, respectively) compared to those of the maxCHM. ALS also produced lower meanCHM values than the other two LiDAR systems. The ALS and TLS datasets, which were acquired on almost the same dates, had higher agreements between the maxCHM and meanCHM values among all the pairs. The Std. of CHM showed overall agreement in the pairs (RMSEs (%) were slightly higher than the other evaluations, but the biases (%) were lower than others). Because the mean CHM and Std. of CHM were calculated based on the surface heights of the canopies, the values showed greater agreement than did those of the ZMEAN and the ZSD (as the CHM showed only the height of the surfaces).

Likewise, in comparing single and clustered trees, the R square values of the single trees were higher than those of the clustered trees except for the MaxCHM (see R^2 in Figure 2.7).

3.3. Comparing the area and the Rumple index determined using the LiDAR systems

Table 2.6 Assessment and comparison of the tree-structure indices determined using the LiDAR systems

Metrics	Area						Rumple index					Plant area index			
Evaluation	**RMSE (m^2)**	**RMSE (%)**	**Bias (m^2)**	**Bias (%)**	**r**	**RMSE (m^2/m^2)**	**RMSE (%)**	**Bias (m^2/m^2)**	**Bias (%)**	**r**	**RMSE (m^2/m^2)**	**RMSE (%)**	**Bias (m^2/m^2)**	**Bias (%)**	**r**
ALS VS. TLS*	8.19	5.89	-8.74	-6.29	0.998	0.15	9.26	-0.02	-1.50	0.892	0.766	24.63	0.69	22.27	0.600
ALS VS. MLS*	15.81	11.38	-16.67	-12.00	0.993	0.17	10.87	0.04	2.70	0.848	0.848	27.27	0.63	20.16	0.463
TLS VS. MLS**	15.00	10.80	-7.93	-5.37	0.995	0.22	13.45	0.07	4.13	0.764	0.290	12.00	-0.07	-2.72	0.877

*Biases were calculated by subtracting the TLS and MLS values from the ALS values.
**Biases were calculated by subtracting the MLS values from the TLS values.

Table 2.6 and Figure 2.8 compare areas, Rumple Index, and plant area index values among the pairs.

The rumple index values showed relatively low agreement among the LiDAR systems (Table 2.6 and Figure 2.8). The ALS-TLS pair showed the highest consistency (RMSE (%) = 9.26 and bias (%) = –1.50), while the TLS-MLS pair had lower values.

The area data were relatively consistent among the LiDAR systems. Table 2.6 and Figure 2.8 describes the higher area values in the MLS than ALS and TLS; biases in Table 2.6 and dots on the plots in Figure 2.8 show that the highest area values were

in the MLS dataset. Moreover, the ALS-TLS pair showed nearly a 1:1 relation in the area comparison (Figure 2.8).

By comparing single and clustered trees, the rumple index for the single trees showed a greater R^2 value than that for clustered trees among the LiDAR datasets. (Figure 2.8). The ALS-TLS and ALS-MLS pairs derived higher R^2 values in area comparisons for clustered trees than single trees. In the case of the TLS-MLS, the R^2 of the area comparison for clustered trees showed a lower value than that for single trees.

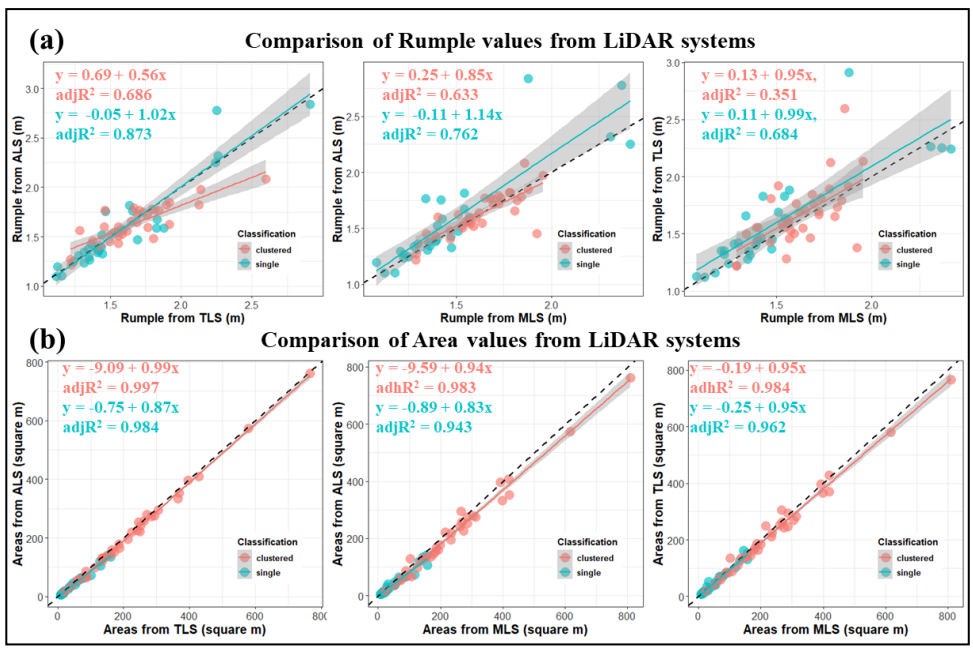

Figure 2.8 Comparison of areas and Rumple Index values among the LiDAR systems (dashed line is the 1:1 line; grey band is the 95 % confidence interval)

Low densities and point clouds were excluded to calculate the PAI; 25 clustered trees and five single trees were used to derive the PAI. Table 2.6 and Figure 2.9 compare the PAI values among the pairs. All pairs showed low linear relations with each other (Pearson's r > 0.4). In particular, the TLS-MLS pair showed a greater consistency (i.e., low RMSE and bias and high Pearson's coefficient r) rather than other two pairs.

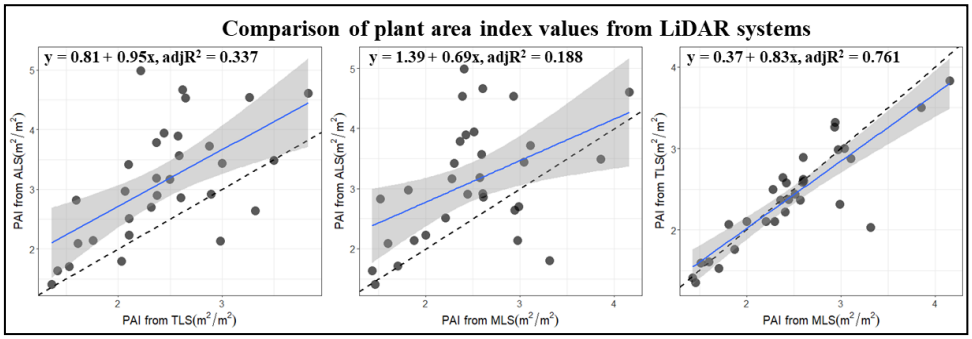

Figure 2.9 Comparison of plant area index values among the LiDAR systems (dashed line is the 1:1 line; grey band is the 95 % confidence interval)

4. Discussion

4.1 LiDAR configurations and data acquisition time intervals

In this study, I investigated ten tree structure metrics (Table 2.3). Most of the metrics derived from each LiDAR system showed linear relationships (values of Pearson's correlation coefficient r was higher than 0.4, and most were strongly correlated, except for the ZMEAN, Rumple Index, and PAI) (Table 2.4, Table 2.5, and Table 2.6).

Consistencies oft height metrics

The ZMAX, maxCHM, and meanCHM, which informed the tree-height values, showed substantial similarity among the LiDAR systems (Table 2.4 and Table 2.5). Although these metrics were highly consistent, differences remained for the bias values. My TLS and MLS data estimated the canopy heights to be higher than estimates by the ALS data at the study sites (Table 2.4 and Table 2.5); the biases in the height comparisons in the ALS-TLS and ALS-MLS pairs showed negative values, although the TLS and MLS data generally tended to underestimate the canopy height compared to ALS data (Hilker et al. 2012; Wang et al. 2019). Since my research sites consisted of small urban parks, with relatively short trees and a sparse canopy density, it was not difficult to set the TLS and MLS locations, which enabled the tops of the canopies to be detected more easily than would be the case in dense forest. Moreover, due to the sparse point density (< 8 points/m^2) provided by ALS, I speculate that ALS missed some tree apices (Zhao et al. 2018), resulting in lower height values (e.g., ZMAX and Max CHM) compared to TLS and MLS (see biases in Table 2.4 and Table 2.5). Therefore, I inferred that the ALS data used in this study missed maximum canopy height detection (Song et al. 2016; Zhao et al. 2018).

Furthermore, since the MLS data were acquired three years after acquiring the ALS and TLS data, ZMAX, maxCHM, and meanCHM metrics derived from the

MLS data, which indicated higher values than those derived by other LiDAR systems (Table 2.4 and Table 2.5), would reflect vertical tree growth in urban parks (e.g., Choi et al. 2019; Song et al. 2016).

More considerable differences in the ZMEAN and Zq95 values may have resulted from the specifications of each LiDAR system (Table 2.1). Because ALS observed its targets from above, the points were concentrated in the higher canopies (skewed towards the top, Figure 2.10) (Hilker et al. 2012). In contrast, the TLS- and MLS-acquired points were concentrated lower in the canopies (skewed towards the bottom, Figure 2.10) (Hilker et al. 2012). These differences in height point densities could have resulted in the large discrepancies observed in the ZMEAN and Zq95 values. Figure 2.11 appropriately represents the distribution of point clouds and their height metrics. Since the ALS dataset was concentrated on the upper canopies, the height metrics were greater than those of TLS and MLS. (Figure 2.8a, Figure 2.8b and Figure 2.8c).

Although there were discrepancies in ZMAX, maxCHM, and meanCHM, I considered the differences sufficiently small (less than 1 m) to allow their use as standard height metrics among the LiDAR systems.

Consistencies oft tree structural metrics

The ZSD, Std. of CHM, area, Rumple Index, and PAI describe the structural diversity of canopies. The Rumple Index, in particular, indicates the vertical diversity of a canopy (Kane et al. 2011; Parker et al. 2004). A comparison of the Rumple Index results derived from each LiDAR system showed relatively low agreement (RMSE (%) = 9.26–13.45 % and bias (%) = –1.50–4.13 %). However, the ALS-MLS and TLS-MLS showed lower consistency than the ALS-TLS pair. Since the Rumple Index was calculated by dividing the areas derived from the CHM surface areas, the 3D surfaces, area, height diversity, ZSD and Std. of CHM could have influenced the results. In particular, the greater area values derived from the MLS than those from the ALS and TLS might have lowered the rumple index values derived from the MLS than those from the ALS and TLS. Moreover, park management efforts, such as pruning, may have affected the decrease in the rumple index in urban parks (e.g., Choi et al. (2019) found that the rumple index value decreases in artificial openings).

Since the MLS data was acquired three years after acquiring the ALS and TLS data, the lateral growth of the trees might have affected the greater biases in the area values of the ALS-MLS and TLS-MLS comparisons. (Choi et al. 2019; Song et al. 2016). Moreover, MLS was able to survey entire targets, and this reduced occlusion effects due to the adoption of the SLAM system. The use of SLAM enabled MLS to obtain an almost complete view of the targets, while TLS missed some points due to issues with sensing locations and shadow effects. Therefore, with the time interval,

the high density of the MLS and an advantage avoiding occlusion effect may affect the greater area values in the MLS.

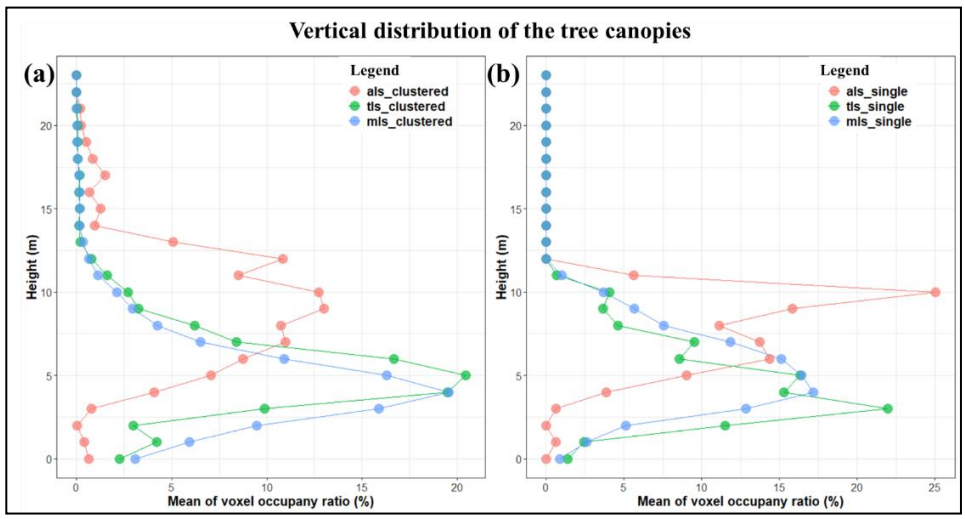

Figure 2.10 Vertical distribution of the clustered trees (a) and single trees (b) by the three LiDAR platforms (The voxel size was 1 m × 1m × 1m, and the dots on the lines indicate the mean values of occupied number of voxels at every 1 m–height)

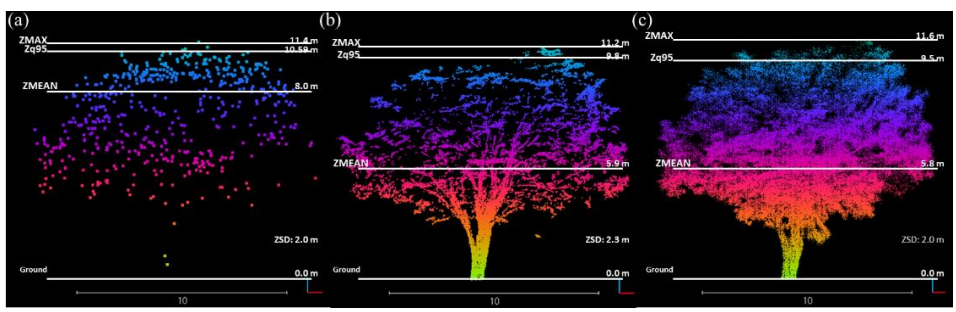

Figure 2.11 Distribution of point cloud from airborne lasers scanning (a), terrestrial laser scanning (b), and mobile laser scanning (c) (White lines indicate height information

In this study, I limited the setting of the parameters to derive the PAI (Table 2.3). The PAI comparison of the TLS-MLS pair showed relatively good consistency. However, the ALS-MLS and ALS-TLS pairs showed low consistencies (Table 2.6). This could have resulted from the wrong grain size, constant K, height threshold, and pulse density used in this study (Almeida et al. 2019; Wang and Fang 2020). In particular, as shown in Figure 2.10 and Figure 2.11, the point density of each LiDAR system was different. I inferred that these differences in point densities among the LiDAR systems resulted in poor agreements in PAI comparisons of ALS-TLS and ALS-MLS pairs. Furthermore, to accurately estimate LAI using LiDAR systems, various factors, such as optimal voxel size, occlusion effect, clumping effect, and others, should be considered with field survey data for calibration (Almeida et al. 2019; Wang and Fang 2020).

4.2. Uncertainty of the structural indices derived from the three LiDAR systems

4.2.1 Evaluation of the degree of differences between the references and observations for the tree classes

Table 2.7 Size comparison of the biases (mean differences between the references and the observations)

Pairs	Tree classification	Biases of ZMAX (m)	Biases of ZMEAN (m)	Biases of Zq95 (m)	Biases of ZSD (m)	Biases of max CHM (m)	Biases of mean CHM (m)	Biases of Std. of CHM (m)	Biases of Rumple index (m^2/m^2)	Biases of Area (m^2/m^2)
ALS VS. TLS*	Single tree	-0.31	1.57	0.69	-0.37	-0.31	-0.14	-0.01	-0.00	-7.30
	Clustered tree	-0.24	2.06	1.37	-0.13	-0.24	-0.15	-0.02	-0.04	-9.90
ALS VS. MLS*	Single tree	-0.60	1.97	1.08	-0.28	-0.60	-0.63	-0.03	0.09	-10.26
	Clustered tree	-0.92	2.97	2.17	0.03	-0.92	-0.68	-0.06	0.00	-21.81
TLS VS. MLS**	Single tree	-0.30	0.40	0.40	0.08	-0.30	-0.49	0.02	0.01	-2.95
	Clustered tree	-0.68	0.91	0.80	0.10	-0.68	-0.53	0.04	0.04	-11.91

* Biases were calculated by subtracting the TLS and the MLS values from the ALS values.
** Biases were calculated by subtracting the MLS values from the TLS values.
Light grey indicates significant differences between tree classification derived from the LiDAR systems ($p < 0.05$).

I assumed that biases (differences between the references: the ALS and the observations: the TLS and the MLS) would be distinct for the different tree classes because of occlusion effect and different point cloud distributions. The t-tests of the mean distances between clustered and single trees were conducted (i.e., testing the mean values of the differences between the references and the observations for single and clustered trees) (Table 2.7).

As shown in Table 2.4 and Figure 2.6, the ZMAX and the area showed great consistencies among the LiDAR systems. However, the biases in the ZMAX and area were not significantly different in the ALS-TLS pair, while the ZMAX and area biases by tree class showed significant differences in the ALS-MLS and TLS-MLS pairs ($p < 0.05$). In the ALS-MLS and TLS-MLS pairs, clustered trees showed greater mean distances (0.92 m and 0.68 m, respectively) than single trees (0.60 m and 0.30 m, respectively) in ZMAX comparisons. Moreover, in the ALS-MLS and TLS-MLS pairs, clustered trees showed greater mean distances (-21.81 m^2 and -11.91 m^2, respectively) than single trees (-10.26 m^2 and -2.95 m^2, respectively) in area comparisons. I think it is likely that additional unknown reasons, such as soil conditions, tree species composition, and stand complexity, may have impacted tree growth and contributed to the higher ZMAX and area estimates in clustered trees as

derived by MLS. Oldfield et al. (Oldfield et al. 2015) found that stand complexity and the existence of the shrubs in stands could enhance tree growth. This study showed more complex structures in the case of clustered trees (rumple index values = 1.63 ± 0.18 m^2/m^2) than single trees (1.57 ± 0.46 m^2/m^2), and clustered trees included shrubs (Figure 2.5). Therefore, I infer that the differences in biases between clustered and single trees might have resulted from the stand complexity and other environmental factors.

ZMEAN and Zq95 values showed significant bias differences for the ALS-TLS and ALS-MLS pairs (Table 2.7). These metrics showed that point densities for heights were skewed as a result of the sensor locations (Figure 2.10). Clustered trees had more data acquisition points at the low heights than did single trees, so both TLS and MLS collected more data for lower heights. This tendency resulted in lower ZMEAN and Zq95 values, especially for clustered trees when the data were derived from TLS and MLS rather than from ALS (Table 2.7). In this study, ZMEAN and Zq95 values showed no significant differences by tree class between TLS and MLS.

In terms of the CHM-related metrics, maxCHM produced exactly the same results as ZMAX, and I assume that differences in the biases were for the same reasons as identified for ZMAX (i.e., tree growth rates might be different depending on soil conditions, stand complexity, and the existence of shrubs). The meanCHM and Std. of CHM showed no significant differences for all the pairs. CHMs (1-m resolution) derived from the LiDAR platforms could be used interactively.

Bias of the rumple index and Std. of CHM by the tree class did not differ significantly in all pairs ($p > 0.05$).

4.2.2 Evaluating the degree of the biases by the tree height, area, and complexity

Metrics	Comparisons	ZMAX and Max CHM (ALS)	Mean CHM (ALS)	Area (ALS)	Rumple (ALS)
ZMAX and Max CHM	ALS- TLS	0.01	-0.03	-0.01	-0.21
	ALS-MLS	-0.23	-0.05	-0.29	-0.29
	TLS-MLS	-0.20	-0.02	-0.24	-0.08
ZMEAN	ALS- TLS	0.77	0.84	0.31	0.44
	ALS-MLS	0.75	0.86	0.38	0.38
	TLS-MLS	0.33	0.42	0.26	0.10
ZSD	ALS- TLS	0.41	0.25	0.25	0.59
	ALS-MLS	0.56	0.45	0.21	0.64
	TLS-MLS	0.17	0.25	-0.05	0.04
Zq95	ALS- TLS	0.71	0.61	0.32	0.45
	ALS-MLS	0.83	0.78	0.35	0.46
	TLS-MLS	0.34	0.38	0.12	0.12
Mean CHM	ALS- TLS	0.28	0.41	0.05	0.23
	ALS-MLS	-0.15	-0.06	-0.07	-0.45
	TLS-MLS	-0.30	-0.31	-0.08	-0.52
Std. of CHM	ALS- TLS	0.08	0.19	0.00	0.42
	ALS-MLS	0.18	0.31	-0.15	0.34
	TLS-MLS	0.15	0.20	-0.18	0.02
Area	ALS- TLS	-0.43	-0.40	-0.17	-0.32
	ALS-MLS	-0.42	-0.32	-0.41	-0.25
	TLS-MLS	-0.24	-0.15	-0.36	-0.12
Rumple	ALS- TLS	-0.20	-0.22	-0.11	0.16
	ALS-MLS	0.16	0.25	-0.15	0.56
	TLS-MLS	0.27	0.36	-0.03	0.33

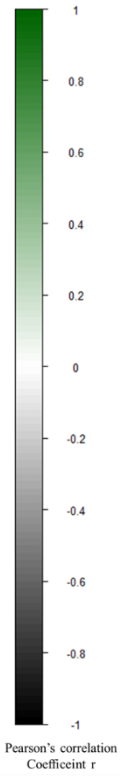

Figure 2.12 Correlation matrix plot between ALS-derived metrics and the biases (color represents only the significant correlations; $p < 0.05$, and differences were calculated by subtracting the observations from the references.)

The biases of the metrics among the sensors were highly correlated with the canopy complexity and tree or canopy heights (Figure 2.12). I infer that bias increased when the trees were tall and the canopy structures were complex (Figure 2.12) because of occlusions effects of the TLS and the MLS, and sparse point density of the ALS. Moreover, more complicated canopy structures imply the difficulties in sensing the tree structures using the LiDAR scanner (Wang et al. 2019).

The biases in the ZMEAN and Zq95 values showed clear linear relationships with tree structures (Figure 2.12). Moreover, a comparison of LiDAR systems revealed significant differences in the biases of the ZMEAN and Zq95 for different tree classes (Table 2.7), highlighting inconsistencies in the application of different LiDAR systems as a standard set of metrics.

Chapter 3. Urban forest growth and gap dynamics detected by yearly repeated airborne LiDAR

1. Introduction

Quantifying forest gaps is essential for monitoring the stability of the forest structure because these disturbances can change the light environment and drive forest dynamics (Asner 2013; Fisher et al. 2008; Kane et al. 2011; Whitmore 1989). Physical disturbances in forest canopies usually result from deforestation (e.g., making space for agricultural fields) and tree-fall events (Asner 2013). Forest gaps could be characterized by their size distribution. The areas of forest gaps in natural forests follow the power-law distribution with the frequencies. Usually, small openings (formed by wind damaged or tree mortality) in natural forests dominate areas in the size distribution and show larger scaling exponents, while frequent large openings show smaller scaling exponents. Therefore, by comparing the scaling exponents with other forests, it is possible to compare the degrees of disturbances (Kane et al. 2011; Whitmore 1989).

Urban forests are usually fragile to disturbances because the dense human population leads to severe conditions that can damage the forest directly (e.g., land-cover changes from forested to urbanized areas) (Steenberg et al. 2016). Forest damage such as deforestation and landcover changes could result in relatively larger openings than small openings in forests and the human activities in there may hinder the forest equilibrium or change the forest ecosystems (Vepakomma et al. 2018). Particularly in South Korea, small and large mountainous urban forests are very common as they remain green areas after development and many people use them for leisure activities, agriculture, and private graveyards that are accompanied with canopy openings (Kim et al. 2013; Kim and Pauleit 2009; Lee et al. 2009; Lee and Kim 2010; Ryu et al. 2017; Youn 2009). Although many policies try to conserve these urban forests in South Korea, land use in urban forests is complexed and can easily undergo harsh disturbances (Koo et al. 2013; Park and Lee 2014; Ryu et al. 2017). Therefore, it is important to monitor forest gaps in urban forests where various natural or anthropogenic disturbances can occur.

Forest surveys are conducted in many countries via onsite sampling of plots that are considered representative of the whole study site. In addition, airborne photogrammetry and satellite imagery are applied to measure the diameter at breast height, stand height, basal area, and species composition using terrestrial field sampling data. However, these traditional methods have certain limitations related to the subjective interpretation of measurement results, low measurement accuracy, and lack of information about vertical canopy structures (Latifi et al. 2016;

Magnussen et al. 2012; Naesset 1997; Sasaki et al. 2013; Thompson et al. 2007; White et al. 2015; Whitehurst et al. 2013). To compensate for the limitations of existing research methods, there is a need to improve techniques that can support the assessment of forest growth and biodiversity such as airborne Light Detection and Ranging [LiDAR] (Whitehurst et al. 2013).

Many studies have suggested that airborne laser scanning (ALS) can be applied to describe vertical forest structures and the accuracy of stand height estimations has been assessed (Magnussen et al. 2012; Naesset 1997). Although ALS-based tree height estimations are less accurate than those using rigorous field measurements (Andersen et al. 2006), the accuracy is acceptable and the more efficient coverage of large areas by ALS offsets this weakness (White et al. 2015). Especially, Vepakomma et al. (2018) reported that the difference between the effects of natural and anthropogenic linear openings (i.e., steam and roads) with LiDAR data. These days, with its acceptable accuracy and advantages in sensing vertical canopy structures, multi-temporal LiDAR survey has also shown great potential for detecting changes in forest structure (Eitel et al. 2016). For example, the use of adequate multi-temporal airborne LiDAR datasets represents a reliable and efficient method for detecting canopy changes and estimating canopy growth and forest biomass dynamics at a fine temporal resolution (Cao et al. 2016; Dalagnol et al. 2019; Dalponte et al. 2019; Hopkinson et al. 2008; Rangel Pinagé et al. 2019; Song et al. 2016; Vepakomma et al. 2012; Vepakomma et al. 2008; Vepakomma et al. 2011; Yu et al. 2008; Zhao et al. 2018). Recently, Song et al. (2016), Zhao et al. (2018), Dalponte et al. (2019) and Cao et al. (2016) successfully estimated forest biomass dynamics and tree growth in forests using repeated airborne LiDAR data. Moreover, Dalagnol et al. (2019) and Rangel Pinagé et al. (2019) reported quantifying canopy dynamics focusing on human-induced disturbances (e.g., logging) by using multi-temporal airborne LiDAR data in Amazon forests. Rangel Pinagé et al. (2019) reported that setting a height differences threshold was an efficient way to map logged trees and small gaps usually closed within short periods (within two years). Dalagnol et al. (2019) found that gap formation occurred more frequently in logged areas than in intact forests.

For applications of multi-temporal ALS in urban forests, a few studies about the forest dynamics (e.g., forest growth and forest gap dynamics) in an urban forest have been conducted. Ossola and Hopton (2018a) measured urban tree loss dynamics in cities' residential landscapes using bi-temporal (five-year period) LiDAR datasets. They particularly noted the changes in urban trees over time caused by human management and urban tree removal for hazard prevention or artistic preference. Since the urban forests are characteristically vulnerable to various and frequent disturbances, particularly in terms of physical damage (Bolund and Hunhammar 1999; Fisher et al. 2008; Lai and Leone 2017; Liu et al. 2015; McWilliam et al. 2010;

Ossola and Hopton 2018b), canopy loss occurs frequently that could finally result in artificial canopy openings. However, to the best of my knowledge, most studies with airborne LiDAR datasets have focused on the forest gaps which are usually treefall gaps in the natural forests (Vepakomma et al. 2012; Vepakomma et al. 2008; Vepakomma et al. 2011) and few studies are related to artificial canopy openings in cities. In the same manner of the effect on the surrounding environment of forest gaps, artificial openings could affect the adjacent environment (Dalagnol et al. 2019; Li et al. 2018) and may also affect the changes in surrounding canopy structures. Therefore, it is important to monitor urban forests continuously (Cumming et al. 2008) including both forest gaps and their artificial canopy openings.

Thus, I estimated the three-dimensional canopy changes in an urban forest using four years of annual LiDAR datasets. To assess how much urban forest structures have changed, I estimated 1) the distribution of the growth area and damaged areas (e.g., vertical and later growth and damaged areas), 2) changes in vertical leaf area density profile, and 3) the dynamics of opening and closing forest canopies during 2012–2015. Accordingly, this study addressed two questions: 1) What are the differences between the canopy structure changes derived from annual change detections and three-year interval change detection? 2) What are the characteristics of structural changes by the different canopy classes (e.g., high canopies and lower canopies) in urban forests?

2. Methods and Materials

2.1 Field survey

The study was conducted at Mt. Bongseo (36.82°N, 127.12°E, altitude: 158 m, area: 124 ha), a remnant patch after urban development located in the center of metropolitan Cheonan, Chungcheongnam-Do, Republic of Korea. The study site is covered with a mixed forest dominated by Quercus acutissima (percent area: 44.8%), Pinus rigida (29.7%), and Larix leptolepis (7.4%). The average age class (as designated by the Korea Forest Service, 2015, http://www.forest.go.kr/) of the forest is 3.8 (i.e., 30–40 years old; the third class). Both managed and unmanaged forest areas can be found within the study site. The forest is easily accessed by citizens and local amenities such as health facilities are present within the forest. Moreover, some of the land in the site is used as a cemetery and some have agricultural activity, which is private land (Figure 3.1).

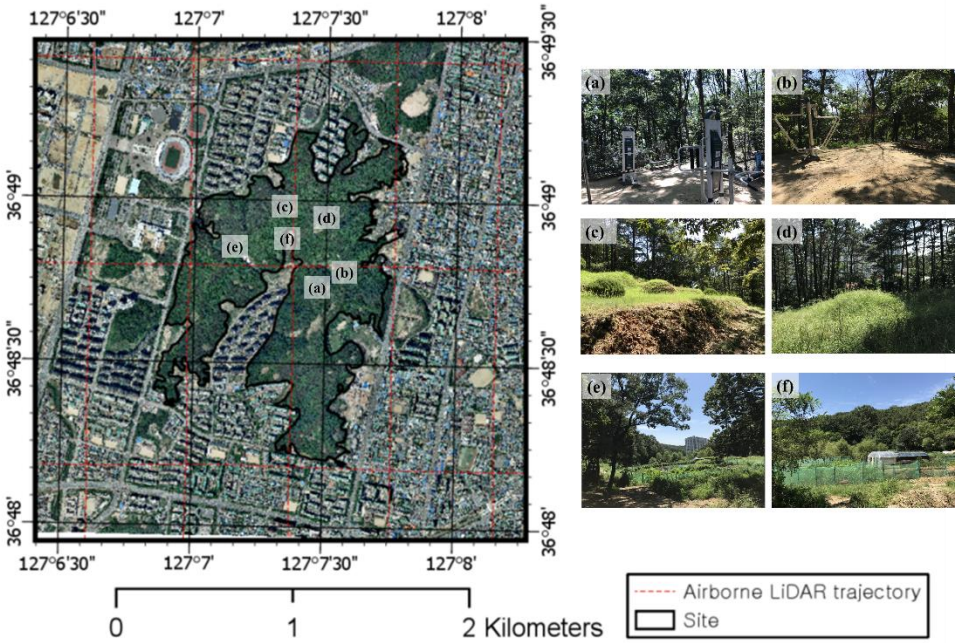

Figure 3.1 Study site (boundary line) and eight airborne LiDAR survey trajectories (red line), and artificial canopy openings or gaps ((a and b): sports facilities, (c and d): private graveyards, and (e and f): agricultural lands)

2.2. Canopy opening detection

To classify open canopy types (e.g., natural treefall or thinning, private graveyards, facilities, and agricultural activities), I conducted field trips on October 7, 2016, August 26, 2017, and September 26, 2017. Moreover, to determine how much canopy should be classified as open canopy, I conducted Simultaneous Localizing and Mapping (SLAM) mobile LiDAR (Stencil, Kaarta, PA, USA) scanning under the tree-fall area (Figure 3.2) at the site on March 26, 2018, when the trees were defoliated. I generated 0.25 × 0.25 m2 digital surface models using the maximum height (HMAX) of all mobile LiDAR datasets with CloudCompare software (https://www.danielgm.net/cc/), and generated CHMs by subtracting the digital terrain models from the digital surface models. Finally, I calculated the gap size in ArcGIS ver. 10.2.2 (ESRI, Redlands, CA, USA). The average area of the 19 open canopies in the nine sampled plots was calculated as 12.48 ± 9.76 m2 with consideration of the foliated season and previous research by Yamamoto (2000) and Runkle and Yetter (1987), who did not consider very small openings (<5 m^2) as gaps, and for the convenience of calculation, I classified gaps as locations where the open area was 10 m^2 or more (Figure 3.3).

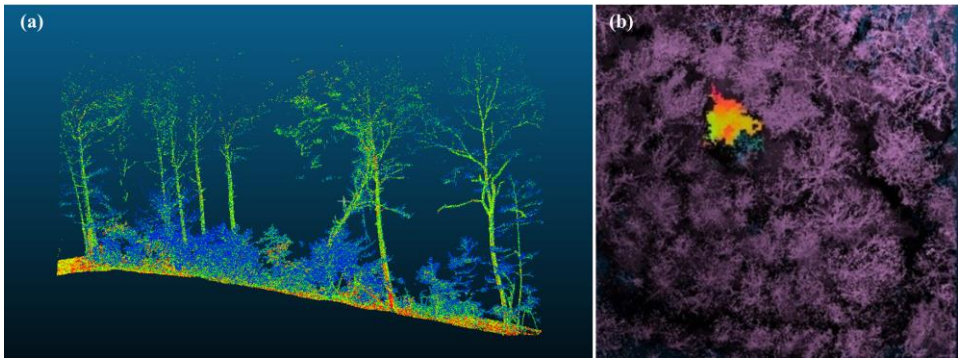

Figure 3.2 Examples of open canopy scanned with mobile LiDAR. (a) Section view of an open canopy formed by a fallen tree. (b) Plane view of an open canopy (highlighted area)

2.3. Airborne LiDAR dataset acquisition and registration

The airborne LiDAR datasets were acquired on October 9, 2012 (day of the year [DOY]: 283), May 16, 2013 (DOY: 136), June 16, 2014 (DOY: 167), and October 30, 2015 (DOY: 303) from IGI LiteMapper 6800 (Samah Aerial Survey) which are all in the foliated season. The LiDAR data were acquired in different months. However, Song and Ryu (2015) reported relatively stable seasonal LAI values in a forest (in the same climate zone as my study site) in South Korea, and my study site experiences for the days with the maximum number of leaves that turned red in the first and last study year were October 28, 2012 and October 26, 2015, respectively (Korea Meteorological Administration, www.kma.go.kr). Therefore, I assumed that my data were acquired in the full-leaved seasons.

The study site was surveyed following eight trajectories (Figure 3.1) by overlapping 50% of the trajectory edges at an altitude of 1,000 m, the beam divergence is 0.3 mrad and field of view is 60°. All annual point densities were higher than 8 points/m^2, which provided sufficiently dense and similar to effectively compare datasets. The airborne LiDAR datasets were preprocessed using algorithms built into the TerraScan (Terrasolid) software on the MicroStation (Bentley) platform. First, I filtered noise at low points and aerial points. Second, I used classification algorithms to classify the points into ground and non-ground classes. I minimized measurement errors by selecting 190 planar areas over the entire year in the digital surface model generated from the point cloud datasets for 2012, 2013, 2014, and 2015 and matched the heights with the average elevation for 2012. Finally, the height was adjusted based on the ground control points (triangulation point: 36°49′02.09″, 127°07′27.31″, ellipsoidal height: 182.17 m; unified control point: 36°48′50.29″, 127°06′55.92″, ellipsoidal height: 906,045 m; National Geographic Information Institute) and points on the roof of a building detected for all years. I selected 70 new random 16 m^2 plots, including building rooftops and roads where the heights were

consistently adjacent to the site, to compare the 2012–2014 airborne LiDAR datasets with the 2015 airborne LiDAR dataset. The average differences from the 2015 dataset were –0.01 m (2012), –0.04 m (2013), and –0.05 m (2014). Although the validation results showed that the heights in 2015 were slightly greater than those in the other years, I concluded that accuracy anomalies in the dataset of within 0.1 m were acceptable.

2.4. Generation of height models and change detection

Since the research site is mountainous and sloped areas may distort the vertical and horizontal locations of the tree canopy and apex (Alexander et al. 2018; Khosravipour et al. 2015), I did not consider segmenting the tree apices. Therefore, I simply calculated the vertical differences in CHMs for 2012–2015 that were generated from the LiDAR datasets and estimated the changes in the canopy throughout the study period. Since quantifying the changes of canopy opening areas and identifying the growth direction (i.e., vertical or lateral direction) both require high-resolution CHMs (e.g., Vepakomma et al. 2012; Vepakomma et al. 2011; Yu et al. 2008) and the beam divergence of the LiDAR sensor is 0.3 mrad, which is a 0.3 m footprint at the ground level (flight altitude: 1,000 m), I assumed that 0.25 × 0.25 m2 grid resolution would be adequate. After preprocessing the LiDAR datasets into 0.25 × 0.25 m^2 (grid level survey) digital surface models and digital terrain models, CHMs were generated using the TerraScan software Figure 3.4 a). The annual average canopy heights for 2012–2015 were 11.09 m, 11.02 m, 12.29 m, and 12.12 m, respectively. The CHMs for each year were classified into two classes: high canopy [HC], with canopy height >5 m and low canopy [LC], with canopy height ≤5 m (Figure 3.3). In addition, I included the subclass canopy closure (CaC), which represents areas with LCs in earlier years that became HCs in later years. Based on the estimated growth rates outlined by Song et al. (2016), I assumed that the average annual growth rate of mature trees could not exceed 50 cm/year. Therefore, after calculating the changes between the two years, I classified the growth regions into four subclasses: vertical growth (VGr) areas with annual mean growth rate ≤50 cm; LGr areas with annual mean growth rate >50 cm; damaged areas with negative growth rates, and no-change areas with –10–+10 cm growth rates.

Since grid size can affect the accuracy of HMAX estimates (Roussel et al. 2017), and canopy metrics based on vertical profiles can be used to accurately estimate forest structure (Hopkinson et al. 2008; Zhang et al. 2017), I generated a larger size of grids for the plot level survey using hexagonal grids with an area of 16.24 m^2 and edge length of 2.5 m (approximately the mean size of a closed gap area during the study periods) to estimate the changes in vertical profiles, leaf area density (LAD), and canopy complexity.

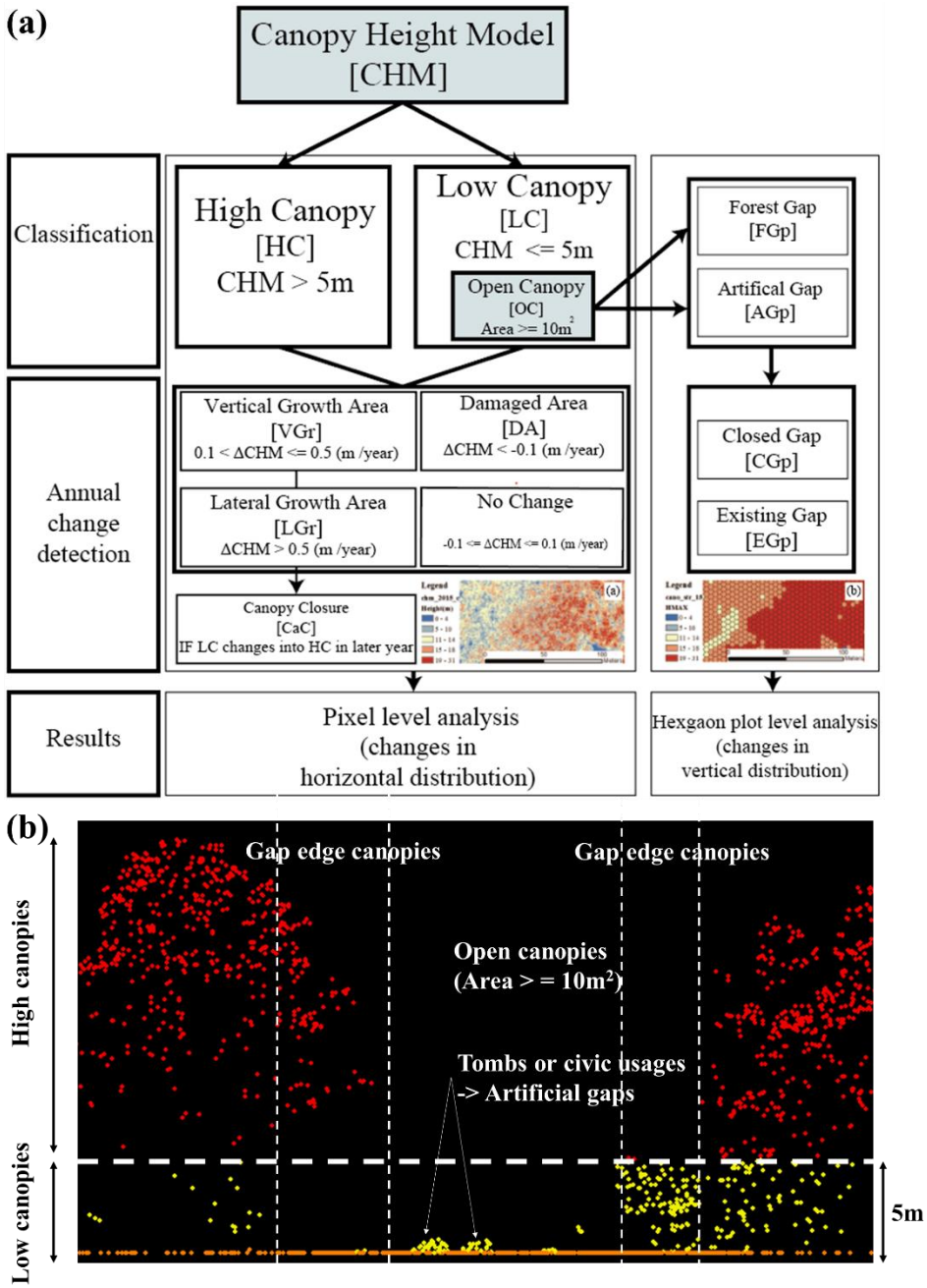

Figure 3.3 Analysis framework for the classification of urban open canopies in this study and a section of a normalized LiDAR dataset at an artificial gap (Figure 3.1c)

2.5. Gap detection and classification

I set the thresholds of height and area for detecting open canopies as 5 m (which was almost half of the CHMs) and 10 m^2 (based on the gap area calculation from mobile LiDAR datasets and for convenience of calculation), respectively, and identified the OCs in each CHM. I defined gaps with canopy openings caused by fallen or dead trees as forest gaps (FGp) and those caused by civic usage as farmland, cemeteries, or trails as artificial gaps (AGp) (Figure 3.1).

To investigate the size distribution of FGp and AGp, I estimated the scaling exponent (λ) that describes the extent to which disturbances are clustered (i.e., lower λ means frequent large disturbances while higher λ means frequent small disturbances) (Asner et al. 2013; Kellner and Asner 2009; Vaughn et al. 2015) using methods from Asner et al. (2013).

2.6. Estimating changes of vertical canopy distribution and canopy complexity

The leaf area index (LAI, m^2/m^2) and canopy complexity (Rumple index, m^2/m^2) are well known to correlate with the productivity of forest ecosystems (Bouvier et al. 2015; Jenness 2004; Parker et al. 2004); LAI is usually calculated as half the total leaf area per unit surface area (Ishii et al. 2004; Jonckheere et al. 2004). I estimated the LAI and leaf area density (LAD, m^2/m^3) using the "lidR" package in R software according to the method of Bouvier et al. (2015), who calculated the LAI based on the Beer–Lambert theory. The LAD was estimated by dividing the LAI values by dz (the profile of LAD). The canopy complexity was also estimated using the Rumple index function within the "lidR" package. Canopy complexity was calculated as a three-dimensional surface area divided by a two-dimensional surface area, which denotes the structural diversity of canopies (Jenness 2004; Parker et al. 2004; Sasaki et al. 2008). Session 2.6 is summarized in Table 3.1 Examples of the canopy height model and hexagon height model and Figure 3.4 .

Table 3.1 Examples of the canopy height model and hexagon height model

	0.25× 0.25 m^2 pixel-level height model	**2.5m hexagon (16.24 m^2) plot-level height model**
Result	Distribution of vertical growth area Distribution of lateral growth area Distribution of damaged area	Leaf area density & leaf area index (Bouvier et al. 2015) Canopy complexity (Parker et al. 2004) Percentile height differences

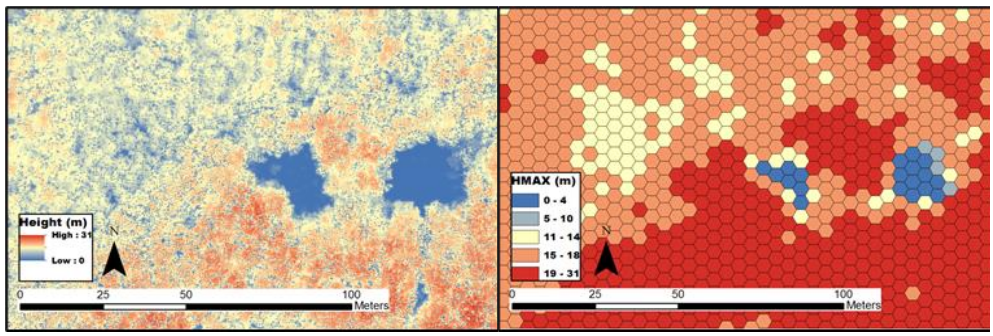

(a) (b)

Figure 3.4 Example of raster grids (height model) (a: 2015 canopy height model, 0.25 × 0.25 m^2 resolution) and hexagon grids (height model) (b: 2015 normalized point cloud, 2.5 m edge length)

3. Results

3.1. Pixel and hexagon height model-based change detection

With change detection, I found that changes in the distribution of canopies were irregular year by year (Figure 3.5), while the annual VGr rates remained relatively stable throughout the study period. There were no great growth rate differences according to either the time interval or the grid size (Table 3.2). Figure 3.5a presents an example of the overall distributions of growth and damaged areas in 2012–2015. Figure 3.5b and c show the vertical changes over two years (i.e., one-year term) to explain the growth and damaged area distributions. Detected growth areas where the canopy height increased usually resulted from lateral growth rather than vertical growth in HCs, which could mean that taller canopy overlapping occurred frequently. In the case of low canopies, lateral growth areas were pervasive in annual change detection, while vertical growth areas were sustained over total periods. Because LC areas included bare lands, the height remained relatively unchanged.

Furthermore, canopy closure (LC to HC) tended to be driven by LGr rather than VGr, possibly because the rate of LGr among taller trees was higher than that of VGr among young trees at the study site (Figure 3.5d). Besides, I found that disturbance and canopy loss were widespread over the whole study period (Figure 3.5b, c).

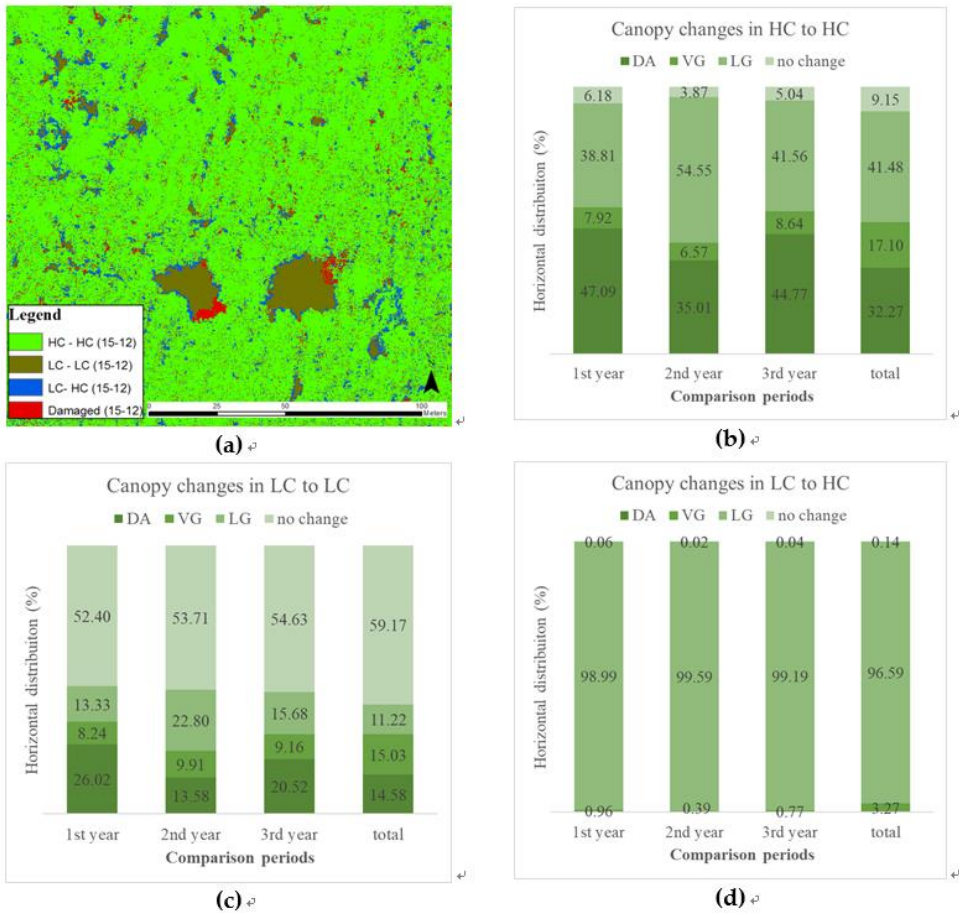

Figure 3.5 Results from pixel-based analysis. (a) Distribution of High Canopy [HC], Low Canopy [LC], Canopy Closure [from LC to HC, CaC], and damaged areas (2012–2015); (b) Distribution of growth and damaged areas in HCs; (c) Distribution of growth and damage areas in LCs; (d) Distribution of growth areas in CaC; first year: 2012–2013, second year: 2013–2014, and third year: 2014–2015; DA: Damaged area, VG: Vertical growth area, LG: Lateral growth area

Table 3.2 Annual mean vertical growth rate (unit: m/year) (First year: 2012–2013, second year: 2013–2014, and third year: 2014–2015; DA: Damaged area, VG: Vertical growth area, LG: Lateral growth area)

Canopy class	Periods (terms)	HMAX (pixel)	HMAX (plot)	H95TH (plot)	HMEAN (plot)
HC to HC	First year (218 days)	0.29	0.25	0.25	0.29
	Second year (396 days)	0.30	0.30	0.29	0.32
	Third year (401 days)	0.29	0.29	0.29	0.30
	Total years (1,015 days)	0.30	0.26	0.27	0.31
LC to LC	First year (218 days)	0.27	0.25	0.25	0.28
	Second year (396 days)	0.28	0.29	0.29	0.30
	Third year (401 days)	0.28	0.29	0.29	0.30

Canopy class	Periods (terms)	HMAX (pixel)	HMAX (plot)	H95TH (plot)	HMEAN (plot)
	Total year (1,015 days)	0.27	0.27	0.27	0.30

3.2. Continuous one-year vertical growth area

Due to widespread canopy loss and the complexity of the dynamics in both canopies (Figure 3.5), I tried to detect continuous growth areas. Table 3.3 shows the proportion of the area in which the canopy continuously grew upward at pixel (via CHMs) and plot (via hexagonal grids) levels. The proportion of overlapping growth areas with positive values (i.e., gradual vertical canopy growth) based on the height difference for 2012–2015 showed a 15.9% correspondence at the pixel scale and a 38.9% correspondence at the plot scale.

Table 3.3 Correspondence of 3-year interval growth grids and annual continuous growth grids (A: growth pixels for 2012-2015, B: continuous growth pixels for 2012-2015

Layers	Overall growth in the mid-term A: (CHM2015 - CHM2012) > 0.1 m	Consistent growth through short terms B: (CHM2013 - CHM2012) > 0.1m & (CHM2014- CHM2013) > 0.1m & (CHM2015- CHM2014) > 0.1m	Consistent growth area ratio (%) B/A * 100
H95TH -hexagon grids (No. of hexagons)	68,381	26,577	39
Hmax-pixel grids (No. of pixels)	10,754,351	1,706,387	16

3.3. Open canopy change detection

Table 3.4 Forest gap information (2012 ~ 2015)

Forest gap 2012-2015				
Year	2012	2013	2014	2015
No. of	925	792	542	601
λ (scaling exponent)	1.28	1.26	1.28	1.28
Mean (m^2)	36 ± 97	42 ± 107	37 ± 84	36 ± 70
Minimum (m^2)	10	10	10	10
Maximum (m^2)	2,251	2,212	1,294	906
Sum (m^2)	33,335	33,512	20,058	21,361

For 2012–2015, the total number of FGps and the sum of the area decreased (Table 3.4). However, the mean FGp area each year did not decrease over time; this might indicate that some forest gaps continued to open and some were closed during the study periods. Moreover, total FGp areas (Sum in Table 3.4) abruptly decreased between 2013 and 2014, which was also present in Figure 5c, as growth distributions increased. Finally, even though the scaling exponent λ in 2013 decreased slightly, λ showed consistent values over the years.

Table 3.5 Existing gaps and closed gaps in forest gaps

Forest gap (FGp)	**Gap continuation (existing gap, EGp)**				**Closed gap (CGp)**
Year	2012	2013	2014	2015	2012~2015
No. of	374	363	387	391	551
Mean (m^2)	65 ± 147	70 ± 153	46 ± 97	46 ± 85	16 ± 9
Minimum (m^2)	10	10	10	10	10
Maximum (m^2)	2,251	2,212	1,294	906	95
Sum (m^2)	24,276	25,237	17,852	17,907	9,059

*The difference in the number of existing gaps in each year might be due to gap coalescence (e.g., Vepakomma et al. 2011)

Forest gaps were classified into two subclasses according to whether they were closed in the study periods (e.g., Vepakomma et al. 2012); existing gap (EGp) and closed gap (CGp) (Table 3.5). The number of existing gaps (EGp) (i.e., FGp in the same location detected for all years) increased slightly from 374 to 391 due to gap coalescence (e.g., Vepakomma et al. 2012), while the mean area of EGp decreased by 19.11 m^2 (Table 3.5). Although the number of EGp patches increased slightly, the mean area and maximum area diminished because some gaps were divided into two or more gaps as a result of tree growth. Moreover, areas of 10.00–94.75 m^2 (mean: 16 ± 9 m^2) were closed for the whole study period (Table 3.5).

In the case of AGp, the mean area was increased by about 10 m2 while the number of patches decreased (Table 3.6). The decrement in the number of patches could result from the LGr of the edge trees (Table 3.5). The notable difference between the changes in forest gap and artificial openings is that artificial opening areas either maintained their position or expanded their area, while natural forest gaps showed more dynamics (i.e., faster canopy closure rates). Moreover, the scaling exponent λ showed lower values than that of forest gaps, which may indicate frequent larger openings in artificial gaps.

Table 3.6 Artificial gap area information (2012 ~2015)

Artificial gap 2012 -2015				
Year	2012	2013	2014	2015
No. of	607	531	540	548
Mean (m^2)	237 ± 750	280 ± 1025	226 ± 628	246 ± 671
λ (scaling exponent)	1.22	1.21	1.22	1.22
Minimum (m^2)	10	10	10	10
Maximum (m^2)	10,694	18,760	7,713	7,736
Sum (m^2)	143,817	148,666	122,241	134,935

3.4. Changes in vertical canopy structures in High Canopy and Open Canopy

The differences in changes to canopy structures by canopy class were more notable in the changes of vertical canopy distribution. In particular, FGp in OC showed both the largest LAI values each year and the largest differences in LAI (0.12 ± 0.62 m^2/m^2) during the study periods, followed by HC and AGp, which could indicate the positive effects of FGp on foliage (Figure 3.6). Furthermore, FGp also exhibited the greatest differences in canopy complexity for 2012–2015 (0.93 ± 4.15 m^2/m^2) followed by HC and AGp (there was no significant difference between HCs and AGp), which possibly indicated that FGp has an important role in increasing canopy structural diversity (Figure 3.6b).

Figure 3.7 shows the LAD of each year and differences in LAD for 2012–2015 (Figure 3.7 'class_dLAD') in FGp (subclassified as EGp and CGp), AGp, and HC at the study site. In the total study period (three-year interval), vertical foliage distribution decreased at a lower height and increased at a higher height for every canopy class. Particularly among high canopies, 12m-height divided the LAD increment and decrement, while 5–10 m heights divided them in the low canopies. Furthermore, in the FGp canopy, the increment in LAD was greater than those in other canopy classes while the differences in LAD among heights in the AGp did not show clear differences. However, looking at the annual changes in Figure 3.7, these

changes were inconsistent throughout the study periods.

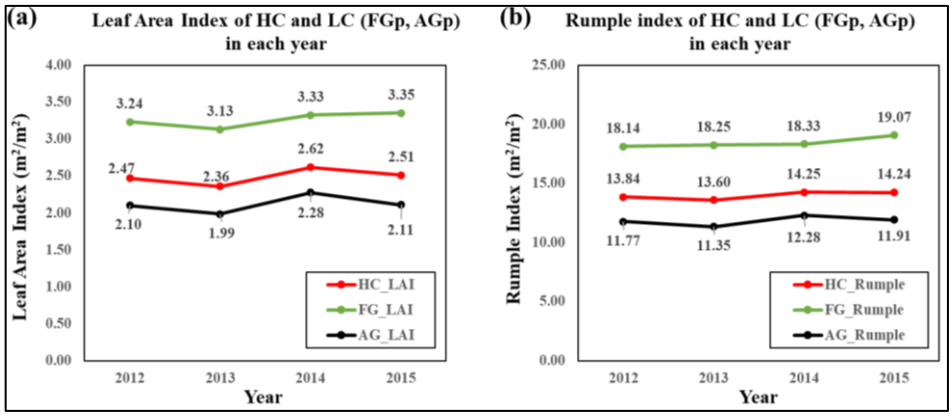

Figure 3.6 Plot-based canopy structure indices of High Canopy and Low Canopy (Forest gap and artificial gap) (a) Yearly LAI for 2012-2015; (a) Yearly rumple index for 2012-2015

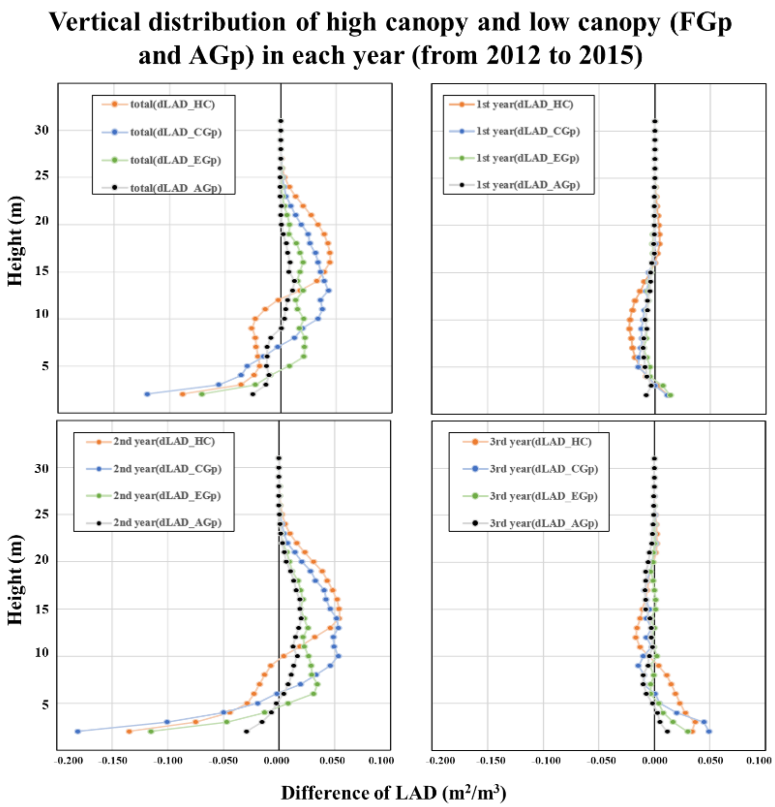

Figure 3.7 Differences in leaf area density (LAD) (m^2/m^3) of high canopy and low canopy in each year from 2012 and 2015; dLAD_'class': differences between 2012 and 2015 in the canopy 'class'; HC: High Canopy; EGp: Exiting Gap; CGp: Closed Gap; AGp: Artificial Gap; total: between 2012 and 2015; First year: 2012–2013, second year: 2013–2014, third year: 2014–2015; DA: Damaged area, VG: Vertical growth area, LG: Lateral growth area)

4. Discussion

4.1. What are the differences between the canopy structural changes derived from annual change detections and three-year interval change detection?

I found that each annual vertical growth rate and total LAI showed almost consistent values, while distributions of changes in the canopies and leaf area profiles were irregular year by year. Moreover, the distribution of the annual growth regions showed low correspondence with the three-year interval growth regions (Table 3). I speculated that this low correspondence and the irregular changes in the canopies might have resulted from frequent changes in urban canopies (i.e., dynamics), weather conditions during data acquisition, grid size, and the DOYs in data acquisition.

4.1.1. In terms of the aspects of the urban canopy dynamics and the DOYs of the data acquisition

I found that the lateral canopy changes were irregular annually. By investigating Figure 3.5b and 5c, the first-year change detection in both HC and LC showed a higher distribution ratio for the damaged area than the others. In addition, the extent of the LGr areas was highest between 2013 and 2014, the second year (Figure 3.5b). Furthermore, Figure 3.6 shows that LAI and the canopy complexity (Rumple index) of all classes in 2013 were slightly lower than in previous years. These may show the importance of the DOYs of data acquisition for the one-year interval LiDAR survey. Since the DOY of data acquisition in 2013 was in the early growing season, while the DOY of data acquisition in 2014 was in the mid-growing season, the phenology might differ. This means that the point density of canopies in 2013 might have been relatively lower than that in other years, which could have resulted from the presence of more extensive damaged areas in the first year and smaller damaged areas in second year. However, considering the third year (the longest term of 401 d) when damaged areas occupied the largest area (Figure 5) and changes in the leaf area density did not show clear differences (Figure 7), I could assume that both the DOY of data acquisition and other environmental variables might have affected the results.

Overall, the forest canopy appeared to change dynamically in each study year (Figure 3.5 and Figure 3.7). This may indicate that growth and disturbance events happened simultaneously and frequently in the study site. Table 3.7 shows the distribution of the yearly canopy changes in damaged area (DA) (HC to LC) and CaC (LC to HC). Row d in Table 3.7 shows the ratio of continuous change areas (open to closed or closed to open), which might indicate that dynamics of the canopy or uncertainty in the change detection using one-year interval LiDAR datasets.

Table 3.7 The ratio of open and closed areas by time (a) open or closed in the first year, (b) open or closed in the second year; (c) open or closed in the third year; (d) continuous changes to open to closed; (e) Total open or closed for 2012–2015, three-year term

Categories	Open area ratio (%)	Close area ratio (%)
Open or closed in the first year (a)	33	50
Newly open or closed in the second year (b)	14	29
Newly open or closed in the third year (c)	69	28
Opened (first year) → Closed (second year) → Opened (third year) or vice versa (d)	15	7
Total (e: a+b+c-d)	100	100

Although the datasets for 2012–2015 were acquired on DOYs 283, 136, 167, and 303, respectively, the one-year interval comparisons showed the potential to estimate the VGr of the canopy surface, given the association between the annual VGr rate and DOY (Table 3.2) and to detect newly opened forest gaps during the study periods.

4.1.2. Regarding the aspect of grid size

For the weather conditions, the canopy heights could have been influenced by windy conditions creating tree canopy movement. Furthermore, I was uncertain whether the trees had grown vertically. These could have resulted in low correspondences when detecting gradual growth areas at smaller grid sizes (Table 3.3), which could indicate that a smaller grid size could be easily affected by canopy movement or growth direction, while a larger grid size would not. In addition, as Roussel et al. (2017) concluded, smaller plot sizes could cause larger errors in HMAX estimations; thus, the plot and grid size may have affected a higher degree of correspondence in the growth area for the plot-level survey. However, in the case of detecting the gap opening areas, change detection with smaller grid sizes could be more useful than a larger size (Table 3.4, Figure 3.5 and Figure 3.6). Since gap edge trees expand their foliage in the lateral direction (Figure 3.5 and Figure 3.7), I might not have seriously considered whether they have exactly grown.

4.2. What are the characteristics of the structural changes according to the different canopy classes (e.g., high canopies and low canopies) in the urban forest?

4.2.1. Forest gap effects on canopy dynamics in urban forests

During the study period (2012–2015), the overall distribution of the canopy growth area in HC was about 58.6% (VGr area: 17.1%, LGr area: 41.5%), while the

damaged areas accounted for about 32.3% of the total area, which suggests active canopy growth and erosion in the study site. Meanwhile, about 26.2% of the LC area exhibited canopy growth, while the remaining 73.8% of the area was either damaged (14.6%) or unchanged (59.2%). The higher percentage of unchanged areas in LC probably resulted from areas of bare land or terrain not covered by canopies. Moreover, based on the VGr rate, both HCs and LCs seemed to grow upward at a steady rate (Table 3.2). However, the VGr rate of LCs was relatively lower than that of HCs; this difference might be due to civic usage and disturbances in LC.

AGp formed via anthropogenic activities (e.g., building graveyards, sports facilities, and recreation areas) has prolonged changes in LAI, canopy complexity, and LAD (Figure 3.6 and Figure 3.7). The particularly slow or lower changes of AGp may have driven the low overall and VGr rates in LC. Regardless, the canopies of FGp showed the greatest changes in canopy complexity, LAI, and complexity (Figure 3.6 and Figure 3.7), exhibiting the well-known effects of FGp, which foster dynamic changes in the forest canopy (Yamamoto 2000). Since canopy complexity and LAI are important parameters of forest health assessments, the FGp at the study site may have positively stimulated vegetation growth (Ishii et al. 2004; Jonckheere et al. 2004). However, Figure 3.8 suggests that FGp could be also vulnerable to disturbances, agreeing with Vepakomma et al. (2012).

In terms of the size distribution of physical disturbances or canopy openings, I could also find notable differences between FGp and AGp. In the case of FGp, the decrement of the scaling exponent in the first year (2012–2013) might result from frequent closures in smaller gaps rather than by opening larger areas (the maximum gap area and total area were similar between 2012–2013). From 2014 to 2015, it seemed that, due to forest gap closure, maximum and total gap area decreased, and the scaling exponent increased slightly. In the case of AGp, the decrement in the number of patches in the first year (2012–2013) and more frequent large openings might reflect slightly lower scaling exponent values in 2013 (the maximum gap area increased in 2013). From 2014 to 2015, it seemed that because of gap closure, maximum gap area was divided into several patches, and the scaling exponent increased slightly. Finally, since AGp had lower λ values, larger mean gap areas, and slower gap closure rates (6% closed in AGp, while 36% closed in FGp in all total periods, 2012–2015), I can assume that AGp was more vulnerable to physical disturbances; therefore, frequent larger openings occurred in AGp than in FGp (Dalagnol et al. 2019; Vepakomma et al. 2018).

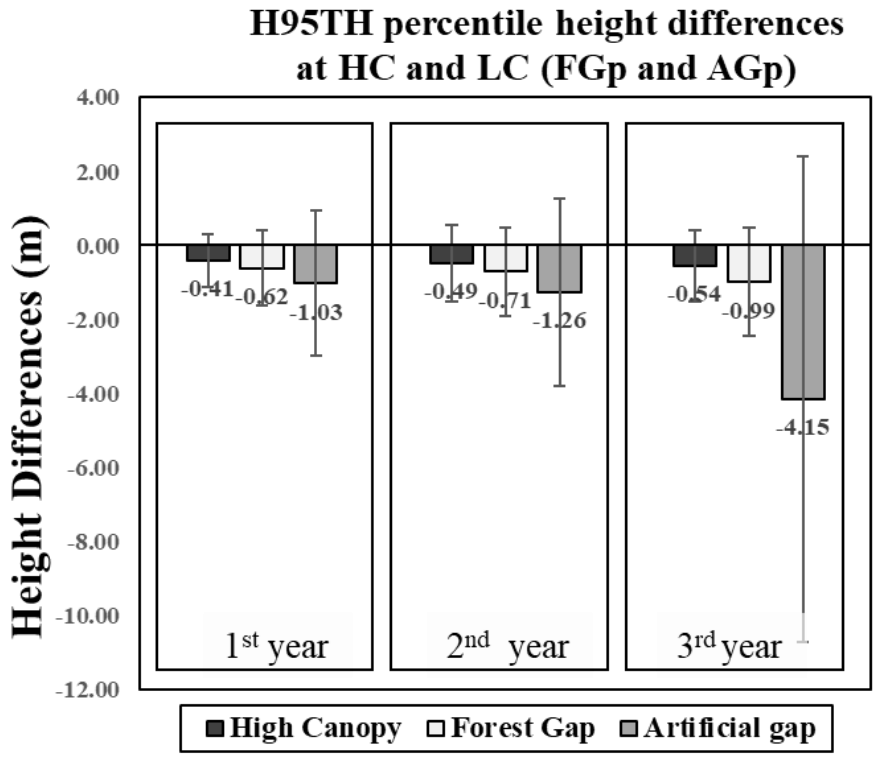

Figure 3.8 Annual height decrements in High Canopy and Low Canopy (FGp and AGp)

4.2.2. Forest gap closure

The FGp exhibited a closure rate of 5.48 m^2/year (Table 3.5), which appeared to be driven by LGr (Figure 3.5d) above a height of 5–10 m (i.e., HC) (Figure 3.7). As shown in Figure 3.5d, LGr occupied most of the area in CaC (96.59%). Based on these results, the LGr rate of maturity consisted of the gap boundaries in trees that appeared to be greater than the VGr rate of the young trees or shorter vegetation on the floor. Many studies have reported that small disturbances such as branch and tree falls could be closed by the lateral extension of gap-edge trees (Runkle 1992; St-Onge et al. 2014; Valverde and Silvertown 1997; Vepakomma et al. 2012). At the present study site, FGps were smaller in size (mean area: 34–42 m^2) than AGp (mean area: 226–279 m^2). Considering a 5.48 m^2/year rate of closure, FGp could close over short time scales. However, the larger gaps and reduced canopy dynamics in AGp areas led to more extensive gaps that remained open over long periods.

Chapter 4. LiDAR-derived three-dimensional ecological connectivity mapping

1. Introduction

Green spaces in cities can enhance biodiversity by providing habitat and food sources. However, as human populations in cities expand globally (United Nations 2019), urban green spaces are in decline (Haaland and van den Bosch 2015) and are increasingly threatened with fragmentation and habitat loss. Due to this threat, it is the role of ecologists and environmental managers to identify biodiversity-based conservation priorities and ecological management for green spaces (Lepczyk et al. 2017). Urban ecological networks provide solutions-based tools to decision-makers regarding urban conservation challenges (Choe and Thorne 2019; Lepczyk et al. 2017; Nor et al. 2017; Sandström et al. 2006). Well-managed ecological networks resulting from the use of these tools could improve biodiversity and sustainability in cities by providing ecosystem services such as hydrological regulation, air purification, and positive effects on human health (Barton and Pretty 2010; Steenberg et al. 2016).

Ecological networks can be quantified by connectivity indices, which provide a measure of how landscape patterns affect ecological processes. Centrality metrics are a form of connectivity indices (Carroll et al. 2012). Centrality values vary among landscape patches and generally imply at least some connectivity within landscapes, at least functionally, even when patches are not physically connected in space (Kindlmann and Burel 2008). Thus, urban ecological connectivity assessments can be effectively used to evaluate landscape function within cities (Casalegno et al. 2017; Cook 2002; Dickson et al. 2019; Grafius et al. 2017; Tian et al. 2017; Urban and Keitt 2001; Zeller et al. 2012).

Networks in urban ecosystems reflect heterogeneous landscape patterns with characteristics such as variation in vegetation patches and both vegetation and anthropogenic structure (e.g., buildings) (Farinha-Marques et al. 2017; Lepczyk et al. 2017). Including vegetation measures as well as measures of building structures (e.g., height and volume) in assessments of urban ecological networks is essential, particularly when considering urban bird species, as these structures represent habitat structure and composition for such species (Xie et al. 2016). Urban ecology studies have often focused on avian species because the extent of ecological connectivity in a given area is related to bird species diversity (Evans et al. 2009a; Goddard et al. 2010; Kang et al. 2015). Avian species typically use green spaces as both corridors and habitat by selecting and moving within vegetation in both vertical and horizontal directions (e.g., by using the top or middle of canopies, and tree interior or edges) (Casalegno et al. 2017; Conole and Kirkpatrick 2011). Therefore, considering the

horizontal and vertical distributions of green spaces is essential to understanding between-patch connectivity for birds (Casalegno et al. 2017). In addition, because buildings in urban ecosystems often segregate urban green patches and act as barriers against the urban bird species (Hale et al. 2012), the configuration of structures including building volume, distribution, and height should be considered when designing urban green space connectivity. However, most urban network studies have treated structures only in 2-dimensions and used vertical information such as tree heights or structures by categorizing values (Grafius et al. 2017; Matsuba et al. 2016).

There are great opportunities for applying 3D datasets to the field of ecology and environment. A 3D dataset could help elucidate the relationship between urban morphologies and urban heat environment. Tian et al. (2019) identified the relationship between air temperature and 3D landscape indices such as building to vegetation volume ratio. Zhang et al. (2019) used the 3D index (e.g., sky fraction) derived from the Google street map to estimate land surface temperatures. Moreover, using a 3D dataset could enhance the understanding of bird species movements. For example, Liu et al. (2020a) and Tattoni and Ciolli (2019) emphasized the importance of 3D data for the bird corridors. Liu et al. (2020a) used digital elevation models (DEMs) and building heights for understanding the impacts of urban vertical expansion on the birds' migratory patterns, and Tattoni and Ciolli (2019) also applied a DEM for finding potential stopover sites in the birds' migratory routes.

Advances in airborne light detection and ranging (LiDAR) (or airborne laser scanning [ALS]) and their availability have made quantifying three-dimensional (3D) structure feasible for ecological applications. LiDAR produces a point cloud which reveals objects in three dimensions at fine scale. This remote sensing can cover wide areas more easily and with higher accuracy than field measurements or aerial photo interpretation (Lefsky et al. 2002; White et al. 2016). Many researchers have successfully applied airborne LiDAR data to quantify vegetation structure in both forestry and urban studies, and many studies have demonstrated that including vegetation structure is critical to assessing ecological connectivity (Casalegno et al. 2017; Chen et al. 2014; Coops et al. 2016; Dalponte et al. 2019; Guo et al. 2018; Melin et al. 2018; Plowright et al. 2017; Shao et al. 2019). For example, Coops et al. (2016) found that airborne LiDAR-derived indices such as the standard deviation of canopy height, green cover ratio, and canopy height diversity were related to bird species diversity; these metrics were successfully used, along with other environmental variables, to estimate bird species diversity across broad areas. Casalegno et al. (2017) characterized urban habitat structure using LiDAR data from local to landscape scales and were among the first to assess connectivity among green space patches in urban areas using LiDAR data. LiDAR-derived structural

variables have enormous potential for assessing connectivity across spatial scales and thus informing biodiversity conservation and monitoring strategies. Finally, Kedron et al. (2019) developed 3D urban landscape indices using a LiDAR dataset.

Although ecological and connectivity networks include both anthropogenic and vegetation structure, existing research has not typically employed 3D analyses to estimate all structural variables. Two-dimensional variables would have limitations in representing these diverse structures of urban ecosystems. Therefore, in this study I evaluate connectivity for avian species in urban areas using both building and vegetation structure variables. My specific research objectives are to define which LiDAR-derived urban bird species diversity variables to use in creating a connectivity surface (landscape resistance and landscape permeability) and then test a modeled urban ecological network created using them. Related research questions are: 1) What are the contributions of the urban green spaces to the 3D connectivity with regard to land-use types; and 2) What are the characteristics of 3D based connectivity results compared to 2D based connectivity results?

2. Materials and Methods

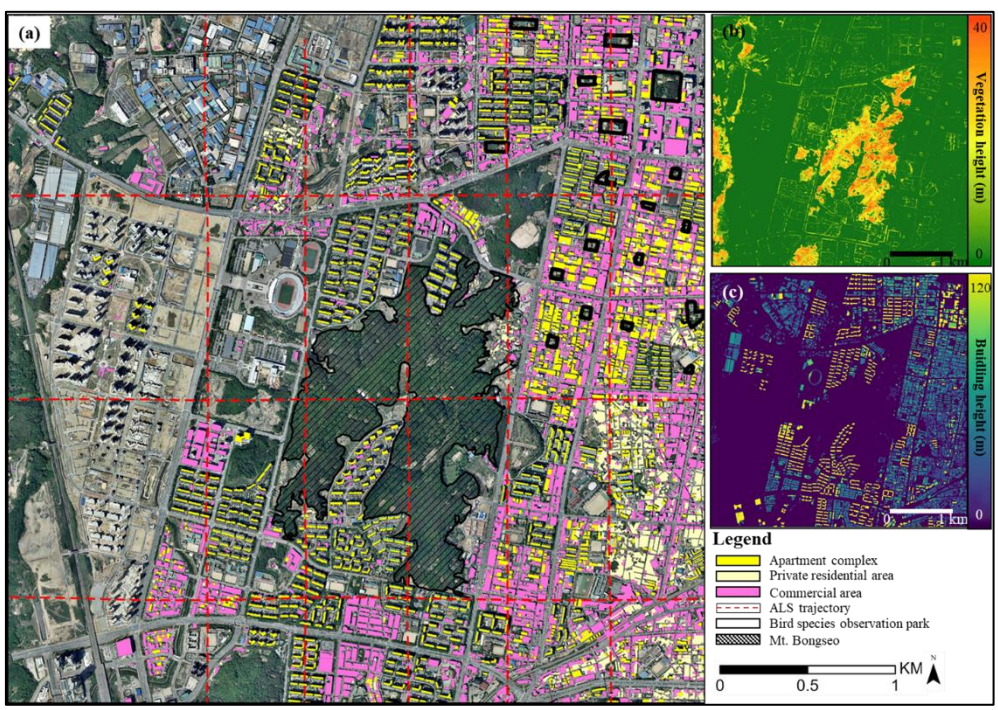

Figure 4.1 Study site (Cheonan city, Republic of Korea) information. (a) Study site mapped with residential areas and commercial areas, (b) map of vegetation height (m), (c) map of building height (m)

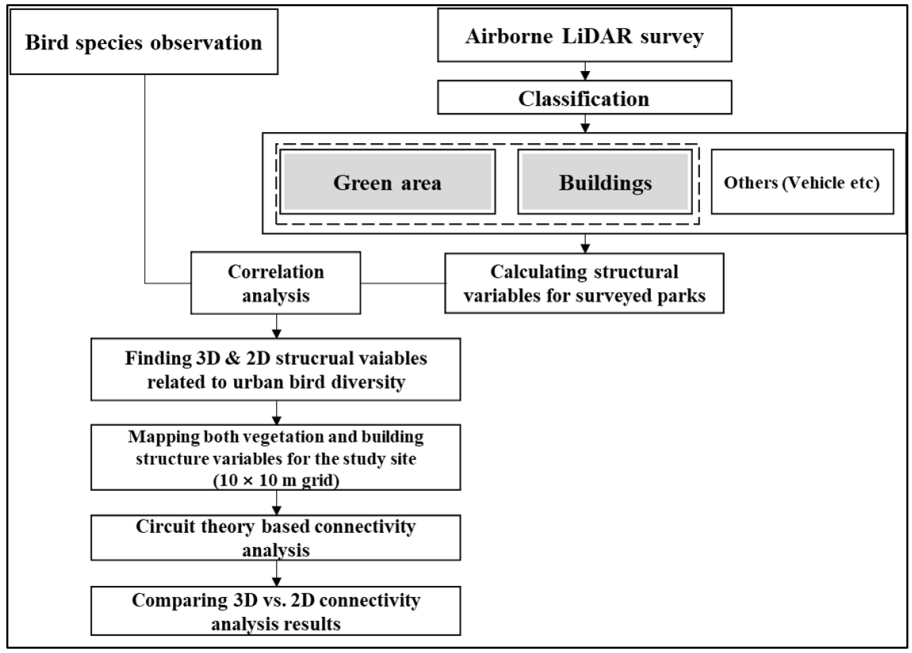

Figure 4.2 Methodological flow chart depicting vegetation and building mapping

2.1. Study area and avian species observation

The study site covers 19.27 km2 in the center of Cheonan, population 600,000 (Korea Statistical Information Service, http://kosis.kr/ 2015), Republic of Korea (Figure 4.1). The city of Cheonan is a major transportation hub connecting the metropolitan areas of Seoul with other provinces in South Korea. The study site has various types of urban green areas, including large urban mountainous forest (Mt. Bongseo located at the center of the research site), urban parks, and street trees. These green areas are surrounded by a variety of urban land-use types including apartment complexes, commercial areas, and private residential areas (Figure 4.1, appendix table 1).

I surveyed bird species during the breeding season (21 April to 15 May 2015) within 18 neighborhood parks (Figure 4.1). Bird species presence and abundance were recorded along line transects (25 m in width) method. Each transect was surveyed three times. Then I summed transect-level observations to determine species richness and abundance. Species richness, abundance, and species richness per unit area for each surveyed park were used in analyses (Figure 4.2). I observed birds using binoculars (Ultraview EX OP 10×32DH II, Kenko Tokina Co., Ltd., Tokyo, Japan) and identified species via sound and visual observation of flight forms ((Bibby et al. 2000; Song 2015, 2017).

The vegetation in the parks consists of general tree species in South Korea. Generally, shrubs (e.g., *Buxus koreana*, *Euonymus alatus* and *Rhododendron*

schlippenbachii), sub-canopy (e.g., *Acer palmatum* and *Chaenomeles sinensis*), and high canopy (e.g., *Zelkova serrata*, *Sophora japonica*, and *Ulmus davidiana* var. *japonica*) formed the canopy structures in the parks. Broad-leave trees such as *Zelkova serrata* and *Sophora japonica* were planted for shading. Some species, such as *Cornus kousa*, *Ginko biloba*, *Prunus sargentii*, *Taxus cuspidate*, and *Pinus densiflora* were planted for landscaping. *Pinus strobus* was planted for screening.

2.2. Airborne LiDAR acquisition, preprocessing and classification and deriving structural variables

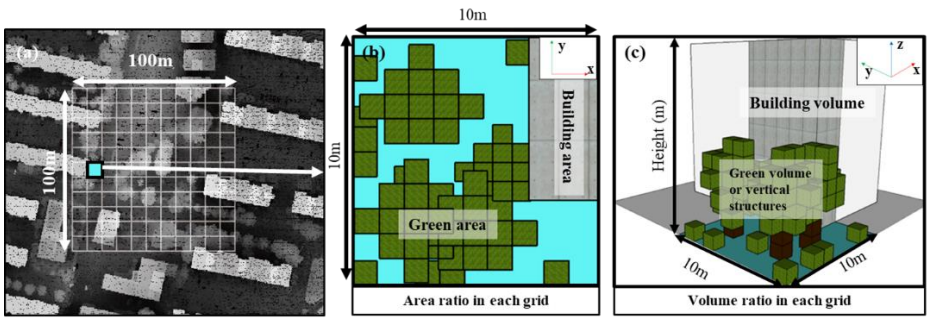

Figure 4.3 Process schematic of LiDAR-derived structure variables for vegetation and buildings. (a) Examples of 10 m×10 m grid cells in the study site, (b) illustration of 2D variables, and (c) illustration of 3D variables.

The airborne LiDAR datasets were surveyed on 30th October 2015 using IGI LiteMapper 6800 sensor (by Samah Aerial Survey CO.) during the foliated season. The study site was surveyed following eight flight lines (Figure 4.1, reds dot lines) at an altitude of 1000 m with a 50% overlap in the width of scanned areas. The beam divergence was 0.3 mrad, and the field of view was 60°. Point density was >5 points/m^2. The dataset was preprocessed and classified using built-in algorithms in TerraScan (Terrasolid, Helsinki, Finland) software on the MicroStation (Bentley Systems, PA, USA) platform.

I classified the LiDAR dataset (point cloud) into buildings, vegetation, ground, and others (e.g., vehicles, streetlights etc.; Figure 4.2) by overlapping and clipping GIS files (vector files at 1:5,000 scale) provided by the National Geographic Information Institute (NGII 2015; https://www.ngii.go.kr/). In addition, I classified green areas into street trees, artificial green areas, natural green areas by overlapping land-use types (appendix table 1). The ground point class was used to normalize the heights and z values of the remaining classes based on the absolute zero height value. Next, I allocated the normalized point cloud into 10 m × 10 m grid cells to generate and map the 3D characteristics of the study site (Figure 4.3). Finally, I mapped both building and vegetation structure variables into every grid cell, after selecting bird diversity-related variables from correlation results (Figure 4.2).

I derived 2D and 3D structural variables from the LiDAR dataset (Figure 4.3). I created 50 m (Andersson and Bodin 2009) buffer zones around the boundary of each surveyed park and then calculated building structure variables within these buffers. Building heights and areas were derived from the airborne LiDAR dataset. The volume of each building was calculated by multiplying its height by its area. Additional building structure variables included mean building area (b_amean), mean building height (b_hmean), the standard deviation of building height (b_hstd), and the ratio of building area for each buffer (b_ratio) (Table 4.1).

To obtain vegetation structure variables for each surveyed park, I estimated the vertical distribution of vegetation structure (i.e., the number of voxels within 1 m^3 at 1 m height increments, g_L01–g_L12) and canopy complexity (obtained by dividing the 3D surface area by the 2D surface area, g_rumple) (Parker et al. 2004). Then I obtained the following four horizontal distribution variables: vegetation area (the amount of area covered by vegetation, g_area), green space perimeter (g_pe), vegetation cover ratio per pixel (g_ratio), and the green space perimeter to area ratio (g_pa_ratio) (Table 4.1). Vertical distribution variables were calculated using the "lidR" package in R (R core team 2018) and horizontal distribution variables were calculated from a canopy height model that I generated using the LiDAR dataset at a cell size of 0.25 m × 0.25 m.

The final resolution of the building structural variables was 0.25 m × 0.25 m in 10 m × 10 m grid cells. In the case of the vegetation structures, the resolution of voxel was 1 m3 and that of area-related variables was 0.25 m × 0.25 m per 10 m × 10 m grid cells.

Table 4.1 Summary of the building and vegetation LiDAR-derived variables used in this study

Variables	Description	2D or 3D
Building structure		
b_amean	mean building area for each buffer around park	2D
b_hmean	mean building height for each buffer around park	3D
b_hstd	standard deviation of building height for each buffer around park	3D
b_ratio	ratio of building area for each buffer around park	2D
b_vmean	mean building volume for each buffer around park	3D
Vegetation structure		
g_L01–g_L12	the number of voxels within 1 m^3 at 1 m height increments	3D
g_rumple	canopy complexity obtained by dividing the 3D surface area by the 2D surface area	3D
g_area	the amount of area covered by vegetation	2D
g_pe	green space perimeter	2D
g_ratio	vegetation cover ratio per pixel	2D
g_pa_ratio	the green space perimeter to area ratio	2D

2.3. Correlation analysis and selection of structural variables

After calculating 2D and 3D structural variables for the 18 surveyed parks, I used the nonparametric Spearman's rank-order correlation (Rho) to assess correlations between bird species richness, abundance, and richness per unit area and horizontal and vertical structure variables of the 18 parks.

I assumed that structural variables that were positively correlated with bird species variables would enhance avian movement, whereas those that were negatively correlated would impede movement. Therefore, I generated 2D and 3D variable maps selecting the vegetation ratio variables by calculating the ratio of vegetation cover (the ratio of vegetated area to total area within each 10 m × 10 m grid cell) and the vegetation volume ratio (the ratio of the volume of vegetation to the total volume in each 1 m3 voxel at each height strata).

I selected LiDAR-derived variables that were significantly correlated ($p < 0.05$), either positively or negatively (Figure 4.4), with the number of species per unit area to generate 2D and 3D landscape permeability maps. Using a 10 m × 10 m cell size, I calculated volume and area ratios as follows:

1) 2D: vegetation area ratio = vegetation area/the area of each grid cell
2) 3D: vegetation volume ratio (8 m to 10 m) = vegetation volume/the volume of each grid cell

2.4. 2D and 3D ecological networks

I applied an electrical current flow-based model provided in the Connectivity Analysis Toolkit (Carroll et al. 2012) to map the connectivity between the parks (Dickson et al. 2019; McRae et al. 2008). I produced current flow betweenness centrality (CFBC) which shows multiple important pathways or alternative pathways surrounding the shortest path (Carroll et al. 2012; Kang et al. 2015). As in the electrical current flow-based model, a high CFBC value means that gird has a greater contribution to connectivity (McRae et al. 2008).

The models were calculated from the landscape permeability maps which reflect how readily target species can move within a landscape. I generated 2D and 3D permeability maps (10 m ×10 m cell size) by normalizing the mapping results of the structural variables from 1–100 linearly after selecting 2D and 3D structural variables from the correlational results (See the Results 3.2 section).

In addition, to visualize which areas were more connected (higher centrality values) or more isolated (lower centrality values), I generated Z-distribution maps for both the 2D and 3D-based connectivity results. I assumed that centrality values that were greater than and less than |0.5SD| reflected connected area and isolated

area, respectively.

Finally, after mapping both 2D and 3D CFBCs, I conducted correlation analyses between those CFBCs and the indices of bird diversity.

3. Results

3.1. Avian species survey

The total number of observed species is 23 and the number of birds is 822. The majority of the observed birds were general species (generalist) living in the city, such as *Passer montanus* (abundance: 486), *Microscelis amaurotis* (abundance: 73), *Pica pica* (abundance: 52), *Carduelis sinica ussuriensis* (abundance: 39), *Streptopelia orientalis* (abundance: 29), *Parus major* (abundance: 24), and *Phylloscopus inornatus* (abundance: 19) (see also appendix table 2). I calculated the bird species richness, abundances, and species richness per square meter at each park for identifying the bird diversity-related LiDAR-derived variables (Figure 4.2).

3.2. Correlation analyses and variable selection

Correlations between bird species diversity and structural variables are shown in Figure 4.4. The results described the importance of amounts of the high canopies (8–10 m height) as well as the structural complexity of canopy (g_rumple) for the species per unit area (Fig. 4). Moreover, Figure 4.4 also showed that building structure variables, especially mean building volume ($p<0.01$, $r= -0.66$), should be considered for the connectivity analysis since there was a negative correlation between the mean building volume and the number of species per unit area.

The 2D variables including the area of vegetation cover and vegetation perimeter (Table 4.1) were negatively correlated with the number of bird species per unit area, whereas these variables were positively correlated with species richness and species abundance. Similarly, structural building variables within 50 m buffers, including mean building area, the standard deviation in building height, and mean building volume were negatively correlated with the number of species per unit area but positively correlated with species richness and abundance. This trend could be explained by data type.

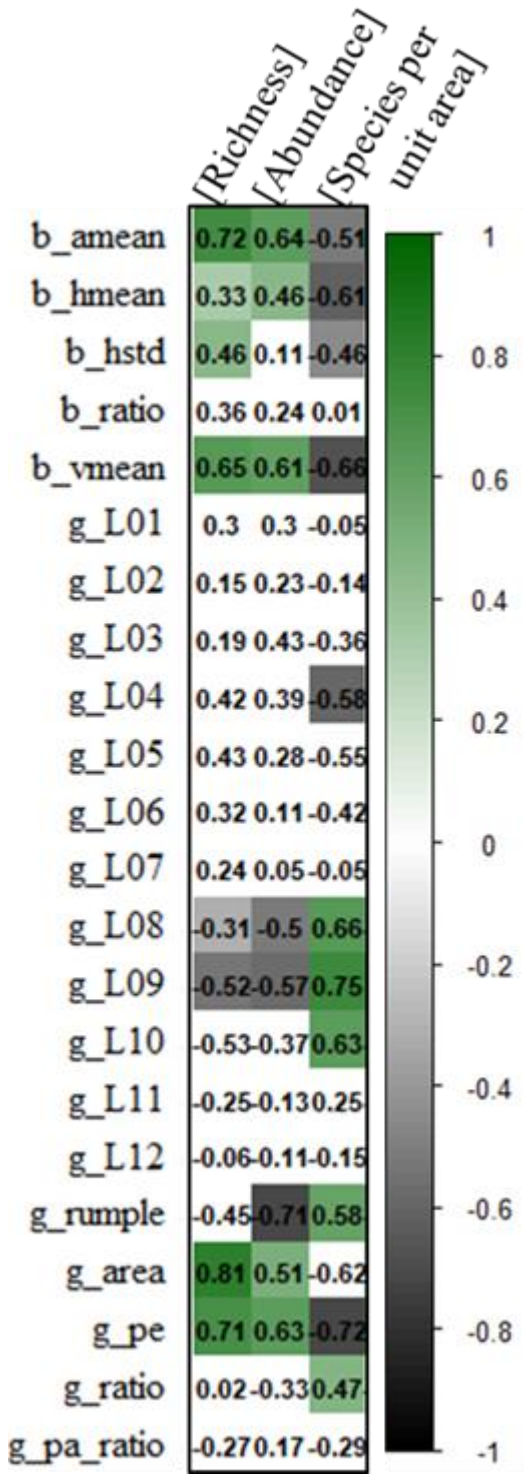

Figure 4.4 Spearman's correlations between the number of species per unit area, species richness, and species abundance with LiDAR-derived variables. Eighteen parks were surveyed in this study. Positive and negative correlations are displayed in green and black, respectively ($p < 0.05$). Color intensity is proportional to the correlation coefficients. See Table 1 for definitions of variables.

3.3. Connectivity analysis results

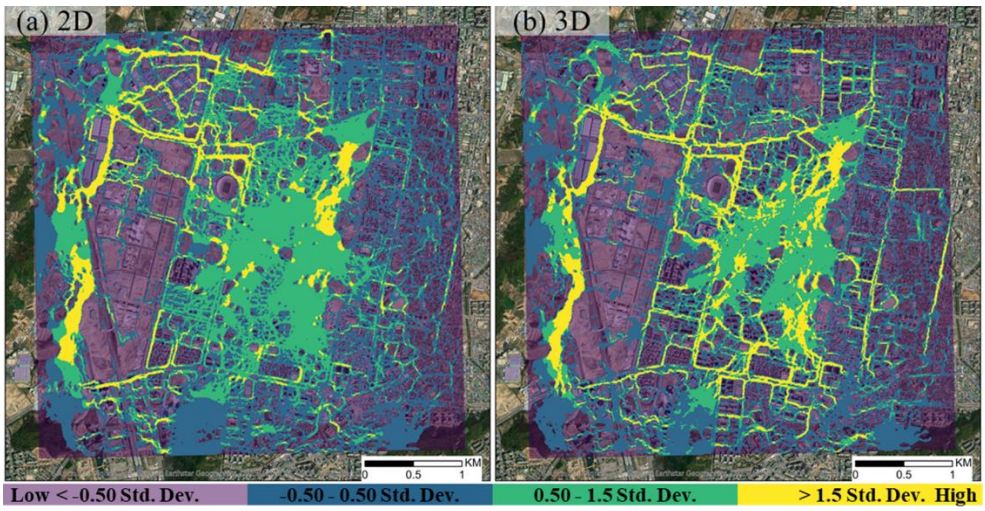

Figure 4.5 Z-distribution maps of all possible alternative pathways (CFBC) derived from the a) 2D permeability map and b) 3D permeability map. Colors indicate standard deviations from each mean centrality value. (See also appendix figure 1)

Although the spatial Z-distributions of possible alternative pathways (i.e., CFBC) derived from both 2D and 3D structural variables (mean CFBC = 0.00241 and 0.00245; SD = 0.00207 and 0.00252, respectively) indicate that boulevards and large green spaces are associated with higher centrality values, there are differences.

In the 3D CFBC, boulevards and large green spaces in the center of the study area appear to be of greater importance than in the 2D CFBC (Figure 4.5).

The occupied connected area (≥0.5 SD) was more extensive in the 2D CFBC (54,209 grid cells, 28.20% of the study area) than in the 3D results (46,292 grid cells, 24.08% of the study area). By contrast, highly connected areas (>1.5 SD) were more universal in the 3D CFBC (8.04% of the study area) than in the 2D (5.96% of the study area). The 3D CFBC results indicated that green spaces within dense residential areas and spaces adjacent to high-rise buildings were more isolated (centrality values < -0.5 SD) than was suggested by the 2D results. Generally, isolated areas (<-0.5 SD) were more extensive in the 3D results (92,842 grid cells, 48.30% of the study area) than in the 2D (80,716 grid cells, 41.99% of the study area).

3.4. Correlation between connectivity results with bird species diversity

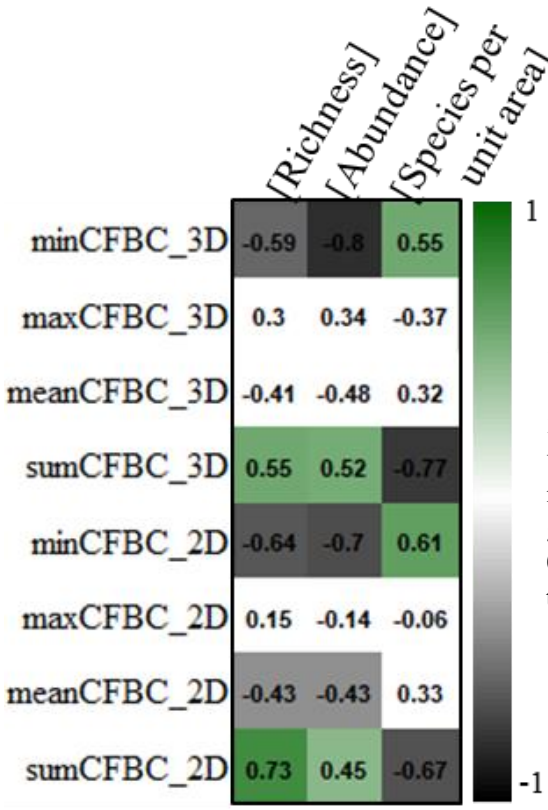

Figure 4.6 Spearman's correlations between the number of species per unit area and species abundance and richness with statistics (minimum [min], maximum [max], mean, and summation [sum]) derived from the 2D and 3D CFBCs within surveyed urban parks (n = 18). Positive and negative correlations are shown in green and black, respectively ($p < 0.05$). Color intensity is proportional to the correlation coefficients.

Both the 2D and 3D CFBCs within urban parks indicated a significant correlation with avian species diversity ($p < 0.05$, Figure 4.6). Species richness and abundance were both positively correlated with the summation of the 2D and 3D CFBCs, whereas the number of species per unit area was negatively correlated with both of these metrics. Although it was not significant, the average of the 3D CFBC appeared to have a positive relationship with the number of species per unit area.

3.5. Differences between 2D- and 3D-based CFBCs

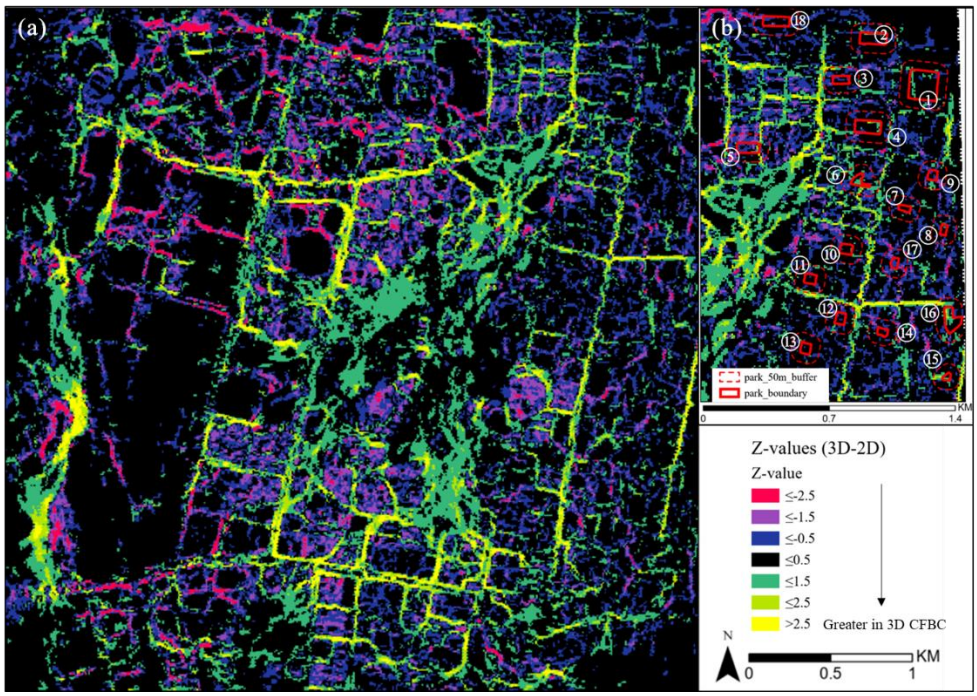

Figure 4.7 Z-distribution map of the differences between the 3D and 2D CFBCs This map was created by subtracting the 2D CFBC from the 3D CFBC for the (a) overall study area and (b) surveyed urban parks. Colors represent standard deviations from the mean difference between CFBC values (mean = 4.22E-05; standard deviation = 1.52E-03). Thick red lines indicate park boundaries and dashed red lines indicate the 50 m buffer zones.

The differences between the 2D and 3D CFBCs are shown in Figure 4.7. Although the mean difference was close to zero (4.2E-05 ± 1.5E-03), notable differences (>±|1.5SD|) occurred in areas adjacent to boulevards and within residential areas and large green space patches (Figure 4.7). In the 3D CFBC results, areas adjacent to apartment complexes (heights>15-20 m) around the mountain displayed significantly less values relative to the 2D CFBC. This is likely because the volume of apartment complexes was incorporated into the 3D-based results, and thus the Z-distribution values in those areas were low (<-1.5SD). Street trees planted along boulevards were also a source of discrepancy between the 2D and 3D CFBCs. Given that boulevards rarely have high structural volumes, the large values observed in the 3D results are likely the result of the volume of street trees 8–10 m in height. Finally, the distribution of the Z-values in large green space patches in the 3D CFBC had relatively high variance, which could be a reflection of diverse canopy structures (canopy volume at 8–10 m) (Figure 4.4). The differences between the 2D and 3D CFBCs for each urban park are shown in Table 2. Although there were no significant

differences between means for each park, some areas of parks 2, 4–6, 9, 16, and 17 were significantly different between the CFBCs (Figure 4.7).

Table 4.2 Differences in the 2D and 3D CFBCs for each surveyed park. Values were obtained by subtracting the 2D CFBC from the 3D CFBC and parks are listed in descending value order.

Park No.	**park06**	**park16**	**park15**	**park01**	**park07**	**park04**	**park10**	**park13**		
3D-2D of CFBC (positive value)	*8.1E-04*	*6.1E-04*	*5.9E-04*	2.6E-04	2.3E-04	1.9E-04	4.5E-05	4.5E-05		
Park No.	**park02**	**park14**	**park08**	**park11**	**park03**	**park12**	**park09**	**park18**	**park05**	**park17**
3D-2D of CFBC (negative value)	-1.6E-05	-1.6E-04	-2.2E-04	-2.8E-04	-4.2E-04	-4.7E-04	-4.8E-04	*-5.5E-04*	*-6.1E-04*	*-1.3E-03*

4. Discussion

4.1. Vegetation and building structures and bird species diversity

I assessed urban connectivity for avian species in the context of urban vegetation and building features. Vegetation volume at heights of 8–10 m (i.e., the number of voxels at those heights) was positively correlated with bird species richness per unit area, whereas at heights of 4 m, vegetation volume was negatively correlated with bird species richness per unit area (see results 3.2). Therefore, I infer well-managed urban parks with high canopies (>8 m height) provide profitable habitats or shelters for the bird species.

Both the volume and average height of buildings within 10 m × 10 m grid cells were negatively correlated with the number of species per unit area. Collectively, these results suggest that 3D structural metrics of vegetation and buildings should be considered in connectivity analyses for birds in urban areas. My results support previous findings of negative effects of the built environment on bird diversity (Xie et al. 2016; Zhou et al. 2012) by providing evidence that high volume or tall buildings are negatively correlated with species metrics.

My results further demonstrate that the number of species per unit area is related to the height and volume of both vegetation and buildings (Results 3.1). The rumple index, which represents complexity in the vertical distribution of vegetation canopies, was a positive correlation with bird species diversity ($r = 0.58$, $p < 0.05$). This indicates that complex canopy composition, such as multi-layered canopies, may relate to greater bird diversity (e.g., Cerra and Crain 2016; Coops et al. 2016; Evans et al. 2009b; Zhou et al. 2012). However, the standard deviation of building height

was negatively related to the number of species found per unit area ($r = -0.46$, $p < 0.05$). There could be a negative impact on the bird diversity caused by the heterogeneity in height of the buildings generally due to high-rise apartment complexes in the site.

4.2. 3D-based connectivity results

The 3D CFBC results indicated that large forested areas (e.g., Mt. Bongseo) and street trees along boulevards appeared to play as key corridors within the study area (Figure 4.8). Mainly, street trees acted to connect isolated areas to areas of higher connectivity, such as boulevards and large green spaces, for avian species (Figure 4.8) (e.g., Grafius et al. 2017; Morelli et al. 2014). For example, in park 6 (Figure 4.8c), where there were adjacent street trees with high canopies (>8m), CFBC values were high relative to other parks (Table 4.2). Street trees contribute to the greater CFBC value of roads compared to other anthropogenic land-use types (Figure 4.9). These contributions of the street trees are due to high canopies (>8 m in height) occurred at equidistant intervals (e.g., Figure 4.10), and the negative impacts of given building volume near roads on bird diversity (Figure 4.4) by acting as barriers (e.g., Hale et al. 2012).

Artificial green areas including residential parks, landscaped green areas, or privately-owned public open spaces also showed great CFBC value (0.003197) among other land-use types except for the natural green spaces and graveyards (graveyards were located inside natural green spaces). However, their contribution to the connectivity could be limited if they are isolated by dense buildings (Figure 4.8b). Therefore, it is required green-infrastructure strategies for improving the connectivity in the isolated areas, such as designing green wall systems and rooftop gardens (Chiquet et al. 2013; Mayrand and Clergeau 2018), or planting and well-managing street trees.

Apartment complexes, owing to their high volume, tended to show lower CFBC values in the 3D analyses. However, if buildings are adequately spaced, adjacent landscaped green spaces or residential parks connected by street trees can improve connectivity inside the apartment complexes (Figure 4.8c). In the case of private residential areas (Figure 4.8d), although the buildings inside the areas are less heights (≦6m), they represented severely isolated areas (Z values of 3D CFBC < -0.5, Figure 4.9). This describes that the extremely isolated areas are decided by the low density of vegetation and high dense building structures in 3D based connectivity analysis.

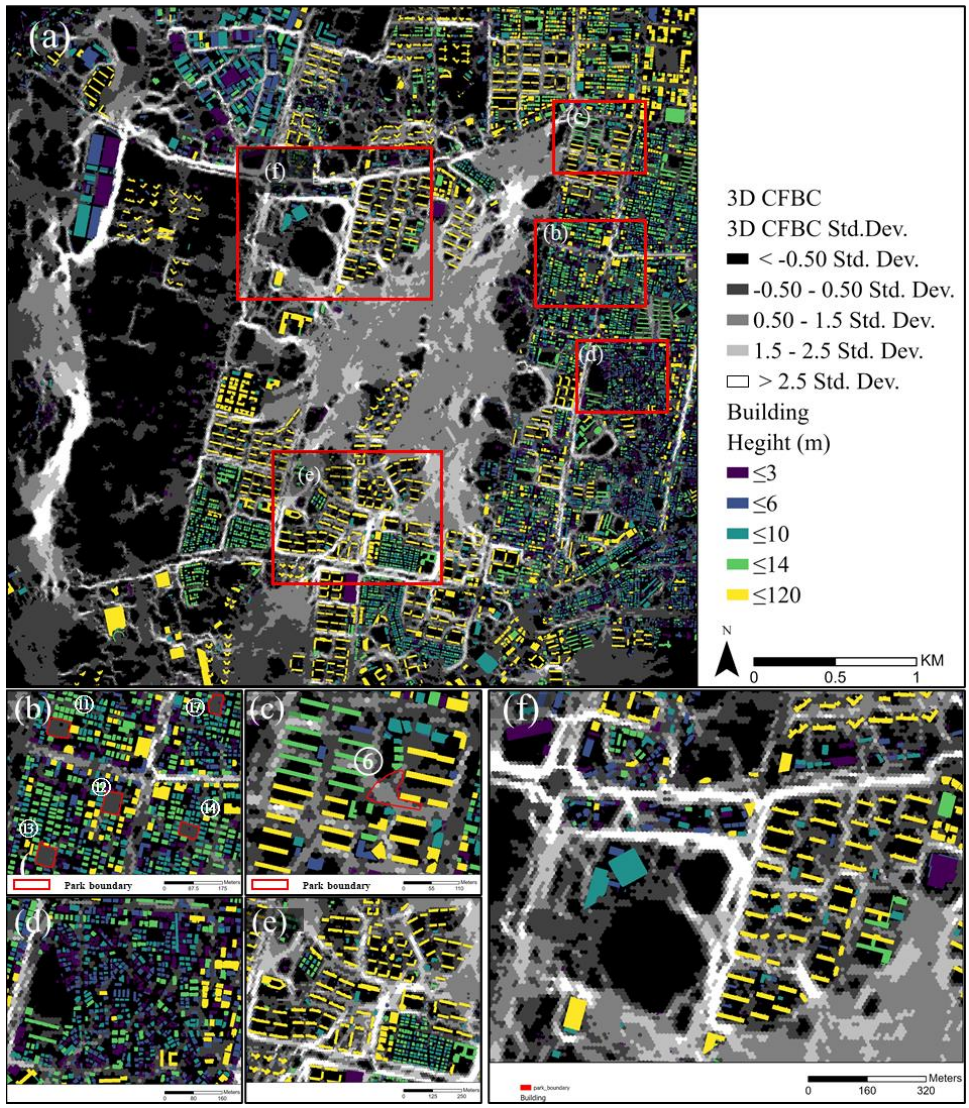

Figure 4.8 Z-distribution map of 3D-based current flow betweenness centrality results with heights of building information (the interval is 20 percentile) for the (a) overall study area, (b) surveyed parks in residential-commercial area, (c) park 6 in an apartment complex, (d) private residential area (e) high-rise apartment complexes and low-rise commercial area adjacent to an urban forest, and (f) high-rise apartment complexes and boulevards adjacent to an urban forest.

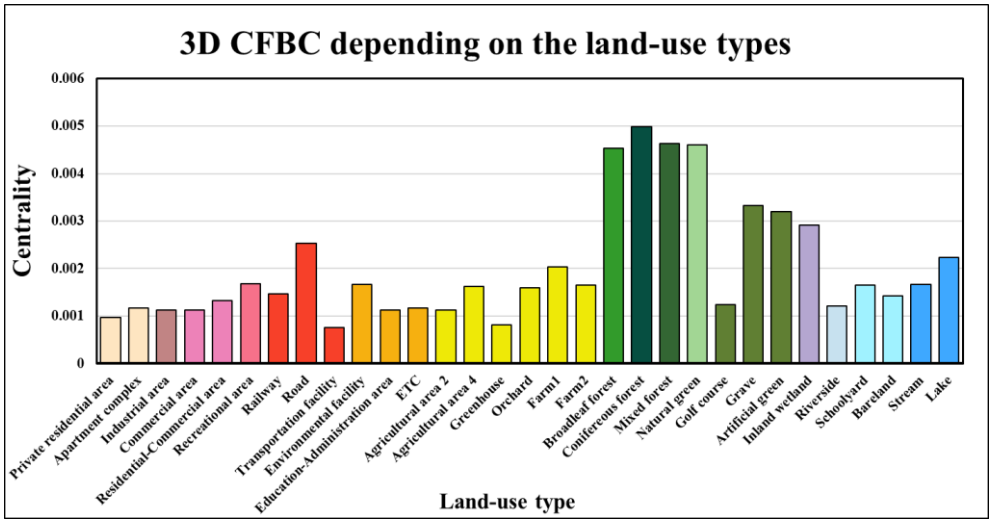

Figure 4.9 3D CFBCs among various land-use types. Colors represent land-use classifications obtained from EGIS, Ministry of Environment, Republic of Korea, https://egis.me.go.kr/)

Figure 4.10 Street view of a boulevard in the study area obtained from Naver Corp., Seongnam, South Korea (http://map.naver.com)

4.3. Differences between 2D and 3D network analyses

Connected areas were more restricted in the 3D CFBC than in the 2D CFBC, and the latter also detected more areas of connectivity (Results 3.3). However, both isolated (<-0.5SD) and highly connected areas (>1.5SD) were more pervasive in the 3D CFBC. I infer that the 3D analyses reflect areas of higher intensity connectivity, whereas the 2D approach can be more generous. I also observed differences in the 2D and 3D CFBCs based on land use types (Figure 4.11).

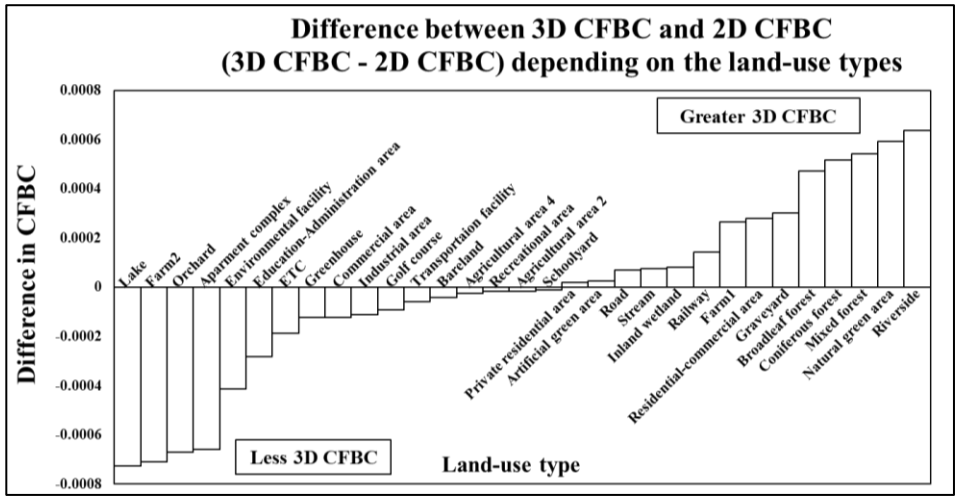

Figure 4.11 Differences between the 2D and 3D CFBC. Centrality values were obtained by subtracting the 2D CFBC from the 3D CFBC, bars represent men differences.

4.3.1. Forest and artificial green area

Both the 2D and 3D CFBCs reflected the importance of natural forests (i.e., broadleaved, coniferous, and mixed) in sustaining connectivity in the study area. However, my results highlighted the importance of considering 3D structures in determining the degree of importance of forest patches to connectivity. The 3D CFBC showed extensive forest patches as more highly connected than the 2D CFBC, and these differences were most pronounced around forest edges facing roads, where adjacent street trees appeared to act as corridors (Figure 4.7). However, I observed little difference between the two CFBCs in a large valley south of the forested patch, which was likely the result of nearby high-volume apartment complexes reducing the contribution of this forested area to connectivity.

I found no evidence of connectivity differences (i.e. mean differences) in artificial green areas (i.e., residential urban parks, landscaped green spaces, or private owned open space) between the two CFBCs. However, my results did suggest that street trees and landscaped green spaces improve connectivity by connecting core areas in the 3D CFBC (Figure 4.8c). In the urban park shown in Fig. 12, the innermost area has a low canopy (less than 5–10 m in height) with open grassland areas and the outermost areas has a high canopy (>10 m). The 3D-based analyses well-described the vertical diversity and volume of these canopies, whereas the 2D-based analyses considered these areas as nearly identical (Figure 4.5 and Figure 4.12).

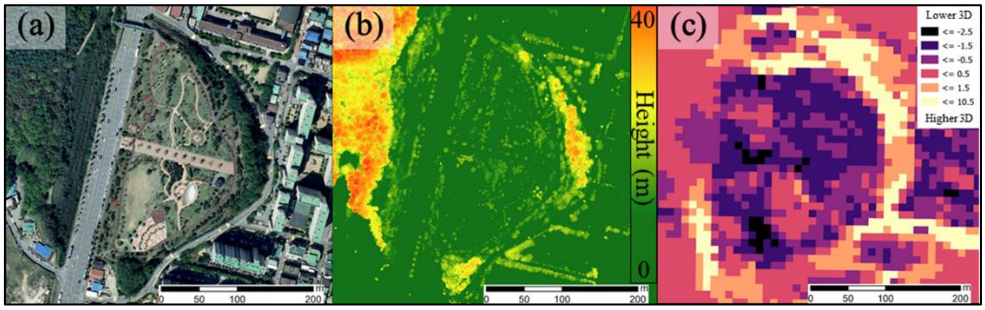

Figure 4.12 A large urban park in the study area showing (a) Ortho-imagery, (b) canopy height (m), and (c) Z-distribution of the difference between the 2D and 3D CFBCs.)

4.3.2. Roads and residential areas

When comparing the 2D and 3D CFBCs for roads I observed a relatively low mean difference (7.E-05) but high standard deviation(i.e. 2.E-03), which indicates that variables such as the volume of street trees or the presence of buildings may affect road contribution to connectivity. The contribution of boulevards was greatest likely because these roads are wide (≥25 m), which may mitigate the effects of building volume. By contrast, narrow alleys had a minimal contribution to connectivity due to adjacent dense buildings (Figure 4.13).

The influence of building volumes on connectivity is seen in the CFBC results in apartment complexes and private residential areas. The connectivity in private residential areas is slightly greater in 3D CFBC results (mean difference of CFBC = 2E-5 ± 8E-4, Z-values≤0.5; Figure 4.7 and Figure 4.11), whereas considerably lower (mean difference of CFBC = 7E-4 ± 1E-3, Z-values≤-1.5) in 3D CFBC in apartment complexes compared to 2D-CFBC results.

I ascertain that 3D connectivity analyses have a great advantage in presenting the difference in building and vegetation structures in the study sit, and that this difference leads to the results of higher intensity connectivity in the 3D analyses and more area selected in 2D analyses.

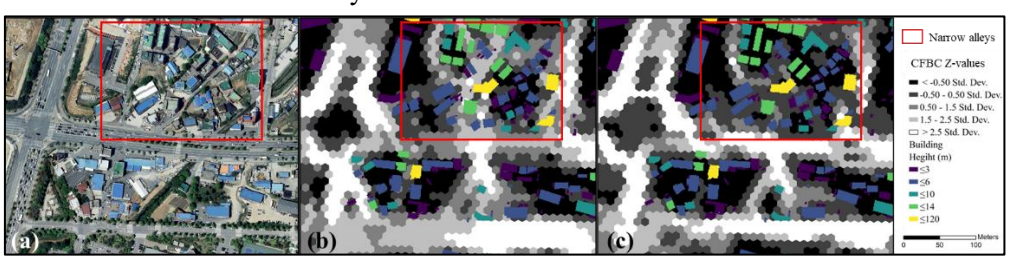

Figure 4.13 Examples of boulevards and narrow alleys in the study site (a: Otho-imagery; b: 2-D based CFBC results; c: 3-D based CFBC results)

Appendix

Appendix table 1 Land-use information* of the study site

Classification	Medium classification code	Area (m^2)	Classification	Medium classification code	Area (m^2)
Road	154	5289,536	Railway	153	124,030
Artificial green	423	2663,816	Schoolyard	622	105,090
Bareland	623	2451,265	Graveyard	422	82,688
Broadleaf forest	311	2048,194	Residential-Commercial area	132	31,158
Commercial area	131	1591,168	Environmental facility	161	28,320
Agricultural area 4	222	1075,865	Inland wetland	511	26,897
Apartment complex	112	876,436	Stream	711	23,016
Coniferous forest	321	750,004	Greenhouse	231	22,021
Industrial area	121	417,343	Farm2	252	9,778
Private residential area	111	393,975	Lake	712	8,649
Agricultural area 2	212	296,987	Farm1	251	7,814
Recreational area	141	229,155	Golf course	421	7,555
Mixed forest	331	219,668	Natural green	411	7,141
Education-Administration area	162	190,865	Transportation facility	155	1,214
ETC	163	150,799	Riverside	612	278
Orchard	241	143,358	**Total**		19,274,082

*Land-use GIS files and information are serviced by EGIS (https://egis.me.go.kr/), Ministry of Environment, Republic of Korea

Appendix table 2 Observed bird species at each park

Park No.	No. of species	No. of birds	Observed species (No. of observed birds)
1	17	127	*Passer montanus (47), Pica pica (1), Microscelis amaurotis (9), Streptopelia orientalis (8), Phoenicurus auroreus (2), Parus major (7), Parus palustris (3), Parus varius (1), Carduelis sinica ussuriensis (24), Sinosuthora webbiana (4), Aegithalos caudatus (2), Picus canus (1), Erithacus sibilans (2), Turdus hortulorum (1), Dendrocopos major (1), Phylloscopus inornatus (3), Emberiza spodocephala (2)*
2	7	63	*Passer montanus (43), Pica pica (3), Microscelis amaurotis (5), Streptopelia orientalis (3), Carduelis sinica ussuriensis (1), Phylloscopus inornatus (3), Emberiza spodocephala (5)*
3	11	42	*Passer montanus (25), Pica pica (5), Microscelis amaurotis (1), Streptopelia orientalis (2), Phoenicurus auroreus (1), Parus*

Park No.	No. of species	No. of birds	Observed species (No. of observed birds)
			major (2), Parus palustris (2), Parus varius (1), Aegithalos caudatus (1), Phylloscopus inornatus (1), Emberiza spodocephala (1)
4	11	86	*Passer montanus (48), Pica pica (9), Microscelis amaurotis (6), Streptopelia orientalis (5), Phoenicurus auroreus (2), Cyanoptila cyanomelana (1), Parus major (3), Carduelis sinica ussuriensis (6), Erithacus sibilans (2), Phylloscopus inornatus (1), Emberiza spodocephala (3)*
5	8	45	*Passer montanus (28), Pica pica (1), Microscelis amaurotis (5), Streptopelia orientalis (3), Parus major (2), Carduelis sinica ussuriensis (3), Sinosuthora webbiana (2), Phylloscopus inornatus (1)*
6	3	16	*Passer montanus (9), Pica pica (4), Microscelis amaurotis (3)*
7	4	26	*Passer montanus (19), Microscelis amaurotis (4), Parus major (2), Tarsiger cyanurus (1)*
8	4	63	*Passer montanus (55), Pica pica (3), Microscelis amaurotis (4), Parus major (1)*
9	3	34	*Passer montanus (28), Pica pica (2), Microscelis amaurotis (4)*
10	8	3	*Passer montanus (14), Pica pica (3), Microscelis amaurotis (6), Streptopelia orientalis (1), Phoenicurus auroreus (1), Parus major (1), Aegithalos caudatus (3), Phylloscopus inornatus (1)*
11	4	35	*Passer montanus (31), Pica pica (2), Microscelis amaurotis (1), Streptopelia orientalis (1)*
12	6	33	*Passer montanus (21), Pica pica (4), Microscelis amaurotis (4), Parus major (2), Parus varius (1), Phylloscopus inornatus (1)*
13	6	25	*Passer montanus (15), Pica pica (4), Microscelis amaurotis (3), Parus palustris (1), Dendrocopos major (1), Phylloscopus inornatus (1)*
14	4	53	*Passer montanus (45), Pica pica (2), Microscelis amaurotis (5), Cyanopica cyanus (1)*
15	4	27	*Passer montanus (2), Pica pica (2), Carduelis sinica ussuriensis (2), Phylloscopus borealis (3)*
16	10	63	*Passer montanus (35), Pica pica (4), Microscelis amaurotis (6), Streptopelia orientalis (1), Parus major (2), Parus palustris (4), Carduelis sinica ussuriensis (2), Sinosuthora webbiana (3), Urosphena squameiceps (1), Phylloscopus inornatus (5)*
17	7	26	*Passer montanus (17), Pica pica (1), Microscelis amaurotis (1), Streptopelia orientalis (2), Parus major (2), Phylloscopus inornatus (1), Phylloscopus borealis (2)*
18	8	55	*Passer montanus (4), Pica pica (2), Microscelis amaurotis (6), Streptopelia orientalis (3), Phoenicurus auroreus (1), Carduelis sinica ussuriensis (1), Phylloscopus coronatus (1), Phylloscopus inornatus (1)*

Shortest path betweenness centrality

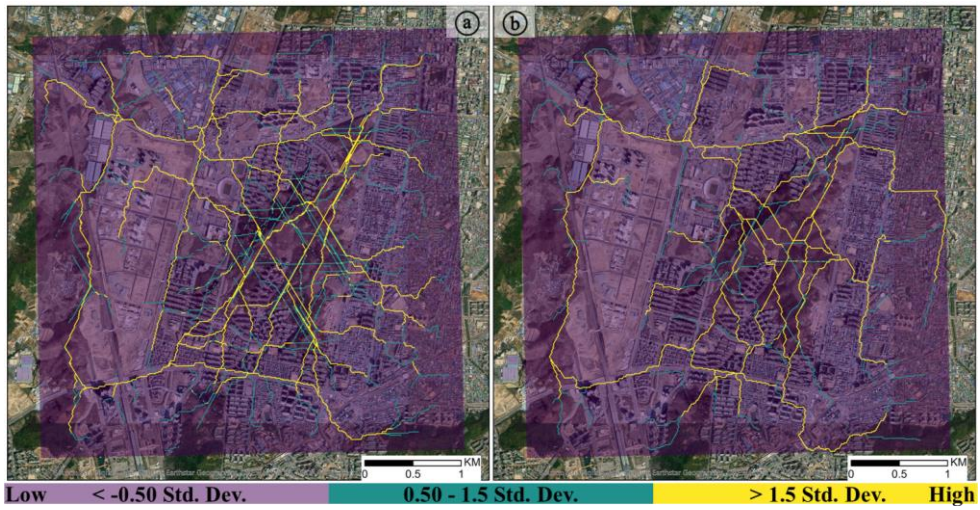

Appendix Figure 1 Z-distribution maps showing the most important pathway (SPBC) derived from the a) 2D permeability map and b) the 3D permeability map. Colors indicate standard deviations from each mean centrality value.

The best single pathways derived from the 2D and 3D SPBCs are shown in Appendix Figure 1. The results of both 2D and 3D SPBCs indicated that core pathways (>0.5 SD) followed boulevards (roads with widths ≥ 25 m) and large green spaces in the center and west (left) portions of the study area. The 2D-based SPBC indicated a core pathway in a dense, highly urbanized area, whereas the 3D-based path did not include this area (Appendix Figure 1). This suggests that green spaces within highly urbanized areas contribute greatly to connectivity when it is assessed in 2D. Moreover, I found that the area of the core pathway (≥0.5 SD) was wider in the 2D SPBC (11,146 grid cells, 5.80% of the study area) than in the 3D SPBC (7,280 grid cells, 3.79% of the study area).

Chapter 5. Conclusion

1. Combination with multiple LiDAR systems for surveying structures of urban green spaces

It is necessary to find common or standard tree structural metrics from the measurements of different LiDAR platforms, and these metrics should be interactively used among the platforms. Moreover, finding common or standard metrics is essential in preventing differences in tree structural metrics from numerous LiDAR platforms that affect the overall monitoring results and cause confusion. Therefore, Chapter 2 attempted to find the consistencies in tree structural variables among the ALS, TLS, and MLS datasets to find alternative structural variables that can be derived from MLS and TLS and applied when ALS datasets are not accessible in urban parks.

My results reveal that ZMAX and CHM-derived structural metrics values showed good agreement among the ALS, TLS, and MLS platforms. These metrics could, therefore, be interchangeable among the three LiDAR systems. ALS-TLS showed better agreement than did the ALS-MLS and TLS-MLS comparisons because the data were acquired on the same dates. The consistency of ZMEAN and Zq95 values between ALS and the other LiDAR systems was low due to the LiDAR scanner locations. There were considerable differences between MLS and the other two LiDAR systems in the values for ZMAX, meanCHM, and area due to the later acquisition date of the MLS data. Although most metrics showed good agreement, errors or differences increased with canopy height and canopy complexity.

This study also emphasized the configuration of LiDAR systems for estimating tree measurements. Depending on the point density and sensing location, the tree measurements could be differently calculated (e.g., ZMEAN and Zq95) and result in different derived outcomes, such as PAI. ZMEAN and Zq95 showed preliminary agreement among the LiDAR systems used in this study. Moreover, in estimating PAI, more factors should be considered in the estimation, and different parameter settings should be required among the ALS and other terrestrial-based systems. Therefore, further studies would be necessary to find methods to alleviate differences in point density and its distribution by different LiDAR configurations. Lastly, using a digital elevation model (DEM) for registering and testing accuracy could enhance the confidence of the comparison results.

Recently, various LiDAR systems, such as the unmanned aerial vehicle laser scanning system and mobile laser scanning system, have been developed. Therefore, there is a great opportunity to combine various LiDAR datasets to monitor tree structures. My results show the potential advantages of combining multiple LiDAR systems to estimate the structural makeup of urban park areas. For example,

researchers have successfully evaluated above-ground biomass by using multiple LiDAR systems, and they recently found that utilizing multiple LiDAR systems at the same time increases the accuracy of tree structure and biomass estimations (Levick et al. 2021; Pyörälä et al. 2019; Zhang and Shao 2021). Given the increasing interest in using multiple LiDAR systems, my results suggest the importance of assessing consistencies among different LiDAR systems before combining multiple LiDAR systems. Finally, as there is an increasing demand for LiDAR technology in urban planning and design and particularly for managing urban green spaces, my results could help when there is a need to fill gaps in datasets in terms of temporal and spatial perspectives.

2. Multi-temporal urban forest gap monitoring

In Chapter 3, I estimated the three-dimensional canopy changes in an urban forest using four-year annual LiDAR datasets. Based on my results, I concluded that the vertical growth rates derived from one-year change detections showed similar values to three-year interval change detection. However, the regions in which the canopies grew up continuously differed according to the grid sizes (pixel- and plot-level grids) and they occupied only 15.9% and 38.9% of the growth areas detected in three-year interval comparison. Moreover, the distributions in VGr, LGr, and damaged areas in the annual change detections showed irregular changes according to the year. These results might indicate that even though three-year interval (or larger) change detection could be a more efficient way to estimate the growth rates in a forest in terms of the costs and efforts, one-year interval change detection with airborne LiDAR datasets would be useful for monitoring and understanding what areas are vulnerable to disturbance (three-year interval change detection might detect open canopies as closed canopies).

I also concluded that the leaf area index showed continuous values year-by-year, while the leaf area profile (e.g., leaf area density) showed irregular yearly changes in both high and low canopies. Among the low canopies, I could conclude that they were vulnerable to physical damage, particularly in AGps. In the case of FGps, they also drove the growth and disturbance aspects of forest dynamics and served to diversify the canopy structure; most of them were closing in a lateral direction by gap-edge trees. Furthermore, high canopies expanded their foliage at a higher height (12 m) than those of low canopies (5 m).

Although I found that the one-year interval change detections showed the potential to achieve detailed information about canopy changes, further study is warranted. For example, since detecting changes in the distribution of canopies might be easily affected by the grid size and the DOY of data acquisitions, an adequate grid size and DOY should be suggested. In particular, in the case of DOY,

seasonal variations in the canopies over a year could be studied with a mobile LiDAR, and this may both hint at the DOY of data acquisition via airborne LiDAR survey and inform about seasonal changes in canopy structures.

3. Ecological connectivity analysis using LiDAR

In Chapter 4, I assessed the urban ecological connectivity by using a LiDAR dataset to evaluate 3D aspect of the urban structures. I found that 3D variables, namely building and vegetation volume, were related to bird diversity in my study area. Building structures including heights, standard deviation of heights, volumes, and areas were negatively correlated with the number of species per unit area. However, vegetation structures including heights, canopy complexity, volumes from 8–10 m heights, and areas were positively correlated with the number of species per unit area.

In 3D connectivity results, the isolated areas are decided by the low density of vegetation and high-density building structures while highly connected areas were detected in sparsely built environment with high tree canopies (>8 m). Moreover, my 3D connectivity results indicated that large green spaces and street trees > 8 m in height act as the key corridors in the study area. Street trees act as major corridors by connecting isolated green spaces patches to larger, more connected patches. Differences between the 2D and 3D connectivity results were substantial in open spaces such as boulevards, forested areas, and apartment complexes. My findings indicate that 3D-based analyses adequately characterize urban building and vegetation structure. This study highlights the value of considering 3D structure in urban planning for ecological networks. Especially, flying species could be affected by the vertical direction of the urbanized areas due to extensive vertical expansion. My findings can be applicable to the network analysis of other urban-dwelling and flying species. I also encourage future studies to assess the effects of changes in the 3D structure on connectivity, assuming applications of green-infrastructure strategies such as roof gardens and green walls.

4. LiDAR application to urban ecosystem monitoring

To monitor urban ecosystems, various spatiotemporal approaches, and advanced remote sensing technologies, such as LiDAR, are required. Chapters 2 to 4 demonstrated the various spatiotemporal applications of the LiDAR dataset; The urban ecosystem structures were quantified using TLS and MLS for the tree-level spatial scale and ALS for the regional-level spatial scale.

The tree metrics calculated in Chapter 2 can be used to assess urban ecosystem structures and their fitness. Furthermore, deriving the tree metrics using a multitemporal LiDAR dataset would enable the investigation of vegetation growth and dynamics. Chapter 3 revealed differences in canopy dynamics by the land use

(i.e., artificial openings and naturally formed gaps) in urban forests. However, acquiring high-temporal-resolution ALS is challenging in terms of cost and operation. The TLS and MLS datasets could offset the gaps in the ALS data of urban forests where frequent disturbances occur and enable consistent monitoring.

The results from the regionals-scale approach in Chapter 4 showed that the distribution of urban components (i.e., vegetation and buildings) impacts ecological connectivity. Applying this approach, urban planners or governors could find ecologically isolated places and make appropriate actions. Furthermore, applying multi-temporal approaches and acquiring a dataset combining TLS and MLS could help in monitoring places where actions need to be implemented.

5. Expanding spatiotemporal scale and further works

In this dissertation, the availability of a 3D dataset was found via three stand-alone studies. I applied LiDAR remote sensing to three different spatiotemporal scales to monitor urban green spaces. I concluded that the 3D information could enhance the quality of urban ecosystem monitoring and ecological connectivity analysis by elaborately explaining spatial structures. However, the spatiotemporal scales of each study were limited to a city scale and within five years. In terms of the environmental monitoring field, this scale-dependent limitation should be overcome to continuously link a city to a national scale and finally to a global scale. Furthermore, long-term monitoring should be done to investigate ecological phenomena (e.g., forest succession) by the fusion of spectral imageries and data processing techniques.

NASA launched the Global Ecosystem Dynamics Investigation (GEDI) mission in 2018, and they provide high-resolution (25 m) 3D structural metrics of the Earth's surface (Dubayah et al. 2020). Furthermore, the GEDI's products include canopy-related variables (e.g., leaf area index, canopy fraction, etc.), above-ground biomass, and biodiversity/habitat model outputs. Therefore, there is great opportunity to expand the spatial and temporal scales of this work by combing it with the GEDI's products. First, since the GEDI's data are brand new, the data used in this dissertation can be used to validate and calibrate the GEDI's products, such as canopy height metrics. Second, with the calibrated GEDI's products and national species observation data, it would be possible to assess ecological connectivity on national, continental, or even global scales. Third, the GEDI's products can be used as link data in a region where the data cannot be easily acquired or when the data is missing.

Future works will focus on finding the relationships between urban landscape structures and their functions using advanced remote sensing and data processing techniques (Figure 5.1). In this dissertation, I concentrated on monitoring and mapping urban ecosystem structures. With these urban ecosystem structures combining other remote sensing and data processing techniques, such as

hyperspectral imageries and high-resolution RGB imageries, I will configure the functions of the urban ecosystem, and classify the urban biotopes or habitats by the structures and functions, spatially. These studies will help assess urban biodiversity and suggest clues about ecological designs and management in urban areas. Lastly, these works will help understand the other ecosystem services in urban areas, such as urban heat reduction and air purification.

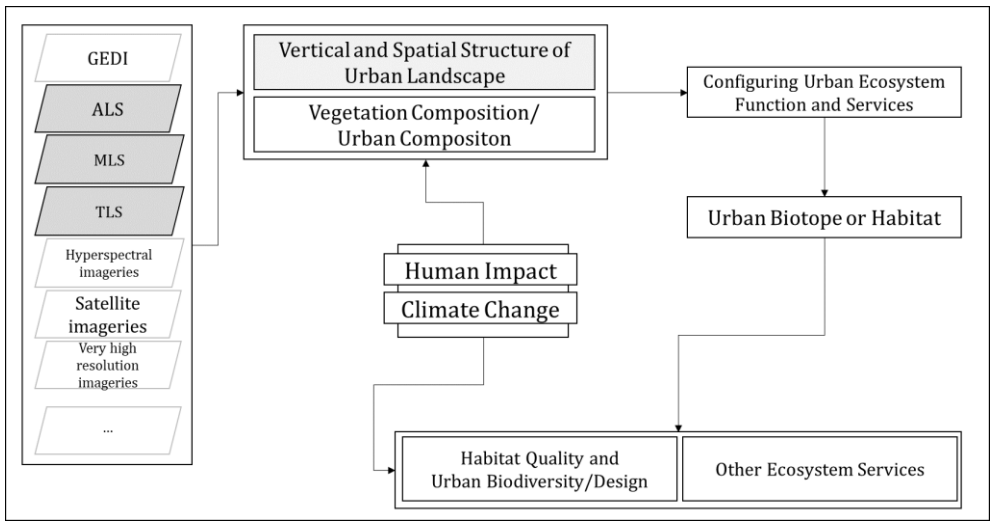

Figure 5.1 Further works after the dissertation (Grey color represents the contents dealt in this dissertation)

Acknowledgments

First, I would like to note my appreciation of my advisor, Prof. Youngkeun Song, for his support of my Ph.D. studies. Thanks to Prof. Song, I had the opportunity to conduct my research under excellent conditions. Furthermore, his sincere advice and guidance on my academic and personal life as a graduate school student greatly encouraged me to persevere. He has inspired me to be confident in my research. I also want to extend my gratitude to my committee members, Prof. Dong-Kun Lee, Prof. Youngryel Ryu, Prof. Junsuk Kang, and Prof. Wanmo Kang, for their outstanding help and direction concerning my academic life at Seoul National University. Thanks to Prof. Dong-Kun Lee, I had a great research experience by participating in a research project. Moreover, his advice always helped me rethink my research implications for deducing meaningful results. I appreciate Prof. Youngryel Ryu for his considerate feedback and direction for my studies and my career. Thanks to Prof. Junsuk Kang, I was able to improve the organization of my dissertation.

I sincerely appreciate Prof. Wanmo Kang at Kookmin University and Dr. James Thorne at the University of California, Davis, for their incredible guidance in publishing Chapter 4 of this dissertation. Their interest and direction for my studies immensely helped me develop my research ability. I thank Satoshi Miyasaka, Masanobu Kondo, and Yoshimichi Senda for training me in LiDAR processing at Nakanihon Air Service Co., Ltd., Nagoya, Japan.

I would also like to thank the lab members of the Landscape and Ecological Planning Lab for their assistance. I especially extend my gratitude to Jonghee Kim, who enables me to overcome difficulties and makes me happy.

Finally, I appreciate my parents, brother, and Dodam for their full support and trust in me during my academic career and life.

Funding: Contents of this dissertation were supported by the National Research Foundation of Korea (NRF) grant funded by the Korea government (Ministry of Education) (No. NRF-2016R1D1A1B03933179), the Korea Environment Industry & Technology Institute (KEITI) through its "*Public Technology Program based on Environmental Policy"* (No. 2016000210004) and "*Urban Ecological Health Promotion Technology Development Project"* (No. 2019002770001 and 2020002770002) and funded by the Korea Ministry of Environment (MOE). Additionally, this work was supported by the BK21 plus Project from 2018-2020 (Seoul National University Interdisciplinary Program in Landscape Architecture, Global Leadership Program towards Innovative Green Infrastructure).

Reference

Alexander, C., Korstjens, A.H., & Hill, R.A. (2018). Influence of micro-topography and crown characteristics on tree height estimations in tropical forests based on LiDAR canopy height models. *International Journal of Applied Earth Observation and Geoinformation, 65*, 105-113

Almeida, D., Stark, S., Chazdon, R., Nelson, B., Cesar, R., Meli, P., Gorgens, E., Duarte, M., Valbuena, R., & Moreno, V. (2019). The effectiveness of lidar remote sensing for monitoring forest cover attributes and landscape restoration. *Forest Ecology and Management, 438*, 34-43

Andersen, H.-E., Reutebuch, S.E., & McGaughey, R.J. (2006). A rigorous assessment of tree height measurements obtained using airborne lidar and conventional field methods. *Canadian Journal of Remote Sensing, 32*, 355-366

Andersson, E., & Bodin, O. (2009). Practical tool for landscape planning? An empirical investigation of network based models of habitat fragmentation. *Ecography, 32*, 123-132

Asner, G.P. (2013). Geography of forest disturbance. *Proceedings of the National Academy of Sciences, 110*, 3711-3712

Asner, G.P., Kellner, J.R., Kennedy-Bowdoin, T., Knapp, D.E., Anderson, C., & Martin, R.E. (2013). Forest Canopy Gap Distributions in the Southern Peruvian Amazon. *PLoS One, 8*, 10

Barton, J., & Pretty, J. (2010). What is the Best Dose of Nature and Green Exercise for Improving Mental Health? A Multi-Study Analysis. *Environmental Science & Technology, 44*, 3947-3955

Bater, C.W., Wulder, M.A., Coops, N.C., Nelson, R.F., Hilker, T., & Nasset, E. (2011). Stability of Sample-Based Scanning-LiDAR-Derived Vegetation Metrics for Forest Monitoring. *IEEE Transactions on Geoscience and Remote Sensing, 49*, 2385-2392

Bauwens, S., Bartholomeus, H., Calders, K., & Lejeune, P. (2016). Forest Inventory with Terrestrial LiDAR: A Comparison of Static and Hand-Held Mobile Laser Scanning. *Forests, 7*, 17

Bazezew, M.N., Hussin, Y.A., & Kloosterman, E.H. (2018). Integrating Airborne LiDAR and Terrestrial Laser Scanner forest parameters for accurate above-ground biomass/carbon estimation in Ayer Hitam tropical forest, Malaysia. *International Journal of Applied Earth Observation and Geoinformation, 73*, 638-652

Bibby, C., Hill, D., Burgess, N., & Mustoe, S. (2000). Bird Census Technique. –Academic Press. In: London

Bienert, A., Georgi, L., Kunz, M., Maas, H.G., & von Oheimb, G. (2018). Comparison and Combination of Mobile and Terrestrial Laser Scanning for Natural Forest Inventories. *Forests, 9*, 25

Bolund, P., & Hunhammar, S. (1999). Ecosystem services in urban areas. *Ecological Economics, 29*, 293-301

Bouvier, M., Durrieu, S., Fournier, R.A., & Renaud, J.-P. (2015). Generalizing predictive models of forest inventory attributes using an area-based approach with airborne LiDAR data. *Remote Sensing of Environment, 156*, 322-334

Cao, L., Coops, N.C., Innes, J.L., Sheppard, S.R.J., Fu, L., Ruan, H., & She, G. (2016). Estimation of forest biomass dynamics in subtropical forests using multi-temporal airborne LiDAR data. *Remote Sensing of Environment, 178*, 158-171

Carroll, C., McRAE, B.H., & BROOKES, A. (2012). Use of Linkage Mapping and Centrality Analysis Across Habitat Gradients to Conserve Connectivity of Gray Wolf Populations in Western North America. *Conservation Biology, 26*, 78-87

Casalegno, S., Anderson, K., Cox, D.T.C., Hancock, S., & Gaston, K.J. (2017). Ecological

connectivity in the three-dimensional urban green volume using waveform airborne lidar. *Scientific Reports, 7*, 45571

Cerra, J.F., & Crain, R. (2016). Urban birds and planting design: strategies for incorporating ecological goals into residential landscapes. *Urban Ecosystems, 19*, 1823-1846

Chen, Z., Xu, B., & Devereux, B. (2014). Urban landscape pattern analysis based on 3D landscape models. *Applied Geography, 55*, 82-91

Chiquet, C., Dover, J.W., & Mitchell, P. (2013). Birds and the urban environment: the value of green walls. *Urban Ecosystems, 16*, 453-462

Choe, H., & Thorne, J.H. (2019). Omnidirectional connectivity of urban open spaces provides context for local government redevelopment plans. *Landscape and Ecological Engineering, 15*, 245-251

Choi, H., Song, Y., & Jang, Y. (2019). Urban Forest Growth and Gap Dynamics Detected by Yearly Repeated Airborne Light Detection and Ranging (LiDAR): A Case Study of Cheonan, South Korea. *Remote Sensing, 11*

Conole, L.E., & Kirkpatrick, J.B. (2011). Functional and spatial differentiation of urban bird assemblages at the landscape scale. *Landscape and Urban Planning, 100*, 11-23

Conto, d. (2020). TreeLS: Terrestrial Point Cloud Processing of Forest Data

Cook, E.A. (2002). Landscape structure indices for assessing urban ecological networks. *Landscape and Urban Planning, 58*, 269-280

Coops, N.C., Tompaski, P., Nijland, W., Rickbeil, G.J.M., Nielsen, S.E., Bater, C.W., & Stadt, J.J. (2016). A forest structure habitat index based on airborne laser scanning data. *Ecological Indicators, 67*, 346-357

Cumming, A.B., Twardus, D.B., & Nowak, D.J. (2008). Urban forest health monitoring: large-scale assessments in the United States. *Aboriculture & Urban Forestry. 34 (6): 341-346., 34*

D'Urban Jackson, T., Williams, G.J., Walker-Springett, G., & Davies, A.J. (2020). Three-dimensional digital mapping of ecosystems: a new era in spatial ecology. *Proceedings of the Royal Society B, 287*, 20192383

Dalagnol, R., Phillips, O.L., Gloor, E., Galvão, L.S., Wagner, F.H., Locks, C.J., & Aragão, L.E. (2019). Quantifying Canopy Tree Loss and Gap Recovery in Tropical Forests under Low-Intensity Logging Using VHR Satellite Imagery and Airborne LiDAR. *Remote Sensing, 11*, 817

Dalponte, M., Jucker, T., Liu, S., Frizzera, L., & Gianelle, D. (2019). Characterizing forest carbon dynamics using multi-temporal lidar data. *Remote Sensing of Environment, 224*, 412-420

Dickson, B.G., Albano, C.M., Anantharaman, R., Beier, P., Fargione, J., Graves, T.A., Gray, M.E., Hall, K.R., Lawler, J.J., & Leonard, P.B. (2019). Circuit-theory applications to connectivity science and conservation. *Conservation Biology, 33*, 239-249

Dubayah, R., Blair, J.B., Goetz, S., Fatoyinbo, L., Hansen, M., Healey, S., Hofton, M., Hurtt, G., Kellner, J., & Luthcke, S. (2020). The Global Ecosystem Dynamics Investigation: High-resolution laser ranging of the Earth's forests and topography. *Science of Remote Sensing, 1*, 100002

Eitel, J.U.H., Höfle, B., Vierling, L.A., Abellán, A., Asner, G.P., Deems, J.S., Glennie, C.L., Joerg, P.C., LeWinter, A.L., Magney, T.S., Mandlburger, G., Morton, D.C., Müller, J., & Vierling, K.T. (2016). Beyond 3-D: The new spectrum of lidar applications for earth and ecological sciences. *Remote Sensing of Environment, 186*, 372-392

Evans, J.S., Hudak, A.T., Faux, R., & Smith, A.M.S. (2009a). Discrete Return Lidar in Natural Resources: Recommendations for Project Planning, Data Processing, and Deliverables. *Remote Sensing, 1*, 776-794

Evans, K.L., Newson, S.E., & Gaston, K.J. (2009b). Habitat influences on urban avian assemblages. *Ibis, 151*, 19-39

Farinha-Marques, P., Fernandes, C., Guilherme, F., Lameiras, J.M., Alves, P., & Bunce, R.G.H. (2017). Urban Habitats Biodiversity Assessment (UrHBA): a standardized procedure for recording biodiversity and its spatial distribution in urban

environments. *Landscape Ecology, 32*, 1753-1770
Fisher, J.I., Hurtt, G.C., Thomas, R.Q., & Chambers, J.Q. (2008). Clustered disturbances lead to bias in large-scale estimates based on forest sample plots. *Ecology Letters, 11*, 554-563
Fontana, S., Sattler, T., Bontadina, F., & Moretti, M. (2011). How to manage the urban green to improve bird diversity and community structure. *Landscape and Urban Planning, 101*, 278-285
Goddard, M.A., Dougill, A.J., & Benton, T.G. (2010). Scaling up from gardens: biodiversity conservation in urban environments. *Trends in Ecology & Evolution, 25*, 90-98
Goodwin, N.R., Coops, N.C., & Culvenor, D.S. (2006). Assessment of forest structure with airborne LiDAR and the effects of platform altitude. *Remote Sensing of Environment, 103*, 140-152
Grafius, D.R., Corstanje, R., Siriwardena, G.M., Plummer, K.E., & Harris, J.A. (2017). A bird's eye view: using circuit theory to study urban landscape connectivity for birds. *Landscape Ecology, 32*, 1771-1787
Guo, S., Saito, K., Yin, W., & Su, C. (2018). Landscape Connectivity as a Tool in Green Space Evaluation and Optimization of the Haidan District, Beijing. *Sustainability, 10*, 1979
Haaland, C., & van den Bosch, C.K. (2015). Challenges and strategies for urban green-space planning in cities undergoing densification: A review. *Urban Forestry & Urban Greening, 14*, 760-771
Hale, J.D., Fairbrass, A.J., Matthews, T.J., & Sadler, J.P. (2012). Habitat Composition and Connectivity Predicts Bat Presence and Activity at Foraging Sites in a Large UK Conurbation. *PLoS One, 7*, e33300
Heo, H.K., Lee, D.K., Park, J.H., & Thorne, J.H. (2019). Estimating the heights and diameters at breast height of trees in an urban park and along a street using mobile LiDAR. *Landscape and Ecological Engineering*, 1-11
Hilker, T., Coops, N.C., Newnham, G.J., van Leeuwen, M., Wulder, M.A., Stewart, J., & Culvenor, D.S. (2012). Comparison of Terrestrial and Airborne LiDAR in Describing Stand Structure of a Thinned Lodgepole Pine Forest. *Journal of Forestry, 110*, 97-104
Hilker, T., van Leeuwen, M., Coops, N.C., Wulder, M.A., Newnham, G.J., Jupp, D.L., & Culvenor, D.S. (2010). Comparing canopy metrics derived from terrestrial and airborne laser scanning in a Douglas-fir dominated forest stand. *Trees, 24*, 819-832
Hopkinson, C., Chasmer, L., & Hall, R.J. (2008). The uncertainty in conifer plantation growth prediction from multi-temporal lidar datasets. *Remote Sensing of Environment, 112*, 1168-1180
Hosoi, F., & Omasa, K. (2009). Estimating vertical plant area density profile and growth parameters of a wheat canopy at different growth stages using three-dimensional portable lidar imaging. *ISPRS Journal of Photogrammetry and Remote Sensing, 64*, 151-158
Hyyppä, E., Kukko, A., Kaijaluoto, R., White, J.C., Wulder, M.A., Pyörälä, J., Liang, X., Yu, X., Wang, Y., Kaartinen, H., Virtanen, J.-P., & Hyyppä, J. (2020). Accurate derivation of stem curve and volume using backpack mobile laser scanning. *ISPRS Journal of Photogrammetry and Remote Sensing, 161*, 246-262
Ishii, H.T., Tanabe, S., & Hiura, T. (2004). Exploring the relationships among canopy structure, stand productivity, and biodiversity of temperate forest ecosystems. *Forest Science, 50*, 342-355
Jenness, J.S. (2004). Calculating landscape surface area from digital elevation models. *Wildlife Society Bulletin, 32*, 829-839
Jonckheere, I., Fleck, S., Nackaerts, K., Muys, B., Coppin, P., Weiss, M., & Baret, F. (2004). Review of methods for in situ leaf area index determination. *Agricultural and Forest Meteorology, 121*, 19-35
Kane, V.R., Gersonde, R.F., Lutz, J.A., McGaughey, R.J., Bakker, J.D., & Franklin, J.F.

(2011). Patch dynamics and the development of structural and spatial heterogeneity in Pacific Northwest forests. *Canadian Journal of Forest Research, 41*, 2276-2291

Kane, V.R., McGaughey, R.J., Bakker, J.D., Gersonde, R.F., Lutz, J.A., & Franklin, J.F. (2010). Comparisons between field- and LiDAR-based measures of stand structural complexity. *Canadian Journal of Forest Research, 40*, 761-773

Kang, W., Minor, E.S., Park, C.-R., & Lee, D. (2015). Effects of habitat structure, human disturbance, and habitat connectivity on urban forest bird communities. *Urban Ecosystems, 18*, 857-870

Kedron, P., Zhao, Y., & Frazier, A.E. (2019). Three dimensional (3D) spatial metrics for objects. *Landscape Ecology, 34*, 2123-2132

Kellner, J.R., & Asner, G.P. (2009). Convergent structural responses of tropical forests to diverse disturbance regimes. *Ecology Letters, 12*, 887-897

Khosravipour, A., Skidmore, A.K., Wang, T., Isenburg, M., & Khoshelham, K. (2015). Effect of slope on treetop detection using a LiDAR Canopy Height Model. *ISPRS Journal of Photogrammetry and Remote Sensing, 104*, 44-52

Kim, E., Song, W., & Lee, D. (2013). A multi-scale metrics approach to forest fragmentation for Strategic Environmental Impact Assessment. *Environmental Impact Assessment Review, 42*, 31-38

Kim, K.-H., & Pauleit, S. (2009). Woodland changes and their impacts on the landscape structure in South Korea, Kwangju City Region. *Landscape Research, 34*, 257-277

Kindlmann, P., & Burel, F. (2008). Connectivity measures: a review. *Landscape Ecology, 23*, 879-890

Koo, J.-C., Park, M.S., & Youn, Y.-C. (2013). Preferences of urban dwellers on urban forest recreational services in South Korea. *Urban Forestry & Urban Greening, 12*, 200-210

Krooks, A., Kaasalainen, S., Kankare, V., Joensuu, M., Raumonen, P., & Kaasalainen, M. (2014). *Predicting tree structure from tree height using terrestrial laser scanning and quantitative structure models*.

Lai, S., & Leone, F. (2017). Bridging biodiversity conservation objectives with landscape planning through green infrastructures: a case study from Sardinia, Italy. In, *International Conference on Computational Science and Its Applications* (pp. 456-472): Springer

LaRue, E.A., Wagner, F.W., Fei, S., Atkins, J.W., Fahey, R.T., Gough, C.M., & Hardiman, B.S. (2020). Compatibility of aerial and terrestrial LiDAR for quantifying forest structural diversity. *Remote Sensing, 12*, 1407

Latifi, H., Heurich, M., Hartig, F., Müller, J., Krzystek, P., Jehl, H., & Dech, S. (2016). Estimating over- and understorey canopy density of temperate mixed stands by airborne LiDAR data. *Forestry: An International Journal of Forest Research, 89*, 69-81

Lee, D.K., Park, C., Kim, E.Y., Song, W.K., & Choe, H.Y. (2009). Classification of Urban Forest Types and its Application Methods for Forests Creation and Management. Journal of the Korea Society of Environmental Restoration Technology. *Journal of the Korea Society of Environmental Restoration Technology, 12*, 101-109

Lee, J.-D., & Kim, M.-H. (2010). Development and practicability evaluation of GIS-based cemetery information management system. *Journal of the Korean Society of Surveying, Geodesy, Photogrammetry and Cartography, 28*, 223-231

Lefsky, M.A., Cohen, W.B., Parker, G.G., & Harding, D.J. (2002). Lidar Remote Sensing for Ecosystem StudiesLidar, an emerging remote sensing technology that directly measures the three-dimensional distribution of plant canopies, can accurately estimate vegetation structural attributes and should be of particular interest to forest, landscape, and global ecologists. *BioScience, 52*, 19-30

Lepczyk, C.A., Aronson, M.F.J., Evans, K.L., Goddard, M.A., Lerman, S.B., & MacIvor, J.S. (2017). Biodiversity in the City: Fundamental Questions for Understanding the Ecology of Urban Green Spaces for Biodiversity Conservation. *BioScience, 67*,

799-807
Lepczyk, C.A., Wedding, L.M., Asner, G.P., Pittman, S.J., Goulden, T., Linderman, M.A., Gang, J., & Wright, R. (2021). Advancing Landscape and Seascape Ecology from a 2D to a 3D Science. *BioScience*
Levick, S., Whiteside, T., Loewensteiner, D., Rudge, M., & Bartolo, R. (2021). Leveraging TLS as a Calibration and Validation Tool for MLS and ULS Mapping of Savanna Structure and Biomass at Landscape-Scales. *Remote Sensing, 13*, 257
Li, Y., Kang, W., Han, Y., & Song, Y. (2018). Spatial and temporal patterns of microclimates at an urban forest edge and their management implications. *Environmental monitoring and assessment, 190*, 93
Liang, D., Ma, C., Wang, Y.Q., Wang, Y.J., & Zhao, C.X. (2016a). Quantifying PM2.5 capture capability of greening trees based on leaf factors analyzing. *Environmental Science and Pollution Research, 23*, 21176-21186
Liang, X.L., Kankare, V., Hyyppa, J., Wang, Y.S., Kukko, A., Haggren, H., Yu, X.W., Kaartinen, H., Jaakkola, A., Guan, F.Y., Holopainen, M., & Vastaranta, M. (2016b). Terrestrial laser scanning in forest inventories. *ISPRS Journal of Photogrammetry and Remote Sensing, 115*, 63-77
Liu, X., Zhou, Y.Y., Yue, W.Z., Li, X.C., Liu, Y., & Lu, D.B. (2020a). Spatiotemporal patterns of summer urban heat island in Beijing, China using an improved land surface temperature. *Journal of Cleaner Production, 257*
Liu, Y., Wang, Y., Peng, J., Du, Y., Liu, X., Li, S., & Zhang, D. (2015). Correlations between Urbanization and Vegetation Degradation across the World's Metropolises Using DMSP/OLS Nighttime Light Data*, 7*, 2067-2088
Liu, Z., Huang, Q., & Tang, G. (2020b). Identification of urban flight corridors for migratory birds in the coastal regions of Shenzhen city based on three-dimensional landscapes. *Landscape Ecology*
Maddern, W., Pascoe, G., Linegar, C., & Newman, P. (2017). 1 year, 1000 km: The Oxford RobotCar dataset. *International Journal of Robotics Research, 36*, 3-15
Magnussen, S., Næsset, E., Gobakken, T., & Frazer, G. (2012). A fine-scale model for area-based predictions of tree-size-related attributes derived from LiDAR canopy heights. *Scandinavian Journal of Forest Research, 27*, 312-322
Matsuba, M., Nishijima, S., & Katoh, K. (2016). Effectiveness of corridor vegetation depends on urbanization tolerance of forest birds in central Tokyo, Japan. *Urban Forestry & Urban Greening, 18*, 173-181
Mayrand, F., & Clergeau, P. (2018). Green roofs and green walls for biodiversity conservation: a contribution to urban connectivity? *Sustainability, 10*, 985
McRae, B.H., Dickson, B.G., Keitt, T.H., & Shah, V.B. (2008). USING CIRCUIT THEORY TO MODEL CONNECTIVITY IN ECOLOGY, EVOLUTION, AND CONSERVATION*, 89*, 2712-2724
McWilliam, W., Eagles, P., Seasons, M., & Brown, R. (2010). Assessing the degradation effects of local residents on urban forests in Ontario, Canada. *Journal of Arboriculture, 36*, 253
Melin, M., Hinsley, S.A., Broughton, R.K., Bellamy, P., & Hill, R.A. (2018). Living on the edge: utilising lidar data to assess the importance of vegetation structure for avian diversity in fragmented woodlands and their edges. *Landscape Ecology, 33*, 895-910
Morelli, F., Beim, M., Jerzak, L., Jones, D., & Tryjanowski, P. (2014). Can roads, railways and related structures have positive effects on birds? - A review. *Transportation Research Part D-Transport and Environment, 30*, 21-31
Nadrowski, K., Wirth, C., & Scherer-Lorenzen, M. (2010). Is forest diversity driving ecosystem function and service? *Current Opinion in Environmental Sustainability, 2*, 75-79
Naesset, E. (1997). Determination of mean tree height of forest stands using airborne laser scanner data. *ISPRS Journal of Photogrammetry and Remote Sensing, 52*, 49-56

Nor, A.N.M., Corstanje, R., Harris, J.A., Grafius, D.R., & Siriwardena, G.M. (2017). Ecological connectivity networks in rapidly expanding cities. *Heliyon, 3*

Ojoatre, S., Zhang, C., Hussin, Y.A., Kloosterman, H.E., & Ismail, M.H. (2019). Assessing the Uncertainty of Tree Height and Aboveground Biomass From Terrestrial Laser Scanner and Hypsometer Using Airborne LiDAR Data in Tropical Rainforests. *IEEE Journal of Selected Topics in Applied Earth Observations and Remote Sensing, 12*, 4149-4159

Oldfield, E.E., Felson, A.J., Auyeung, D.S.N., Crowther, T.W., Sonti, N.F., Harada, Y., Maynard, D.S., Sokol, N.W., Ashton, M.S., Warren II, R.J., Hallett, R.A., & Bradford, M.A. (2015). Growing the urban forest: tree performance in response to biotic and abiotic land management. *Restoration Ecology, 23*, 707-718

Omasa, K., Hosoi, F., & Konishi, A. (2006). 3D lidar imaging for detecting and understanding plant responses and canopy structure. *Journal of Experimental Botany, 58*, 881-898

Ossola, A., & Hopton, M.E. (2018a). Climate differentiates forest structure across a residential macrosystem. *Science of the Total Environment, 639*, 1164-1174

Ossola, A., & Hopton, M.E. (2018b). Measuring urban tree loss dynamics across residential landscapes. *Science of the Total Environment, 612*, 940-949

Pandey, G., McBride, J.R., & Eustice, R.M. (2011). Ford Campus vision and lidar data set. *International Journal of Robotics Research, 30*, 1543-1552

Park, M., & Lee, H. (2014). Forest policy and law for sustainability within the Korean Peninsula. *Sustainability, 6*, 5162-5186

Parker, G.G., Harmon, M.E., Lefsky, M.A., Chen, J., Pelt, R.V., Weis, S.B., Thomas, S.C., Winner, W.E., Shaw, D.C., & Frankling, J.F. (2004). Three-dimensional Structure of an Old-growth Pseudotsuga-Tsuga Canopy and Its Implications for Radiation Balance, Microclimate, and Gas Exchange. *Ecosystems, 7*, 440-453

Plowright, A.A., Coops, N.C., Chance, C.M., Sheppard, S.R., & Aven, N.W. (2017). Multi-scale analysis of relationship between imperviousness and urban tree height using airborne remote sensing. *Remote Sensing of Environment, 194*, 391-400

Plummer, K.E., Gillings, S., & Siriwardena, G.M. (2020). Evaluating the potential for bird-habitat models to support biodiversity-friendly urban planning. *Journal of Applied Ecology, 57*, 1902-1914

Pyörälä, J., Saarinen, N., Kankare, V., Coops, N.C., Liang, X., Wang, Y., Holopainen, M., Hyyppä, J., & Vastaranta, M. (2019). Variability of wood properties using airborne and terrestrial laser scanning. *Remote Sensing of Environment, 235*, 111474

Rangel Pinagé, E., Keller, M., Duffy, P., Longo, M., dos-Santos, M.N., & Morton, D.C. (2019). Long-Term Impacts of Selective Logging on Amazon Forest Dynamics from Multi-Temporal Airborne LiDAR. *Remote Sensing, 11*, 709

Roussel, J.-R., Auty, D., Coops, N.C., Tompalski, P., Goodbody, T.R.H., Meador, A.S., Bourdon, J.-F., de Boissieu, F., & Achim, A. (2020). lidR: An R package for analysis of Airborne Laser Scanning (ALS) data. *Remote Sensing of Environment, 251*, 112061

Roussel, J.-R., Caspersen, J., Béland, M., Thomas, S., & Achim, A. (2017). Removing bias from LiDAR-based estimates of canopy height: Accounting for the effects of pulse density and footprint size. *Remote Sensing of Environment, 198*, 1-16

Runkle, J.R. (1992). *Guidelines and sample protocol for sampling forest gaps*.

Runkle, J.R., & Yetter, T.C. (1987). Treefalls Revisited: Gap Dynamics in the Southern Appalachians. *Ecology, 68*, 417-424

Rutten, G., Ensslin, A., Hemp, A., & Fischer, M. (2015). Vertical and Horizontal Vegetation Structure across Natural and Modified Habitat Types at Mount Kilimanjaro. *PLoS One, 10*, e0138822

Ryu, J., Hwang, J., Lee, J., Chung, H.-I., Lee, K.-i., Choi, Y.-Y., Zhu, Y., Sung, M.-J., Jang, R., & Sung, H.-C. (2017). Analysis of changes in forest according to urban expansion pattern and morphological features-Focused on Seoul and Daegu. *Korean Journal of Remote Sensing, 33*, 835-854

Sahraoui, Y., De Godoy Leski, C., Benot, M.-L., Revers, F., Salles, D., van Halder, I., Barneix, M., & Carassou, L. (2021). Integrating ecological networks modelling in a participatory approach for assessing impacts of planning scenarios on landscape connectivity. *Landscape and Urban Planning, 209*, 104039

Sandström, U., Angelstam, P., & Mikusiński, G. (2006). Ecological diversity of birds in relation to the structure of urban green space. *Landscape and Urban Planning, 77*, 39-53

Sandstrom, U.G., Angelstam, P., & Mikusinski, G. (2006). Ecological diversity of birds in relation to the structure of urban green space. *Landscape and Urban Planning, 77*, 39-53

Sasaki, T., Imanishi, J., Ioki, K., Morimoto, Y., & Kitada, K. (2008). Estimation of leaf area index and canopy openness in broad-leaved forest using an airborne laser scanner in comparison with high-resolution near-infrared digital photography. *Landscape and Ecological Engineering, 4*, 47-55

Sasaki, T., Imanishi, J., Ioki, K., Song, Y., & Morimoto, Y. (2013). Estimation of leaf area index and gap fraction in two broad-leaved forests by using small-footprint airborne LiDAR. *Landscape and Ecological Engineering, 12*, 117-127

Savard, J.-P.L., Clergeau, P., & Mennechez, G. (2000). Biodiversity concepts and urban ecosystems. *Landscape and Urban Planning, 48*, 131-142

Schneider, F.D., Kükenbrink, D., Schaepman, M.E., Schimel, D.S., & Morsdorf, F. (2019). Quantifying 3D structure and occlusion in dense tropical and temperate forests using close-range LiDAR. *Agricultural and Forest Meteorology, 268*, 249-257

Shao, G., Stark, S.C., de Almeida, D.R.A., & Smith, M.N. (2019). Towards high throughput assessment of canopy dynamics: The estimation of leaf area structure in Amazonian forests with multitemporal multi-sensor airborne lidar. *Remote Sensing of Environment, 221*, 1-13

Smith, M.N., Stark, S.C., Taylor, T.C., Ferreira, M.L., de Oliveira, E., Restrepo-Coupe, N., Chen, S., Woodcock, T., dos Santos, D.B., Alves, L.F., Figueira, M., de Camargo, P.B., de Oliveira, R.C., Aragão, L.E.O.C., Falk, D.A., McMahon, S.M., Huxman, T.E., & Saleska, S.R. (2019). Seasonal and drought-related changes in leaf area profiles depend on height and light environment in an Amazon forest. *New Phytologist, 222*, 1284-1297

Song, W. (2015). Analysis of Bird Species Diversity Response to Structural Conditions of Urban Park -Focused on 26 Urban Parks in Cheonan City-. *Journal of the Korea Society of Environmental Restoration Technology, 18*, 65-77

Song, W. (2017). Analysis of Bird Diversity According to Landscape Connectivity and Structure of Urban Park. *Journal of the Korea Society of Environmental Restoration Technology, 20*, 131-142

Song, Y., Imanishi, J., Sasaki, T., Ioki, K., & Morimoto, Y. (2016). Estimation of broad-leaved canopy growth in the urban forested area using multi-temporal airborne LiDAR datasets. *Urban Forestry & Urban Greening, 16*, 142-149

Song, Y., & Ryu, Y. (2015). Seasonal changes in vertical canopy structure in a temperate broadleaved forest in Korea. *Ecological Research, 30*, 821-831

St-Onge, B., Vepakomma, U., Sénécal, J.-F., Kneeshaw, D., & Doyon, F. (2014). Canopy Gap Detection and Analysis with Airborne Laser Scanning. In M. Maltamo, E. Næsset, & J. Vauhkonen (Eds.), *Forestry Applications of Airborne Laser Scanning: Concepts and Case Studies* (pp. 419-437). Dordrecht: Springer Netherlands

Steenberg, J.W., Millward, A.A., Nowak, D.J., & Robinson, P.J. (2016). A conceptual framework of urban forest ecosystem vulnerability. *Environmental Reviews, 25*, 115-126

Su, Y., Guo, Q., Jin, S., Guan, H., Sun, X., Ma, Q., Hu, T., Wang, R., & Li, Y. (2020). The Development and Evaluation of a Backpack LiDAR System for Accurate and Efficient Forest Inventory. *IEEE Geoscience and Remote Sensing Letters*, 1-5

Tattoni, C., & Ciolli, M. (2019). Analysis of Bird Flyways in 3D. *Isprs International Journal*

of Geo-Information, 8, 535
Thompson, I.D., Maher, S.C., Rouillard, D.P., Fryxell, J.M., & Baker, J.A. (2007). Accuracy of forest inventory mapping: some implications for boreal forest management. *Forest Ecology and Management, 252*, 208-221
Tian, Y., Liu, Y., Jim, C., & Song, H. (2017). Assessing Structural Connectivity of Urban Green Spaces in Metropolitan Hong Kong. *Sustainability, 9*, 1653
Tian, Y., Zhou, W., Qian, Y., Zheng, Z., & Yan, J. (2019). The effect of urban 2D and 3D morphology on air temperature in residential neighborhoods. *Landscape Ecology, 34*, 1161-1178
Urban, D., & Keitt, T. (2001). LANDSCAPE CONNECTIVITY: A GRAPH-THEORETIC PERSPECTIVE. *Ecology, 82*, 1205-1218
Valverde, T., & Silvertown, J. (1997). Canopy closure rate and forest structure. *Ecology, 78*, 1555-1562
Vaughn, N.R., Asner, G.P., & Giardina, C.P. (2015). Long-term fragmentation effects on the distribution and dynamics of canopy gaps in a tropical montane forest. *Ecosphere, 6*, 1-15
Vepakomma, U., D Kneeshaw, D., & De Grandpre, L. (2018). *Influence of Natural and Anthropogenic Linear Canopy Openings on Forest Structural Patterns Investigated Using LiDAR*.
Vepakomma, U., Kneeshaw, D., & Fortin, M.J. (2012). Spatial contiguity and continuity of canopy gaps in mixed wood boreal forests: persistence, expansion, shrinkage and displacement. *Journal of Ecology, 100*, 1257-1268
Vepakomma, U., St-Onge, B., & Kneeshaw, D. (2008). Spatially explicit characterization of boreal forest gap dynamics using multi-temporal lidar data. *Remote Sensing of Environment, 112*, 2326-2340
Vepakomma, U., St-Onge, B., & Kneeshaw, D. (2011). Response of a boreal forest to canopy opening: Assessing vertical and lateral tree growth with multi-temporal lidar data. *Ecological Applications, 21*, 99-121
Wang, Y., & Fang, H. (2020). Estimation of LAI with the LiDAR Technology: A Review. *Remote Sensing, 12*, 3457
Wang, Y., Lehtomäki, M., Liang, X., Pyörälä, J., Kukko, A., Jaakkola, A., Liu, J., Feng, Z., Chen, R., & Hyyppä, J. (2019). Is field-measured tree height as reliable as believed – A comparison study of tree height estimates from field measurement, airborne laser scanning and terrestrial laser scanning in a boreal forest. *ISPRS Journal of Photogrammetry and Remote Sensing, 147*, 132-145
White, J., Stepper, C., Tompalski, P., Coops, N., & Wulder, M. (2015). Comparing ALS and Image-Based Point Cloud Metrics and Modelled Forest Inventory Attributes in a Complex Coastal Forest Environment. *Forests, 6*, 3704
White, J.C., Coops, N.C., Wulder, M.A., Vastaranta, M., Hilker, T., & Tompalski, P. (2016). Remote Sensing Technologies for Enhancing Forest Inventories: A Review. *Canadian Journal of Remote Sensing, 42*, 619-641
Whitehurst, A., Swatantran, A., Blair, J., Hofton, M., & Dubayah, R. (2013). Characterization of Canopy Layering in Forested Ecosystems Using Full Waveform Lidar. *Remote Sensing, 5*, 2014-2036
Whitmore, T.C. (1989). Canopy Gaps and the Two Major Groups of Forest Trees. *Ecology, 70*, 536-538
Wu, D., Johansen, K., Phinn, S., Robson, A., & Tu, Y.H. (2020). Inter-comparison of remote sensing platforms for height estimation of mango and avocado tree crowns. *International Journal of Applied Earth Observation and Geoinformation, 89*, 15
Xie, S., Lu, F., Cao, L., Zhou, W., & Ouyang, Z. (2016). Multi-scale factors influencing the characteristics of avian communities in urban parks across Beijing during the breeding season. *Scientific Reports, 6*
Yamamoto, S.-I. (2000). Forest gap dynamics and tree regeneration. *Journal of forest research, 5*, 223-229

Youn, Y.-C. (2009). Use of forest resources, traditional forest-related knowledge and livelihood of forest dependent communities: Cases in South Korea. *Forest Ecology and Management, 257*, 2027-2034

Yu, X., Hyyppa, J., Kaartinen, H., Maltamo, M., & Hyyppa, H. (2008). Obtaining plotwise mean height and volume growth in boreal forests using multi-temporal laser surveys and various change detection techniques. *International Journal of Remote Sensing, 29*, 1367-1386

Zeller, K.A., McGarigal, K., & Whiteley, A.R. (2012). Estimating landscape resistance to movement: a review. *Landscape Ecology, 27*, 777-797

Zhang, J., Grabe, V., Hamner, B., Duggins, D., & Singh, S. (2016). Compact, real-time localization without reliance on infrastructure. In, *Proc. 3rd Annu. Microsoft Indoor Localization Competition*

Zhang, Y., Middel, A., & Turner, B.L. (2019). Evaluating the effect of 3D urban form on neighborhood land surface temperature using Google Street View and geographically weighted regression. *Landscape Ecology, 34*, 681-697

Zhang, Y., & Shao, Z.F. (2021). Assessing of Urban Vegetation Biomass in Combination with LiDAR and High-resolution Remote Sensing Images. *International Journal of Remote Sensing, 42*, 964-985

Zhang, Z., Cao, L., & She, G. (2017). Estimating Forest Structural Parameters Using Canopy Metrics Derived from Airborne LiDAR Data in Subtropical Forests. *Remote Sensing, 9*, 940

Zhao, K., Suarez, J.C., Garcia, M., Hu, T., Wang, C., & Londo, A. (2018). Utility of multitemporal lidar for forest and carbon monitoring: Tree growth, biomass dynamics, and carbon flux. *Remote Sensing of Environment, 204*, 883-897

Zhou, D., Fung, T., & Chu, L.M. (2012). Avian community structure of urban parks in developed and new growth areas: A landscape-scale study in Southeast Asia. *Landscape and Urban Planning, 108*, 91-102

Zhou, W.Q., Huang, G.L., & Cadenasso, M.L. (2011). Does spatial configuration matter? Understanding the effects of land cover pattern on land surface temperature in urban landscapes. *Landscape and Urban Planning, 102*, 54-63

Zhu, X., Liu, J., Skidmore, A.K., Premier, J., & Heurich, M. (2020). A voxel matching method for effective leaf area index estimation in temperate deciduous forests from leaf-on and leaf-off airborne LiDAR data. *Remote Sensing of Environment, 240*, 14

Abstract in Korean

다중 규모 LiDAR 데이터를 활용한 도시생태계 구조 및 연결성 평가

최희준
서울대학교 대학원 협동과정 조경학
논문지도교수: 송영근

본 학위논문은 다양한 시공간 스케일에서 도시생태계 모니터링을 위한 LiDAR 데이터의 활용과 생태적 의미 도출에 관한 내용을 다룬다. LiDAR란 Light Detection and Ranging의 약어로, LiDAR 센서에서 발사된 레이저가 대상에 도달한 뒤 반사되어 돌아오는 레이저의 세기와 시간을 계산하여 대상의 위치 정보를 3차원 점군 데이터로 변환해주는 능동형 원격탐사 도구이다. LiDAR 원격탐사 도구의 등장으로 자연과 도시의 3차원 공간정보의 취득이 기능해짐에 따라, 서식지의 3차원 공간정보와 생물 종 사이의 관계 도출, 시계열 LiDAR 데이터를 활용한 녹지 모니터링 연구 등이 이뤄지고 있다. 또한 항공 LiDAR(ALS), 지상 LiDAR(TLS), 이동형 LiDAR(MLS) 등 다양한 LiDAR 시스템의 개발로 연구 목적에 알맞은 시공간 해상도의 3차원 공간정보를 취득할 수 있게 되었다. 본 학위논문에서는 도시녹지를 대상으로 LiDAR 원격탐사 도구의 다양한 시공간 스케일 적용 측면에서, Chapter 2 항공, 지상, 이동형 LiDAR 시스템 사이 수목구조관련 변수들의 일치성 평가, Chapter 3 시계열 분석을 통한 도시녹지 동태 모니터링, Chapter 4 도시의 생태적 연결성 분석을 진행하였다.

Chapter 2: 도시의 수목정보를 취득하는 것은 도시녹지 관리에 있어 필수적이다. LiDAR 기술의 발달로 도시수목의 3차원 정보를 취득할 수 있게 되었으며, 이를 통해 수목높이와 수목구조, 지상 바이오매스 등을 높은 정확도로 산출할 수 있게 되었다. 항공 LiDAR는 넓은 범위의 공간정보를 높은 정확도로 측정하는 특성을 지녀 산림 모니터링

분야에서 활발히 활용되고 있다. 하지만 항공 LiDAR 데이터의 취득은 항공기 운용비, 장비관련 막대한 비용이 발생하고 운용에 있어 전문성을 요구하며 대상의 점군밀도가 상대적으로 낮다는 단점을 지닌다. 반면 지상 LiDAR와 이동형 LiDAR는 운용하기 편리하고 높은 점군밀도를 출력한다는 점에서 항공 LiDAR의 단점을 극복할 수 있다. 이처럼 다양한 LiDAR 시스템의 등장과 이를 활용한 생태계 모니터링 연구 시도가 증가하면서 LiDAR 시스템간 효율적인 운용과 데이터의 보완 방법들이 요구되고 있다. 하지만 현재까지 ALS, TLS, MLS의 3개의 시스템을 통해 취득된 수목 정보를 서로 비교하고, 서로 대체가능한 수목정보를 도출한 연구는 많이 진행된 바 없다. 따라서 본 학위논문의 Chapter 2에서는 ALS, TLS, MLS 통해 취득된 도시의 수목정보를 서로 비교하여 일치성을 평가하고, 어떠한 수목구조관련 지표가 세 LiDAR 시스템 사이에서 대체가능한지 다루고 있다. 세부적으로 Chapter 2는 수목구조관련 지표가 단목차원과 군집차원, 수목구조에 따라 ALS, TLS, MLS 시스템에서 차이가 발생하는지에 대한 내용을 담고 있다. 천안시 도시공원 9개소에서 ALS 데이터는 2017년 5월 14일, TLS 데이터는 2017년 5월 10일과 11일, MLS 데이터는 2020년 4월 21에서 25일 취득되었다. 취득된 데이터셋은 수관의 겹침 여부에 따라 단목과 군집으로 분류되었으며, 3개의 페어(ALS-TLS, MLS-TLS, ALS-MLS)로 수관의 퍼센타일 높이, 수관복잡성, 면적 등의 수목구조관련 변수들을 1:1 비교하였다. 항공 LiDAR 데이터를 통해 도출된 수목구조관련 변수들을 참조로 하여 평균제곱근오차(RMSE), 편향(bias), 피어슨 상관계수(r) 등을 계산하고 세 LiDAR 시스템 사이의 일치성을 평가하였다. 평가 결과 ZMAX, CHM관련 수관높이 관련 변수들, 그리고 수관면적이 높은 일치성을 보였다(RMSE% < 15 %, Bias% < 15 %, and r > 0.900). 특히 CHM을 통해 도출된 수관높이 관련 변수들은 단목과 군집에서 세개의 LiDAR 시스템간 통계적인 차이를 보이지 않았다($p > 0.05$). 반면 퍼센타일 수관높이와 평균 수관높이 등은 매우 낮은 일치성을 나타냈으며, 세 페어에서 도출된 편향은 수고, 수관복잡성과

약한 선형관계를 나타냈다($r > |0.29|$, $p < 0.05$).

Chapter 3: 수관동태는 숲의 건강성을 반영한다. 특히, 자연적·인위적인 교란에 의해 발생한 숲틈은 숲 내부에 빛의 투과율, 온도, 습도 등에 영향을 끼쳐 주변 환경의 변화를 야기한다. 따라서 숲틈을 탐지하고 모니터링하는 것은 숲의 동태를 이해하는데 있어 매우 중요하다. 항공 LiDAR 센서를 활용할 경우 위성영상이나 항공사진 등 2차원 데이터로 탐지하기 어려운 숲틈 또는 개방공간의 탐지와 수관의 3차원 형상의 취득이 가능하다. Chapter 3에서는 2012년도부터 2015년도 4개년의 항공 LiDAR를 활용하여 자연형 도시공원(봉서산)의 수관과 숲틈의 수평적 수직적 변화양상을 추정하였다. 수관은 높이 5m를 기준으로 상층부와 하층부 수관으로 분류되었으며, 수관높이모델(canopy height model, CHM)을 생성하여 연간변화를 탐지하였다. 연구결과 상층부 및 하층부 수관의 수직생장량과 엽면적지수는 일정한 연간 변화양상을 보인 반면, 수평적 변화와 엽면적밀도는 불규칙적인 연간 변화양상을 보였다. 전반적으로 상층부 수관은 높이 12m에서 측방향 생장을 하는 것으로 나타났으며, 하층부 수관 중 숲틈에서는 높이 5m에서 측방향 생장이 활발하게 나타났다. LiDAR 데이터의 연간 변화 탐지를 통해 자연적으로 형성된 숲틈의 경우 생장과 교란 측면에서 매우 활발한 동태가 발생하고 있으며, 인위적으로 형성된 개방공간의 경우 수관의 동태가 다소 침체됨을 도출하였다.

Chapter 4는 도시 내 건물과 녹지의 3차원 구조를 입력자료로 활용하여 도시의 생태적 연결성을 평가하는 연구를 다룬다. 도시 내 생태적 연결성 도출과 관련한 연구는 도시와 녹지의 형태 등을 주요 변수로 하여 진행이 되고 있다. 그러나 3차원적인 특성인 도시 건물의 부피, 수목의 수직적인 구조 등을 고려한 연결성 분석은 많이 진행된 바 없다. 연구 대상지는 천안시 시청을 중심으로한 4 km × 4 km 지역으로, 2015년에 취득된 항공 LiDAR와 같은 해 취득된 조류 종 조사 데이터를 활용하여 1)도시 내 건물과 녹지의 3차원 구조와 조류 종 다양성 사이 관계를 살피고, 2)조류 종 다양성과 상관관계를 가지는 3차원 구조변수를

활용하여 전류흐름기반 매개중심성 연결성 분석(CFBC)을 진행하였다. 연구결과 건축물의 부피와 수목높이 8-10m의 녹지 부피비가 면적당 조류 종 풍부도와 스피어만 순위상관관계에서 높은 상관관계($|\rho| > 0.6$)를 나타냈다. 연결성 분석의 결과는 입력변수의 공간차원(2D 및 3D)에 따라 다르게 나타났다. 특히 도시숲, 대로변, 아파트단지내 녹지 등에서 2D 기반 CFBC와 3D기반 CFBC는 통계적으로 유의미한 차이를 보였다. 또한 도시녹지의 3D 기반 CFBC의 경우 같은 녹지 면적임에도 수관의 구조적인 특성에 따라 높은 차이가 나타남을 확인하였다. 3D CFBC 분석결과를 통해 고층 건물 주변부, 고밀도 아파트단지, 고밀 시가화지역 등이 낮은 중심성을 보여 고립지역으로 나타났으며, 건물 사이 공지 내 식생은 연결성이 고립된 지역과 핵심지역을 연결하는 기능을 나타냈다.

이 학위논문은 서로 다른 LiDAR 시스템을 활용하여 단목, 경관 지역단위 등 다양한 공간 스케일에서의 도시경관구조 분석, 도시녹지구조와 토지이용 등에 따른 시간적 변화양상, 도시경관구조가 가지는 생태적 의미 등과 관련된 내용을 다루고 있다. 향후 Global Ecosystem Dynamics Investigation(GEDI) 미션의 데이터를 활용하여 본 학위논문에서 다루는 지역규모의 연구를 국가단위, 대륙단위 등으로 확장할 수 있을 것이며 이를 통해 도시생태계 구조와 그 기능 사의 관계를 이해하는데 도움을 줄 수 있을 것이다.

Keyword: LiDAR, 레이저 스캐닝, 3차원 데이터, 식생구조, 도시경관구조, 도시생태계

학번: 2018-35951